

# Biomechanics of the Achilles tendon and midportion Achilles tendinopathy

**Chia-Han Yeh** 葉嘉漢

**Dissertation submitted in fulfilment of the requirements for the  
degree of:**

**Doctor of Philosophy**

Department of Bioengineering, Imperial College London

Mar 2019

## **Declaration of originality**

The work presented in this thesis is my own and all else is appropriately referenced.

## **Copyright declaration**

The copyright of this thesis rests with the author. Unless otherwise indicated, its contents are licensed under a Creative Commons Attribution-Non Commercial 4.0 International Licence (CC BY-NC). Under this licence, you may copy and redistribute the material in any medium or format. You may also create and distribute modified versions of the work. This is on the condition that: you credit the author and do not use it, or any derivative works, for a commercial purpose. When reusing or sharing this work, ensure you make the licence terms clear to others by naming the licence and linking to the licence text. Where a work has been adapted, you should indicate that the work has been changed and describe those changes. Please seek permission from the copyright holder for uses of this work that are not included in this licence or permitted under UK Copyright Law.

## Acknowledgements

I would first like to thank my supervisors, Dr Angela Kedgley, Professor Anthony Bull, and Professor James Calder for their guidance throughout this period. Angela provided me with all the support and help when I have problems with my research and gave me detailed comments on my writing. Anthony's critical big-picture thinking and encouragement is invaluable for this thesis. I would like to thank James for his sharp clinical perspective and providing all the connections and supports from Fortius Clinic. I would like to thank Jon and Jarrod for their clinical supports and guidance. I would like to thank staff in the Fortius clinic, Shane, Lucy, and Mary for the supports for carrying out clinical research.

I would like to thank all my colleagues from Angela's and Anthony's groups who kindly offered help when I was in need. I would like to thank all the participants who kindly took part in my experiment.

I would like to thank TUSA scholarship from Taiwan Government for the generous funding for my study in London.

I am extremely grateful to all my friends I have made during my times in London for those happy times when we played basketball and football, went to bars, and went to conferences.

Finally, I am extremely thankful to my father (葉武三), mother (陳小燕), sister (葉上琳) and my wife (Hsin-Ru Huang) for their unconditional love, support and encouragement for the whole time. This allowed me to focus on research wholeheartedly and make this PhD journey possible.

## **Abstract**

The Achilles tendon is the largest tendon in the human body and correspondingly it transmits large forces during everyday activities. Such frequent loading makes it prone to injury. Achilles tendinopathy is the most common injury of the Achilles tendon with two-thirds of cases being midportion Achilles tendinopathy. Midportion Achilles tendinopathy is a debilitating condition for both athletes and people with a sedentary lifestyle. People affected with midportion Achilles tendinopathy often significantly reduce their activity level, in some cases even quitting physical exercise completely. This has a negative effect on their overall health.

The exact mechanism of midportion Achilles tendinopathy is not clear. Two mechanical hypotheses have been proposed: differential loading within the Achilles tendon and interaction of the plantaris tendon. The first objective of this thesis was to clarify the role of these two hypotheses. The potential for differential loading within the Achilles tendon was analysed using musculoskeletal modelling, while the interaction of the plantaris tendon was investigated by categorizing the plantaris tendon geometry using MRI and ultrasound.

The differential loading within the Achilles tendon was modelled by including the Achilles tendon fibre bundle rotation in the musculoskeletal modelling. It was observed that the medial gastrocnemius force increased as the degree of rotation of the fibre bundle increased. As the medial gastrocnemius fibre accounts for the lateral aspect of the Achilles tendon, such increased load could also increase the risk of midportion Achilles tendinopathy. The process of predicting the muscle forces, using constrained optimization, was further analysed and a novel presentation of ‘Lagrange Vector’ was proposed to facilitate the understanding of the model prediction process.

The plantaris tendon geometry was also investigated by analysing MRI scans in a case-control study. The plantaris tendon geometry was associated with plantaris-involved midportion Achilles tendinopathy. The odds ratio of the plantaris directly inserting into the Achilles tendon was significantly higher in the symptomatic group.

Rehabilitation is one of the first lines of treatment for midportion Achilles tendinopathy. Such rehabilitation induces tendon healing by loading the tendon in a controlled manner. However, the relationship between external loading and Achilles tendon force during different rehabilitation activities is not clear. Thus, the second objective was to analyse the Achilles tendon force during rehabilitation.

It was observed that the force exerted on the Achilles tendon was not associated with the direction (eccentric or concentric) but strongly correlated with the maximum dorsiflexion angle reached during the exercises. As the ankle dorsiflexed, the Achilles tendon force increased. These findings could be used to estimate the tendon loading during rehabilitation and modify the current rehabilitation to improve clinical results.

This thesis investigates the Achilles tendon and midportion Achilles tendinopathy. For the two mechanical hypotheses, the role of plantaris tendon in midportion Achilles tendinopathy was further clarified, but the intra-tendon loading simulated cannot be validated as the tendon force measurement *in vivo* was infeasible. For the rehabilitation, the role of dorsiflexion angle during the rehabilitation was identified and a regression equation that clarifies the role of external loading and dorsiflexion angle was proposed.

Future work including a prospective study comparing the plantaris tendon geometry for patients diagnosed with midportion Achilles tendinopathy and a prospective study comparing the effectiveness of the modified Achilles tendon rehabilitation regimen is now required.

# Contents

Declaration of originality .....	3
Copyright declaration.....	3
Acknowledgements.....	4
Abstract.....	5
Contents .....	7
List of figures.....	11
List of tables.....	14
List of abbreviations .....	15
Chapter 1 Introduction .....	16
1.1 Motivation.....	16
1.2 Aims.....	17
1.3 Thesis structure .....	17
Chapter 2 Literature review .....	20
2.1 Anatomy.....	22
2.1.1 Bones and joints in the foot and ankle.....	22
2.1.2 Triceps surae .....	25
2.1.3 The plantaris muscle and plantaris tendon.....	27
2.1.4 Achilles tendon .....	30
2.2 Midportion Achilles tendinopathy .....	33
2.2.1 Epidemiology and clinical symptoms .....	34
2.2.2 Mechanical hypothesis I: Plantaris involvement .....	36
2.2.3 Mechanical hypothesis II: Differential stress within the tendon .....	38
2.3 Rehabilitation of midportion Achilles tendinopathy.....	40
2.3.1 Tendon healing mechanism and tendon adaptation.....	41
2.3.2 Rehabilitation protocol I: Eccentric loading training.....	43
2.3.3 Rehabilitation protocol II: Heavy slow resistance training.....	44
2.4 Biomechanical methodologies for investigating Achilles tendon and midportion Achilles tendinopathy.....	47
2.4.1 Mechanical testing with cadaveric specimens .....	48
2.4.2 Mechanical testing <i>in vivo</i> .....	50
2.4.3 Medical imaging .....	50
2.4.4 Electromyography.....	51
2.4.5 Computational modelling.....	52
2.5 Mechanical properties of the Achilles tendon <i>in vitro</i> and <i>in vivo</i> .....	56
2.5.1 In vitro measurement of mechanical properties of the Achilles tendon and plantaris tendon .....	56

2.5.2	In vivo measurement of mechanical properties of the Achilles tendon	56
2.6	Summary	57
Chapter 3	Plantaris tendon geometry <i>in vivo</i>	59
3.1	Introduction	60
3.2	Method	62
3.2.1	Participants	62
3.2.2	MRI protocol	64
3.2.3	Ultrasonography protocol	66
3.2.4	Image segmentation protocol	66
3.2.5	Plantaris tendon categorization	67
3.2.6	Statistical analysis	70
3.3	Results	70
3.4	Discussion	80
3.4.1	Plantaris tendon geometry	81
3.4.2	The attachment between the Achilles and plantaris tendons	82
3.4.3	The absence rate of plantaris	83
3.4.4	Limitation	84
3.5	Conclusion	85
Chapter 4	Plantaris tendon geometry in patients with plantaris-involved midportion Achilles tendinopathy	86
4.1	Introduction	87
4.2	Methods	89
4.2.1	Participants	89
4.2.2	Image segmentation and categorization	89
4.2.3	Statistical analysis	90
4.3	Results	90
4.4	Discussion	95
4.5	Conclusion	98
Chapter 5	Effect of the twisted fibre structure of the Achilles tendon on loading	99
5.1	Introduction	100
5.2	Methods	106
5.2.1	Anatomical datasets	106
5.2.2	Rotational tendon fibre structure	106
5.2.3	Kinematic marker datasets	108
5.2.4	Musculoskeletal model	109
5.2.5	Statistical analysis	111
5.3	Results	111

5.4	Discussion.....	116
5.4.1	Rotational insertions vs. simplified insertions.....	116
5.4.2	The effect of rotation on modelling output.....	118
5.5	Conclusion.....	120
Chapter 6	A biomechanical comparison of rehabilitation protocols for midportion Achilles tendinopathy: eccentric loading and heavy slow resistance training.....	122
6.1	Introduction.....	123
6.2	Methods.....	124
6.2.1	Participants.....	124
6.2.2	Experimental protocol.....	125
6.2.3	Kinematic and kinetic data collection.....	129
6.2.4	Musculoskeletal modelling.....	130
6.2.5	Achilles tendon force estimation.....	131
6.2.6	Statistical analysis.....	134
6.3	Results.....	135
6.3.1	The ankle torque and the Achilles tendon moment arm estimated during ECC and HSR.....	135
6.3.2	Achilles tendon force estimation from FreeBody model.....	139
6.3.3	Achilles tendon force estimation from the subject-specific MRI model	141
6.3.4	Multivariate analysis.....	143
6.4	Discussion.....	145
6.4.1	Achilles tendon moment arm at extreme dorsiflexion.....	146
6.4.2	Eccentric loading protocol vs. heavy slow resistance protocol	147
6.5	Conclusion.....	150
Chapter 7	Summary, discussion, and future work.....	151
7.1	Summary.....	151
7.2	Discussion.....	153
7.2.1	Mechanism of midportion Achilles tendinopathy.....	153
7.2.2	Limitations.....	156
7.3	Future work.....	158
7.4	Conclusion.....	159
References.....		160
Publications and presentations.....		178
Appendix A	The role of Lagrange multipliers in lower limb musculoskeletal modelling	179
A.1	Introduction.....	180
A.2	Methods.....	181



A.2.1 Anatomical parameters and kinematic data .....	181
A.2.2 Musculoskeletal model .....	181
A.3 Results.....	188
A.4 Discussion.....	193
A.4.1 The magnitude of Lagrange multipliers.....	193
A.4.2 Lagrange Vector.....	195
A.5 Conclusion .....	198
Appendix B Permissions for reproduction of figures .....	200
Appendix C Waiver statement.....	206

## List of figures

Figure 2.1 – (a) The bones and (b) the major joints (green lines) of the foot.....	23
Figure 2.2 – The motion and axes of an ankle.....	24
Figure 2.3 – Functional axis of the ankle joint. The axis has a mean deviation of 6° posterolaterally and 10° inferiorly from the anatomical coordinate frame (Nordin and Frankel, 2001).....	24
Figure 2.4 – Illustration of the triceps surae muscle.....	26
Figure 2.5 – Illustration of the plantaris tendon .....	28
Figure 2.6 – The plantaris tendon insertion categorised into nine different types.....	29
Figure 2.7 – Achilles tendon insertion. The Achilles tendon (red triangle) attaches to the posterior aspect of the calcaneus with a crescent-shaped insertion. (a) Horizontal section of calcaneal bone. (b) MRI axial view of the right foot.....	30
Figure 2.8 – The Achilles tendon rotational structure of the beaver. ....	32
Figure 2.9 – The rotational structure of the Achilles tendon presented in the literature. ....	39
Figure 2.10 – The eccentric loading training for midportion Achilles tendinopathy. ....	44
Figure 2.11 – The heavy slow resistance training includes three exercises: seated calf-raise, ankle push in a leg press machine and standing heel rise bearing a barbell. ....	46
Figure 3.1 – The wedge and coil setting for MRI scanning. ....	65
Figure 3.2 – Down-categorization of the classification system proposed by van Sterkenberg et al. (2011).....	69
Figure 3.3 – The types of plantaris tendon geometry and their presentation in MRI and ultrasound (US).....	72
Figure 3.4 – The variation within Type 1 plantaris tendons, illustrated by images of participants S26 and S20. Some Type 1 geometries have a gap (*) between the Achilles and Plantaris tendons. ....	74
Figure 3.5 – Different gap changes from dorsiflexion (-) to plantarflexion (+). ....	75
Figure 3.6 - Change of the gap size from dorsiflexion to plantarflexion in Type 1 tendons... ..	76
Figure 3.8 – The attached segment (arrow) between the Achilles tendon and plantaris tendon for participant S04. ....	77
Figure 3.9 – Fanning Type 2 plantaris tendon becoming untraceable.....	78
Figure 3.10 – The Type 2 plantaris tendon and Achilles tendon of representative participant S05 during motion. ....	79
Figure 4.1 – Frequency of plantaris tendon anatomical variants (number of tendons) for the tendinopathy group and a healthy control group. ....	91
Figure 4.2 – Representative segmented models and corresponding ultrasound (US) images and MRI sections of the plantaris tendon geometry from a group of 36 tendons in 33 patients with plantaris tendon involved midportion Achilles tendinopathy. ....	92

Figure 4.3 – Representative Type 1 plantaris tendon geometry variants from a group of 18 tendons in 17 patients with plantaris-involved midportion Achilles tendinopathy. ....	93
Figure 4.4 – Representative Type 2 plantaris tendon geometry variants from a group of 5 tendons in 4 patients with plantaris-involved midportion Achilles tendinopathy. ....	94
Figure 4.5 – Representative Type 4 plantaris tendon geometry in a group of 11 tendons in 9 patients with plantaris-involved midportion Achilles tendinopathy.....	95
Figure 5.1 – Categorisation of Achilles tendon fibre rotation into (a) least, (b) moderate, and (c) extreme rotation.....	101
Figure 5.2 – Achilles tendon fibre configuration reported by Szaro et al. (2009).....	102
Figure 5.3 – Achilles tendon fibre configurations reported by Edama et al. (2015). Reproduced with permission of Edama et al. (2015).....	103
Figure 5.4 – Perturbation of the Achilles tendon insertion modelled as a single point. ....	104
Figure 5.5 – Representation of different degrees of rotation of the Achilles tendon insertion in a musculoskeletal model.....	107
Figure 5.6 – The median and interquartile range of the triceps surae muscle forces and the Achilles tendon force (n=9).....	112
Figure 5.7 – Box plots of the peak forces of medial gastrocnemius, lateral gastrocnemius, overall gastrocnemius, soleus and Achilles tendon force (n=9) for different insertion types.....	113
Figure 5.8 – The median muscle activation (n = 9) of the of different insertional variants of the Achilles tendon compared with normalized EMG from the literature.....	117
Figure 5.9 – The difference between of medial gastrocnemius insertion locations (triangles) in different Achilles tendon insertion patterns.....	119
Figure 6.1 – The (a) standing heel rise and (b) seated calf-raising performed with a Smith machine.....	126
Figure 6.2 – (a) Anterior and (b) posterior views of the twenty-three reflective markers used in the trial, consisting of 12 single markers and 9 clusters, each of three markers.....	129
Figure 6.3 – Determination of a subject-specific ankle centre of rotation of the ankle, and Achilles tendon line of action and moment arm. ....	133
Figure 6.4 - Normalized ankle torque (mean $\pm$ one standard deviation) for 18 participants over the range of motion for eccentric loading (ECC) and heavy slow resistance (HSR)....	136
Figure 6.5 - The Achilles tendon moment arm (mean $\pm$ one standard deviation) from the scaled model and subject-specific MRI scans of 18 participants over a range of joint angles. ....	138
Figure 6.6 - Achilles tendon force (mean $\pm$ one standard deviation) over ankle joint range of motion estimated by FreeBody for 18 participants, during the eccentric loading (ECC) and heavy slow resistance protocol (HSR) for different external loading conditions ..	139

Figure 6.7 - Achilles tendon force (mean $\pm$ one standard deviation) over ankle joint range of motion estimated by subject-specific MRI model for 18 participants, during the eccentric loading (ECC) and heavy slow resistance protocol (HSR) for different external loading conditions.....	141
Figure 8.1 – The median trajectory of two Lagrange multipliers during a walking trial (n = 9) .....	189
Figure 8.2 – The median trajectory of the norms of all the Lagrange Vectors for all nine participants.....	191
Figure 8.3 – The anterior and medial projection of the Lagrange Vector. ....	192
Figure 8.4 – The illustration of a spatial understanding of the Lagrange Vector. ....	196
Figure 8.5 – The orientation of the Lagrange Vector (LV) is decisive as to muscle activation. ....	197

## List of tables

Table 2.1 – Heavy slow resistance protocol suggested by Beyer et al. (2015) .....	46
Table 3.1 – Participants’ anthropometric data.....	63
Table 3.2 – The plantaris tendon incidence of each type, compared with those from the literature.....	71
Table 5.1 – The nomenclature of the insertional types.....	108
Table 5.2 – The coefficient of multiple correlations of the activation pattern during a gait cycle (n=9) between different insertional variants. ....	115
Table 6.1 – The loading condition and the activity performed.....	128
Table 6.2 – The peak normalized torque in eccentric loading (ECC) and heavy slow resistance exercise (HSR). *:p<0.05, **:p<0.01 , Wilcoxon signed rank test with Bonferroni correction. ....	137
Table 6.3 - The peak Achilles tendon force predicted by FreeBody in eccentric loading (ECC) and heavy slow resistance (HSR) exercise. *: p<0.05, **:p<0.01, Wilcoxon signed rank test, with Bonferroni correction.....	140
Table 6.4 - The peak Achilles tendon force predicted by subject-specific MRI model in eccentric loading (ECC) and heavy slow resistance (HSR) exercise. *: p<0.05, **:p<0.01, Wilcoxon signed rank test, with Bonferroni correction. ....	142
Table 6.5 – Multivariate regression analysis of the normalized peak Achilles tendon force during standing and seated motions in the heavy slow resistance protocol.....	144
Table 8.1 – The Lagrange multipliers in the FreeBody model and corresponding kinetic constraints.....	184
Table 8.2 – The 15 joint contact forces in the FreeBody model.....	186
Table 8.3 – The median and IQR of extrema of Lagrange multipliers and Lagrange vectors. ....	190

## List of abbreviations

---

Abbreviation	Explanation
3D	Three dimensional
EMG	Electromyography
MRI	Magnetic resonance image
PCSA	Physiological cross-sectional area
RM	Repetition maximum
TR	Repetition time
TE	Echo time

---

# Chapter 1

## Introduction

### 1.1 Motivation

Midportion Achilles tendinopathy is a debilitating condition, in which patients may experience pain with every step. This causes great discomfort during daily activities. It has been estimated that long-distance runners have a lifetime risk of developing midportion Achilles tendinopathy of 50% (Kujala et al., 2005). However, the precise mechanism is not fully understood. In this thesis, the mechanical hypotheses of the initiation of the midportion Achilles tendinopathy –plantaris tendon involvement and the differential loading within the Achilles tendon– are examined with medical imaging and musculoskeletal modelling. The hypotheses are i) the anatomical variation of the plantaris tendon can be associated the occurrence of plantaris tendon involvement and ii) the differential loading within the Achilles tendon will be affected by the rotation of the fibre structure. This is followed by an investigation into the biomechanics of two

common Achilles tendon rehabilitation protocols: the eccentric loading exercise and the heavy slow resistance exercise. Musculoskeletal modelling was used to estimate the forces transmitted by the Achilles tendon during rehabilitation activities. The findings in this thesis can bridge the gap between the biomechanical aspects of midportion Achilles tendinopathy and provide insights into rehabilitation regimens.

## 1.2 **Aims**

The aims of this thesis are to examine the possible mechanisms in the development of midportion Achilles tendinopathy and to investigate the relationship between the external load and force through the Achilles tendon during rehabilitation exercises. To achieve these aims, musculoskeletal modelling and medical imaging, MRI and ultrasound, are used. The musculoskeletal model allows personalised quantification of the forces created by the muscles that insert on the Achilles tendon, while MRI and ultrasound enable anatomical variance to be captured. The ultimate goal is to apply these methods and results to improve patient treatment and preventive measures.

## 1.3 **Thesis structure**

Chapter 2 provides a literature review of the relevant topics, including the anatomical background and terminology, hypotheses and supporting evidence, and rehabilitation regimens. This chapter also reviews the current clinical views regarding



midportion Achilles tendinopathy and the methodology behind musculoskeletal modelling.

Chapter 3 investigates the first hypothesis for the development of midportion Achilles tendinopathy –involvement of the plantaris tendon. The high anatomical variation of the plantaris tendon has not been investigated *in vivo* previously. A healthy cohort of 34 volunteers recruited from a university environment was investigated. MRI and ultrasound were used to evaluate and classify the various geometries. Multiple static MRIs were taken at a range of ankle joint angles to visualize the plantaris tendon's relationship with the Achilles tendon.

Chapter 4 applies the categorization of the plantaris tendon that was developed in Chapter 3 to a cohort of 36 plantaris tendons from 29 individuals who had received a clinical diagnosis of midportion Achilles tendinopathy with plantaris tendon involvement. Their anonymised MRI and ultrasound scans were retrospectively collected from the Fortius Clinic. A chi-squared test was used to identify the proportion difference between two groups. By comparing the difference in the prevalence of plantaris tendon types, the correlation between plantaris type and midportion Achilles tendinopathy can be further clarified.

Chapter 5 examines the second hypothesis of midportion Achilles tendinopathy – differential loading within the tendon. This is achieved by modelling the different degrees of rotation of the fibre bundles within the Achilles tendon. By modelling different tendon insertions, the effect of the differential loading within the tendon can be analyzed.

Chapter 6 compares the load of the Achilles tendon in two different rehabilitation regimens: eccentric load training and heavy slow resistance training. Musculoskeletal modelling and a subject-specific modelling based on moment arm were used to analyse

the effectiveness of loading the Achilles tendon during the different protocols. These findings can be used to further optimise the rehabilitation protocol.

Chapter 7 provides a summary of all the findings and an integrated discussion of the potential mechanism of midportion Achilles tendinopathy development. It also discusses the contribution of this thesis to the current knowledge of midportion Achilles tendinopathy, the limitations of the work, and future research directions.

In Appendix A, a further investigation of the optimization process that is used in the musculoskeletal model is shown. This provides a mathematical perspective on how muscle forces are distributed within the model, which is fundamental to determining the muscle activation patterns. This analysis also provides insights into the modelling of muscle coordination and co-contraction.

## Chapter 2

### Literature review

The Achilles tendon, also termed the calcaneal tendon, is the thickest tendon in the human body. It is named after the legendary warrior, Achilleas, from Greek mythology. When Achilleas was a baby, his mother Thetis dipped Achilleas, head down, into the River Styx. The magical river water offered invulnerability to the baby Achilleas, except on his heel, which was held by his mother, and thus become his only weakness. Achilleas grew up to be a famous warrior and survived many great battles. However, the weakness on his heel eventually caused his death, when it was punctured by a poisoned arrow during the Trojan War (Walton, 2003).

The Greek myth of the Achilles tendon is justified by its powerful biomechanical role in human movement. The cyclic stretch and relaxation of the Achilles tendon drives human locomotion. From routine daily activities to artistic dancing to vigorous competitive sports, all these fantastic activities cannot be achieved without a healthy, competent Achilles tendon. Although the Achilles is the largest tendon, it's one of the

most frequently injured tendons in the human body. Injury of the tendon body is broadly termed Achilles tendinopathy.

This chapter provides an overview of the functional anatomy and biomechanics of the Achilles tendon, including the ankle joint and the muscles connected to the tendon. This is followed by an introduction to the pathological condition termed Achilles tendinopathy, and two biomechanical hypotheses for its predisposition. Two rehabilitation exercise protocols are then introduced and the mechanisms by which these exercises rehabilitate the Achilles tendon are discussed.

There are many unknowns in the relationship between Achilles tendon force and injury because the muscle/tendon forces are difficult to measure *in vivo*. Therefore, the methods for investigating the force through the Achilles tendon and Achilles tendinopathy in the literature are reviewed and the logic for the choice of methods in this thesis is discussed.

## 2.1 Anatomy

In order to understand the biomechanics of the Achilles tendon, the anatomy of the foot and ankle must first be reviewed. The foot and ankle are naturally designed to provide the human with a stable and adaptable interface between the body and the external environment. This is achieved by a flexible joint motion during initial contact with the surroundings, maintaining the stability of the superincumbent bony structure of the lower limb whilst transmitting the body weight, and finally becoming rigid. From 20% to 70% of the stance phase, the stiffness of ankle joint increased from 1.5 to 6.5 Nm/rad/kg (Rouse et al., 2014), before pushing off and propelling the body forward. This cannot be achieved without proper coordination of the associated muscles (Nordin and Frankel, 2012; Zelik and Honert, 2018).

### 2.1.1 Bones and joints in the foot and ankle

The human foot is composed of 28 bones (including sesamoids) and 31 articulating surfaces. It is separated into forefoot, midfoot and hindfoot. The dome-shaped talus acts as the major articulating interface between the foot and shank. (Figure 2.1)

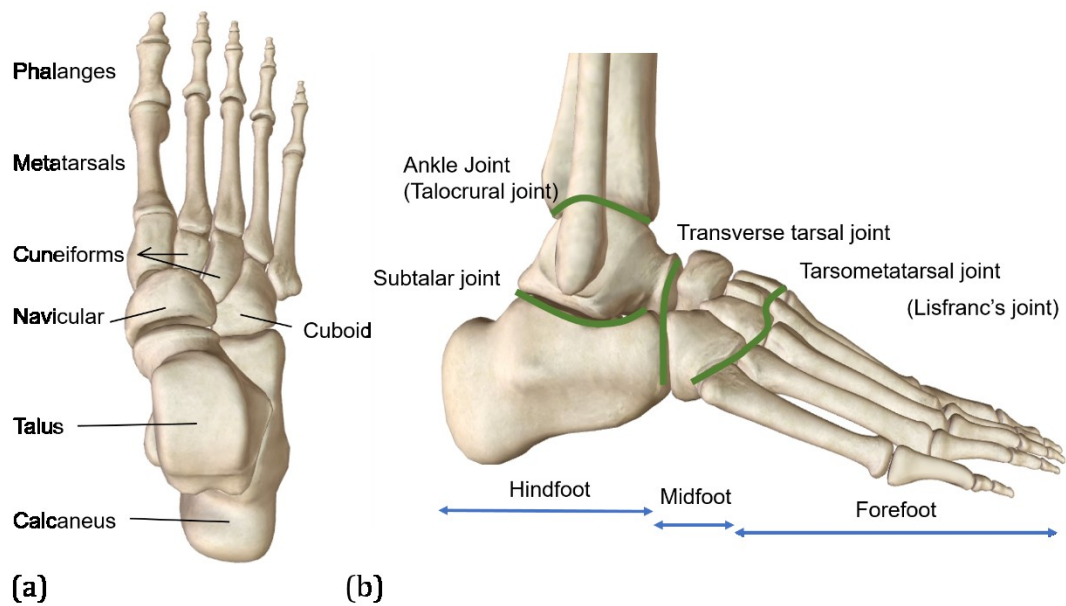


**Figure 2.1 – (a) The bones and (b) the major joints (green lines) of the foot.**

The transverse tarsal joint and tarsometatarsal joint separate the forefoot, midfoot and hindfoot. Reproduced and modified with permission from BioDigital Human (<https://www.biodigital.com/>).

Most of the foot range of motion is provided by the combination of the ankle joint and the subtalar joint. The ankle joint is defined as the joint complex between the distal tibia, distal fibula, and the dome of the talus (Drake, 2015), and it is also called the ‘talocrural articulation’, which means the ‘joint between talus and leg’.

The ankle joint motions and degrees of freedom are shown in Figure 2.2. The motions of the ankle are commonly defined based on a Cartesian coordinate frame on the shank. However, the functional joint axes are slightly oblique to the long axis of tibia (Figure 2.3). The ankle joint provides the primary axis for dorsiflexion and plantarflexion. The range of motion of the ankle joint varies between people. Clinical measurement using goniometry results in a normal range of motion of  $10^{\circ}$  to  $20^{\circ}$  for dorsiflexion and  $40^{\circ}$  to  $55^{\circ}$  of plantarflexion (Nordin and Frankel, 2012).

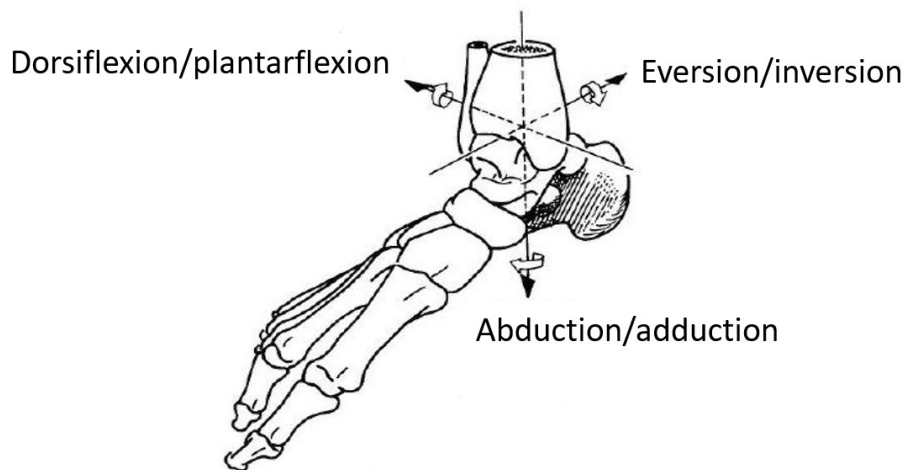


**Figure 2.2 – The motion and axes of an ankle.**

Reproduced with permission from Nordin and Frankel (2012).

---

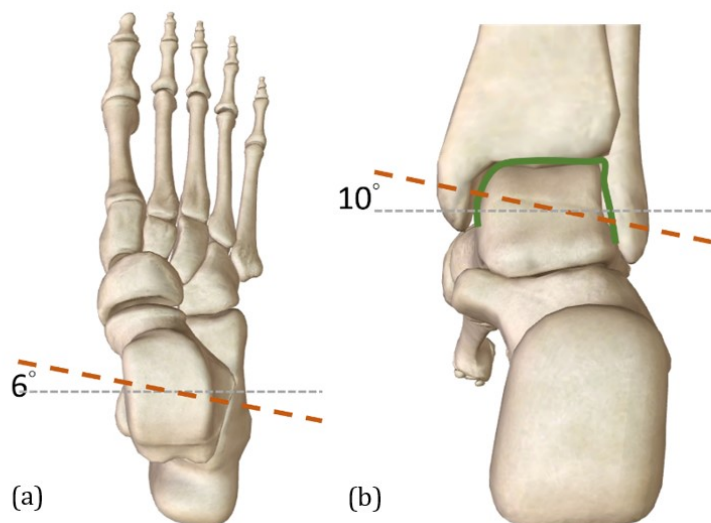


**Figure 2.3 – Functional axis of the ankle joint. The axis has a mean deviation of 6° posterolaterally and 10° inferiorly from the anatomical coordinate frame (Nordin and Frankel, 2001).**

Reproduced and modified with permission from BioDigital Human (<https://www.biodigital.com/>).

---

The subtalar joint is defined by the articulation between the talus and calcaneus. The joint axis is set at an oblique angle to the anatomical axis and provides 20° of inversion

and 10° of eversion. Although the subtalar joint provides a small amount of motion for plantarflexion and dorsiflexion, it is not considered clinically meaningful and is often neglected (Nordin and Frankel, 2012). When motion about the ankle joint and subtalar joint axes were analysed using dynamic MRI, it was found that nearly all the motion can be attributed to the ankle with extreme consistency across people (Sheehan, 2010).

### **2.1.2 Triceps surae**

The cardinal human plantarflexors are collectively called triceps surae, which means ‘the three muscles of the leg’. They are composed of three muscles: the medial head of the gastrocnemius (also termed ‘gastrocnemius medialis’), the lateral head of the gastrocnemius (‘gastrocnemius lateralis’) and the soleus muscle. The gastrocnemius is a biarticular muscle with its medial head attached to the posterior aspect of the medial femoral condyle and its lateral head to the posterior aspect of the lateral femoral condyle, while the soleus is a monoarticular muscle with a broad inverted U-shaped origin along the soleal line on the tibia and proximal posterior fibula (Figure 2.4). The muscle fibres of gastrocnemius fuse distally and form the gastrocnemius aponeurosis and then converge with the soleus fibre underneath to form the Achilles tendon, which inserts onto the posterior superior end of the calcaneus (Drake, 2015).



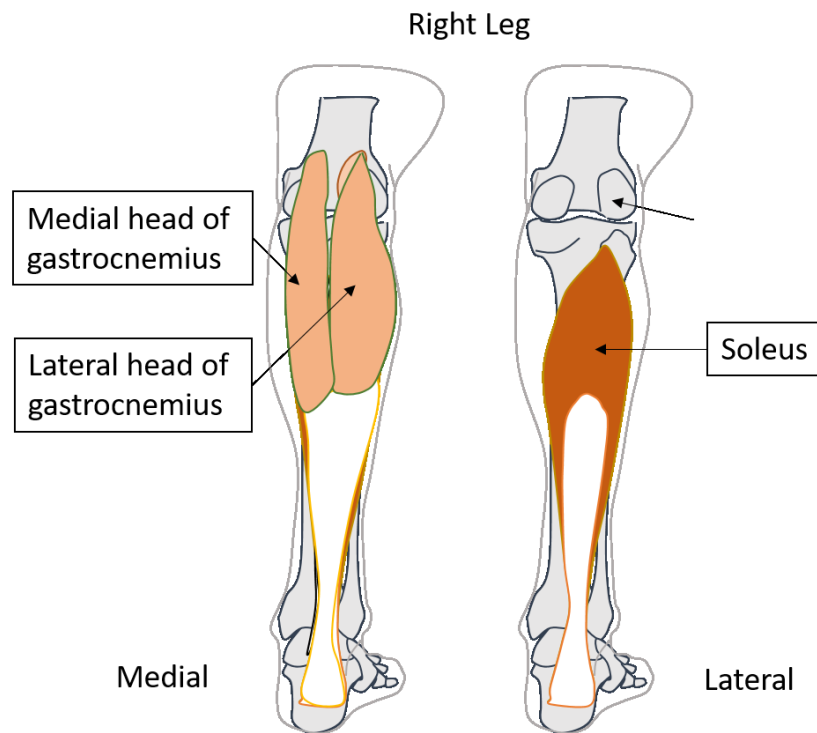


**Figure 2.4 – Illustration of the triceps surae muscle.**

---

Triceps surae is innervated by the tibial nerve, which originates from the S1 nerve root. This shared innervation underlies the functional similarity between gastrocnemius and soleus. During a normal gait cycle, they are estimated to generate together 90% of the torque for plantarflexion and the activation periods are primarily overlapping (Nordin and Frankel, 2012). However, there are still some functional differences in the triceps surae. For complicated activities, the function of gastrocnemius largely depends on the knee joint angle. As a biarticular muscle, the contribution to ankle torque greatly decreases when the knee joint is flexed (Cresswell et al., 1995). Another difference is in the muscle fibre type. Half of the muscle fibres in gastrocnemius are fast twitch fibres and thus it is characterized by fast force-generating capacity but short endurance. In contrast, soleus is made up of 70% slow twitch fibres, which contract slowly but can provide a stable force over a long period of time (Edgerton et al., 1975).

Because of its endurance, the soleus muscle is regarded as an evolutionary landmark for bipedalism (Hanna and Schmitt, 2011). The soleus muscle provides one of the main forces to support and propel the human body during the stance phase (Hamner et al., 2010). With soleus, humans can stand and perform most activities in the upright posture.

### **2.1.3 The plantaris muscle and plantaris tendon**

The plantaris muscle has a short spindle-shaped muscle belly, but a long tendon. The muscle belly length is 5-10 cm, but the tendon length is approximately 30 cm (Spina, 2007). It originates from the supracondylar line of the femur and travels between the gastrocnemius and soleus muscles (Figure 2.5). The plantaris muscle belly is small (mass: 12 g, physiological cross-sectional area: 2.4 cm<sup>2</sup>) (Klein Horsman et al., 2007) and can only provide a weak force. Therefore, it has been generally considered vestigial (Spina, 2007), yet it is of interest due to its bi-articular nature and the high variation in insertion locations.

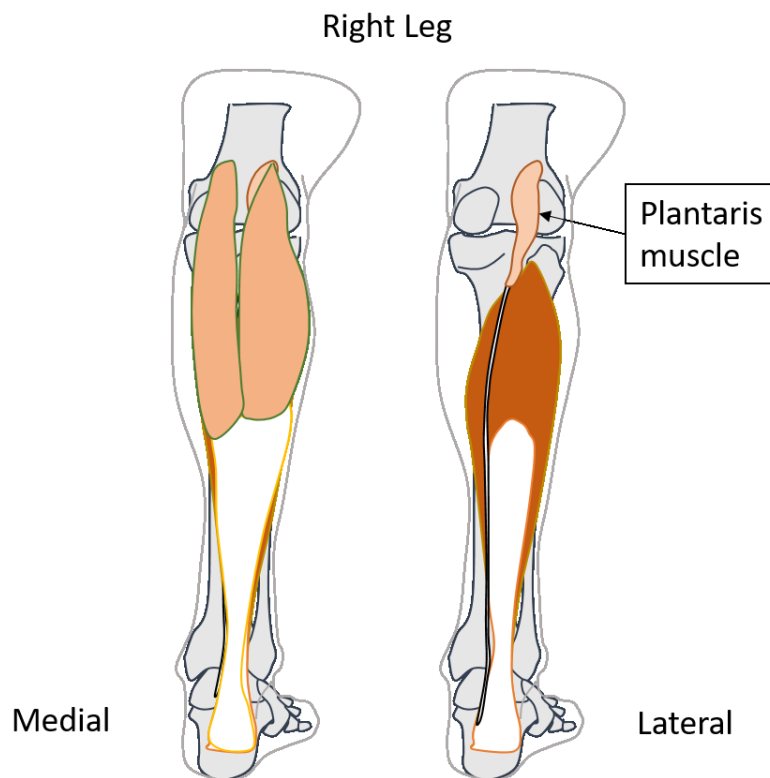











**Figure 2.5 – Illustration of the plantaris tendon**

---

Using cadaveric specimens, plantaris has been categorized by several authors into between three and nine different types, with an absence rate of between 0% and 20% (Daseler and Anson, 1943; Dos Santos et al., 2009; Joshi et al., 2014; Spang et al., 2016; van Sterkenburg et al., 2011a) (Figure 2.6).

The great anatomical variation in plantaris means that there could potentially be differences in muscle path and moment arm; however, when this is considered in combination with its very small volume, it is possible that the biomechanical importance of the plantaris muscle could also be insignificant.

Site of insertion Plantaris tendon	Medial onto calcaneus	Medial, fan- shaped onto calcaneus	Medial onto calcaneal tendon	Medial with thin slips onto calcaneus
Image				
Frequency (n = 107) (%)	21 (20)	26 (24)	3 (2.8)	5 (4.7)
Anteromedial onto calcaneus	Anteromedial, fan- shaped onto calcaneus	Posteromedial, fan-shaped onto calcaneus	Anterior onto calcaneus	Deep fascia
				
15 (14)	18 (17)	16 (15)	2 (1.8)	1 (0.9)

**Figure 2.6 – The plantaris tendon insertion categorised into nine different types.**

Reproduced with permission from van Sterkenburg et al. (2011).

However, despite its small size, the plantaris muscle could play another important role in human mobility. A high density of muscle spindles, structures that function as sensors for muscle tension, has been observed in the plantaris (Peck et al., 1984; Spina, 2007). This implies that the plantaris potentially acts as a sensor for human posture, which is also termed proprioception. This hypothesis could explain its unique shape. With a short compliant muscle belly and a long stiff tendon, the force sensing process can be more efficient when compared to a long muscle belly and short tendon structure. As the muscle lengthens and shortens, the force will stretch the compliant muscle more than the stiff tendon; the small muscle belly design may increase its sensitivity in detecting small changes in force (Peck et al., 1984).

## 2.1.4 Achilles tendon

The Achilles tendon is the largest tendon in the human body, measuring approximately 15 cm in length. The Achilles tendon originates from the aponeurosis formed by the gastrocnemius and soleus and inserts into the calcaneus with a crescent-shaped insertion (Figure 2.7). The Achilles tendon is composed of multiple fascicles, which are made up of bundles of collagen fibres. These fibre bundles are derived from the muscle fibres of gastrocnemius and soleus. These fibre bundles twist as they descend to the insertion like a biological spring (Cavagna et al., 1977).

---

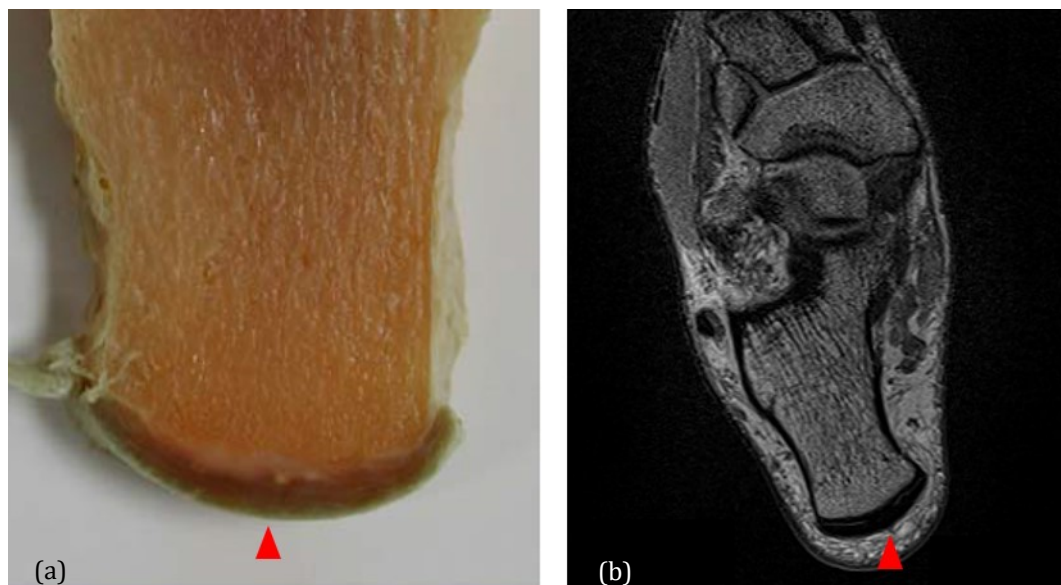


**Figure 2.7 – Achilles tendon insertion. The Achilles tendon (red triangle) attaches to the posterior aspect of the calcaneus with a crescent-shaped insertion. (a) Horizontal section of calcaneal bone. (b) MRI axial view of the right foot.**

(a) Reproduced and modified with permission from Lohrer et al. (2008).

---

A similar rotational tendon structure has been found in many mammals. Parsons et al. (1894) reported a similar rotational tendon structure in the Achilles tendon of

beavers, kangaroos, rodents, and dogs (Figure 2.8). In a horse tendon study by Birch et al. (2007), the Achilles tendon equivalent, superficial digital flexor tendon, transmits a large force during running and was categorized as a 'functional tendon'. To the contrary, thin tendons made up of parallel fibres, such as the common digital extensor tendon, were categorized as 'positional tendons'. As the name suggests, positional tendons maintain joint position and hence are not exposed to large forces during motion, while the functional tendons are often connected to strong muscles and drive a certain activity. The Young's modulus of functional tendons is lower than that of positional tendons (Birch, 2007). Such compliance has been described as a biological spring in reference to the fact that elastic energy may be stored when stretching the tendon. Such energy will be released when the tendon is relaxed, reducing the energy consumption of the muscles. However, due to their compliant nature and frequent force transmission, a large strain of the tendon is seen in functional tendons and they are therefore prone to injury (Birch, 2007). On the other hand, Ker et al. (2002) categorize tendons as over-strong and low safety-factor tendons based on the force that the tendon normally sees *in vivo*. Some tendons have a high safety factor, ranging from 8 to 15, and normally have lower 'stress-in-life'. To the contrary, other tendons, especially those found in the ankle, have low safety factors. When two types of tendon were loaded with same stress, the tendons with a lower safety factor showed higher fatigue lifetime. It was suggested that these low safety factor tendons are evolved to sustain larger forces. However, when the two tendons were loaded with the normal forces they sustain *in vivo*, their fatigue lifetime is the same. Such a finding suggests that the tendons have evolved to match their mechanical purpose. (Gosline et al., 2002)

Both fatigue and tendon material property have been suggested to be associated with the risk of tendon injury (Neviaser et al., 2012). The works from Birch et al. (2007) and

Ker et al. (2002) presented different information about tendon structure and property, which is likely due to the difference in tendon samples. More studies are needed to clarify the relationship among different tendon mechanical properties of different types, tendon structures and risk of injury.

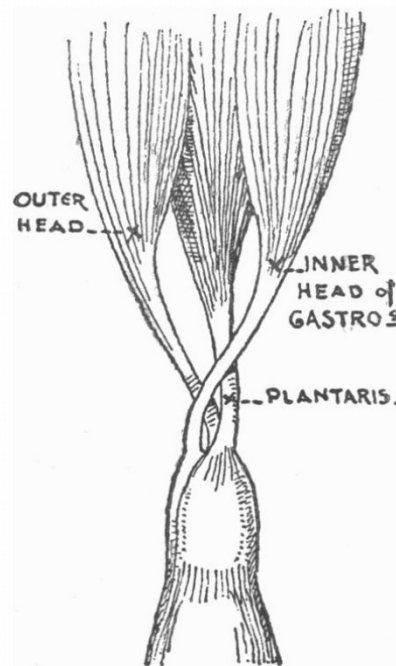


**Figure 2.8 – The Achilles tendon rotational structure of the beaver.**

Reproduced with permission from Parsons (1894).

---

Unlike most tendons in the human body, which are covered by a synovial sheath, the Achilles tendon is covered by a double-layered ‘paratenon’. This is a connective tissue richly vascularized to provide blood supply to the tendon and facilitate gliding. As the tendon body is not innervated, injury of the fibres within the Achilles tendon should not cause pain. It has been suggested that the neovascularization and innervation around the paratenon are the cause of pain sensation in the injury of the Achilles tendon (van Sterkenburg et al., 2011a).

## 2.2 Midportion Achilles tendinopathy

The term ‘Achilles tendinopathy’ was proposed by Maffulli et al. (1998) to describe the combination of clinical symptoms including pain, swelling and impaired performance. In the past, it was thought that inflammatory cells infiltrated into the injured tissue, causing subsequent swelling and pain. Therefore, many similar terms were used to name the pain around the Achilles tendon, such as ‘paratendinitis’, ‘peritendinitis’, ‘tenosynovitis’ and ‘tendinitis’ (Khan et al., 1996), which literally defined this disease entity as an inflammatory process.

However, later pathological evidence indicated that only minimal inflammatory cell infiltration was presented in the injured tendon (Astrom and Rausing, 1995; Khan et al., 1996; Nirschl and Pettrone, 1979; Uthoff and Sano, 1997). Therefore, Achilles tendinopathy is a process of tendon degeneration, a process characterized by disorganized healing response, possibly after overuse (Maffulli et al., 2004). The painful Achilles tendon comes from a complicated degeneration process, including tendon fibre disarrangement in the tendon body (Cook et al., 2002; Fredberg and Stengaard-Pedersen, 2008; Khan et al., 1996), neovascularization (de Vos et al., 2007; Peers et al., 2003; Reiter et al., 2004; van Sterkenburg et al., 2010; Zanetti et al., 2003) and neoinnervation to the paratenon (Bjur et al., 2005) that causes pain and swelling sensation. In other words, the injury is a ‘tendinosis’ instead of ‘tendinitis’, as the degeneration plays a major role most of the time. Interestingly, such degeneration often precedes clinical symptoms and is not necessarily symptomatic (Kannus and Jozsa, 1991).



Achilles tendinopathy is categorized into insertional Achilles tendinopathy and midportion Achilles tendinopathy based on the location of the symptoms (Almekinders and Temple, 1998). Insertional Achilles tendinopathy occurs at the insertion site on the calcaneus, while midportion Achilles tendinopathy occurs at 2-7 cm above the insertion site. (Abramowitch et al., 2010; Li and Hua, 2016) This categorization also implies its different histopathology. Ossification of the tendon enthesis and bone spurs are often noticed in patients with insertional Achilles tendinopathy (Den Hartog, 2009), while tendinosis and degeneration are associated with midportion Achilles tendinopathy (van Dijk et al., 2011).

### **2.2.1 Epidemiology and clinical symptoms**

Among all the activities associated with midportion Achilles tendinopathy, middle- and long-distance running have the greatest risk. The annual incidence for high-level club runners is 7-10% (Jarvinen et al., 2005), and professional long-distance runners have a lifetime risk of 52% (Kujala et al., 2005). Five percents of athletes with an occurrence will face a premature career termination (Kujala et al., 2005). In the general population, it is estimated to affect 2.35 per 1000 people (de Jonge et al., 2011). However, the incidence of Achilles tendinopathy is rising as many people engage in recreational and competitive sports (Selvanetti et al., 1997b).

Patients with midportion Achilles tendinopathy present with pain and stiffness at 2-7 cm above the calcaneus (van Sterkenburg and van Dijk, 2011). Some patients report these symptoms after their training regimen increases. The pain typically worsens as the activity increases and will be relieved after resting. A thickened Achilles tendon at the level 4-7 cm above the insertion site can often be found under ultrasound in chronic midportion Achilles tendinopathy.

Many risk factors have been identified to be associated with Achilles tendon problems: engaging in stop-and-go sports such as basketball and football, a sudden increase of training intensity and duration, male gender, obesity, increasing age and poor running mechanics (Holmes and Lin, 2006). Poor running mechanics include: over and under pronation of the foot, excessive supination, flat foot, high foot arch, leg length discrepancy, foot malalignment and inadequate dorsiflexion (Jarvinen et al., 2001). An observational study on UK elite athletes over a 4 year period found that 22% of all sprinters and 18% of all endurance runners developed an Achilles tendinopathy (Pollock et al., 2016). In bend sprinters, the condition was more common on the right side, with 80% of cases occurring in the right leg.

These risk factors and observations suggest that the biomechanics of the foot and ankle play a major role in predisposing Achilles tendinopathy. Therefore, one hypothesis about the aetiology of Achilles tendinopathy is associated with the adjacent plantaris tendon (Alfredson, 2011). This is based on the clinical observation of some midportion Achilles tendinopathy patients presenting with a focal medial side pain at the level of 4-8 cm above the insertion site. This is the very level where the plantaris tendon may contact the Achilles tendon. Friction or compression between these two tendons has been suggested as a cause for midportion Achilles tendinopathy (Alfredson, 2011; Calder et al., 2016; Masci et al., 2016; Spang et al., 2016). However, confirmation bias could exist in these case series studies. The most effective way to avoid confirmation bias is a blinded study, but it is not always possible in clinical research. Alternatively, confirmation bias could be mitigated by a prospective study that includes all patients with the diagnosis of Achilles tendinopathy rated by multiple independent specialists. Thus, the symptoms and association with the plantaris tendon could be further clarified.

Another hypothesis regarding the pathophysiology of mid-portion Achilles tendinopathy is based on the inadequate force distribution within the tendon during activity (Arndt et al., 1998b; Kader et al., 2002). As the Achilles tendon sustains different individual muscle forces from the gastrocnemius and soleus, a non-uniform stress may occur within the tendon, causing microtrauma between the fibrils (Kader et al., 2002; Selvanetti et al., 1997a). Degeneration of the tendon could occur if the microtrauma accumulation is faster than repair (Arndt et al., 1998a; Kader et al., 2002; Toumi et al., 2016). Such differential stress could be supported by the observation of the differential intra-tendon displacement.(Finni et al., 2018; Franz et al., 2015; Slane and Thelen, 2014)

### **2.2.2 Mechanical hypothesis I: Plantaris involvement**

Involvement of the plantaris tendon has been identified in some midportion Achilles tendinopathy patients, and it could be associated with the pain experienced on the medial aspect of the leg. The anatomical adjacency of the tendon has been suggested to be one important factor that could lead to the shear and compression of the Achilles tendon (Alfredson, 2011).

During surgery for Achilles tendinopathy, the plantaris tendon was found to be in close contact with the Achilles tendon in 80% of patients. Some plantaris tendons were even invaginated into the Achilles tendon (Alfredson, 2011). In some of these patients, ultrasound tissue characterization recognized a fibre disarrangement of the Achilles tendon localized to the side where it contacts the plantaris tendon. After the plantaris tendon was removed, the clinical symptoms improved, as did the Achilles tendon fibre arrangement (Calder et al., 2016; Masci et al., 2015, 2016). Plantaris tendon removal

can be done with a minimally invasive procedure and it has become a popular treatment choice for athletes, as it greatly reduces the return-to-sports time from 18 months to 10 weeks (Alfredson, 2011; Calder et al., 2015; Calder et al., 2016; Masci et al., 2015).

Besides the clinical observations, this hypothesis is also supported by other biomechanical evidence. From a cadaveric study, it is reported that 10.3% of plantaris tendons cannot freely glide relative to the Achilles tendon (van Sterkenburg and van Dijk, 2011). In these cases, the plantaris tendon either inserts directly onto the Achilles tendon or is tethered to the Achilles tendon by a retinaculum-like tissue structure, which prohibits free sliding between the two tendons (van Sterkenburg and van Dijk, 2011). Mechanical testing has shown that the parallel-fibred plantaris tendon is five times stiffer and seven times higher ultimate strength than the rotational-fibred Achilles tendon (Lintz et al., 2011). The stiffness represents the tendon elongation in response to the external loading, and the ultimate strength represents the maximum loading before the tendon breaks.

Cadaveric loading simulations have shown that the differential displacement between the Achilles and plantaris tendons is dependent on the plantaris tendon insertion, and that compression between tendons is more likely to occur at extreme plantarflexion, especially in hindfoot valgus compared with a neutral position (Stephen et al., 2018). As the magnitude of compression during simulations is significantly lower than the ultimate strength of the Achilles tendon (0.2-0.4 MPa vs. 72 MPa), the difference in stiffness between the two tendons is likely to be the main factor.

### **2.2.3 Mechanical hypothesis II: Differential stress within the tendon**

The Achilles tendon experiences large forces during everyday activities. *In vivo* measurement using a buckle transducer attached to the tendon reported a peak force of 2233 N during a squat jump, 1895 N in a countermovement jump, 3786 N in hopping (Fukashiro et al., 1995), 9000 N in running (Komi, 1990), 661N in cycling at 90rpm (Gregor et al., 1987) and 2600 N in slow walking (Komi et al., 1992). It is very likely that muscle fibres derived from the gastrocnemius and soleus might contribute differently to the Achilles tendon force. The gastrocnemius is a bi-articular muscle, so the muscle force is dependent on the knee flexion angle. In knee flexion, the gastrocnemius is slackened and contributes less to the Achilles tendon force. In addition, the ratio of the physiological cross-sectional area (PCSA) of the gastrocnemius medialis, gastrocnemius lateralis and soleus are 4:2:15, which suggests that soleus has larger force generating capacity than gastrocnemius (Klein Horsman et al., 2007). The PCSA was calculated as muscle volume divided by muscle fibre length, and it has been shown to be correlated to the maximum muscle force capacity (Bodine et al., 1982).

In addition, as mentioned earlier in this Chapter, the Achilles tendon fibre bundles have a rotational structure. At the origin of the Achilles tendon, where the soleus fibres confluence with the gastrocnemius aponeurosis, the soleus fibres comprise the deep layer of the Achilles tendon, the gastrocnemius medialis fibres comprise the superficial medial aspect, and the gastrocnemius lateralis fibres comprise the superficial lateral aspect. As the tendon descends to its insertion, the fibre bundles of the gastrocnemius and soleus rotate, and the degree of rotation varies among the population (Ballal et al., 2014; Cummins et al., 1946; Edama et al., 2015; Szaro et al., 2009; van Gils et al., 1996) (Figure 2.9).

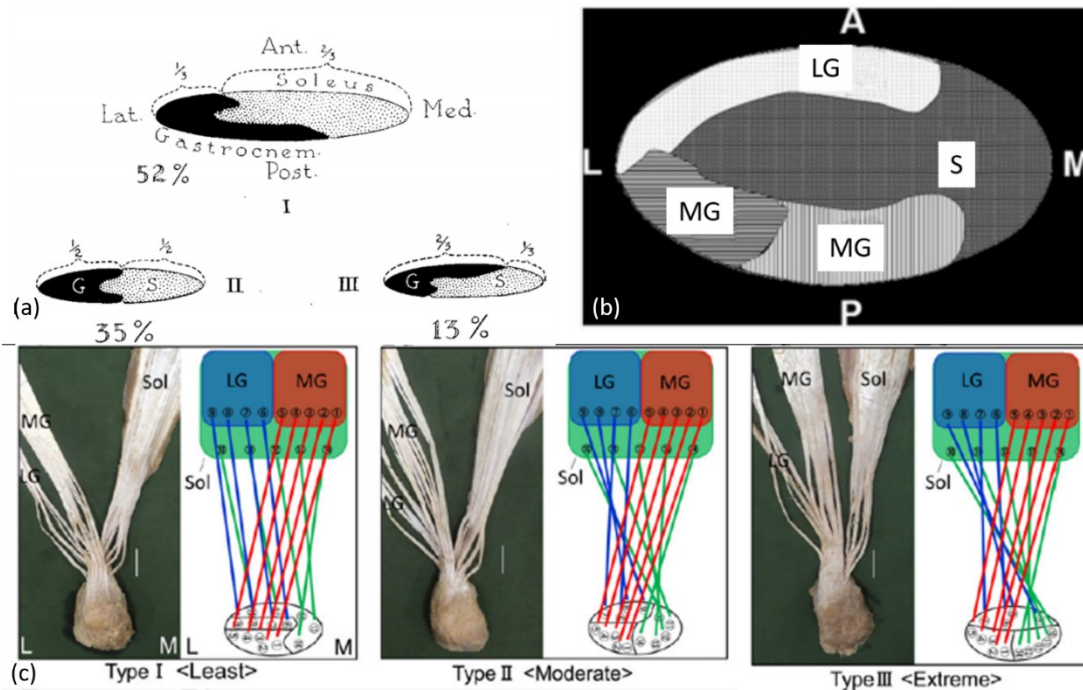


**Figure 2.9 – The rotational structure of the Achilles tendon presented in the literature.**

The Achilles insertion has been separated schematically into (a) gastrocnemius (G) and soleus (S), and (b) medial (MG), lateral gastrocnemius (LG), and soleus (S). (c) The tendon fibre pathways have been identified. Reproduced and modified with permission from (a) Cummins et al (1946), (b) Edama et al (2015) and (c) Szaro et al (2009).

The loading conditions and the rotational structure likely cause differential loading within the Achilles tendon. This theory is supported by the non-uniform displacement of the tendon fibres observed using B-mode ultrasound and ultrasound elastography. In B-mode ultrasound, the differential displacement has been identified from the aponeurosis of the medial gastrocnemius and soleus muscles (Bojsen-Moller et al., 2004; Maganaris et al., 2004). In ultrasound elastography, the superficial layer of the Achilles tendon has been shown to have smaller displacements than the deep layer of the tendon during walking and larger differential displacement was observed as walking

speed increased (Franz et al., 2015; Slane and Thelen, 2015). These observations suggested the existence of non-uniform stress within the tendon, which could cause friction and shear between fibrils and lead to microtrauma. Once the accumulation of microtrauma is such that the rate of repair will not be sufficient to overtake that of damage, degeneration of the Achilles tendon occurs (Kader et al., 2002).

This rotational structure of the Achilles tendon has been modelled with finite element analysis. The observed non-uniform displacement was reduced by 85% if the differential muscle force was eliminated, and reduced by 35% if the rotational structure was eliminated (Handsfield et al., 2017). This study from the literature only modelled one rotational variant (Figure 2.9b).

## **2.3 Rehabilitation of midportion Achilles tendinopathy**

Rehabilitation exercises are the first line treatment for chronic midportion Achilles tendinopathy. The protocol typically involves concentric and/or eccentric exercises. Concentric exercises involve shortening of muscles while resisting a load, while eccentric exercises lengthen muscles while resisting a load.

Two major protocols for midportion Achilles tendon rehabilitation are used clinically: eccentric loading training and heavy-slow resistance training. Alfredson et al. (1998) introduced the eccentric loading protocol. This protocol includes eccentric standing heel drop exercises with a knee flexed and a knee extended position. It has been widely adopted as the mainstream treatment for midportion Achilles tendinopathy over the past decade.

The heavy slow resistance training was developed for rehabilitation in patellar tendinopathy and was found to yield superior results over traditional eccentric loading regimens (Kongsgaard et al., 2009). The approach was then adjusted for midportion Achilles tendon rehabilitation. One randomised controlled trial compared the effects of traditional eccentric loading training and heavy slow resistance training and found no significant differences in improvement of symptoms at 52 weeks follow-up, but the overall training time for the heavy slow resistance group was only one third of that of the eccentric loading group (Beyer et al., 2015).

It is not fully understood which of the loading or the training frequency contributes more to the tendon repair. It is worth noting that not all Achilles tendinopathy patients are responsive to the protocol; one study reported that up to 45% of patients did not improve after 12 weeks of eccentric loading rehabilitation (Sayana and Maffulli, 2007).

There are a lot of question marks in the rehabilitation of midportion Achilles tendinopathy. Does the magnitude of load matter more than the frequency of training? If a patient does not improve, is it because of a failure of the regimen or a misdiagnosis of the patient? Or should we stratify patients and offer personalized protocols?

The following sections will introduce the tendon healing mechanism and provide the details of eccentric loading and heavy slow resistance rehabilitation.

### **2.3.1 Tendon healing mechanism and tendon adaptation**

The natural tendon healing process after injury includes three stages: inflammation, matrix production and remodelling (Sandrey, 2003; Sharma and Maffulli, 2005). The inflammation stage typically lasts for a week after injury. In this stage inflammatory cells, including neutrophils, monophils and macrophages, infiltrate into the local tissue and neovascularization is observed. In the next stage, fibroblasts are activated and start



to produce extracellular matrix proteins, such as collagen fibres. This process takes a further three weeks. During the final remodelling and maturation process, the synthesized fibrins are remodelled into an organized structure through a scar formation. The cell density and vascularity decrease as a tendon heals. The overall healing process can take from 6 to 12 months (Sandrey, 2003; Sharma and Maffulli, 2005).

There is still controversy regarding the existence of remodelling of the Achilles tendon. Thorpe et al. (2010) quantified the racemization of the aspartic acid between injury-prone tendons and rarely-injured tendons to estimate the half-life of the collagenous and non-collagenous components within the tendons. The injury-prone tendons showed a significantly higher half-life for collagen, a lower non-collagen half-life, and fewer collagen-degradation markers, than rarely-injured tendons. This suggested partially degraded proteins could accumulate in injury-prone tendons and could lead to decreased mechanical integrity (Thorpe et al., 2010). On the contrary, Heinemeier et al. (2013) quantified the  $^{14}\text{C}$  level within the Achilles tendon core and found the  $^{14}\text{C}$  level in the Achilles tendon was remained from decades before being sampled. This suggests that the Achilles tendon core tissue is formed by the age of 17 years and does not renew.

The mechanical environment will also affect the healing of a tendon (Galloway et al., 2013; Heinemeier and Kjaer, 2011; Kjaer, 2004; Lavagnino and Arnoczky, 2005; Wang, 2006). Changes in tendon material properties (Arampatzis et al., 2007b; Kongsgaard et al., 2007; Kubo et al., 2002; Reeves et al., 2003) and morphology, such as cross-sectional area (Arampatzis et al., 2010; Bohm et al., 2014; Seynnes et al., 2009), are seen because of increasing collagen synthesis following a period of enhanced mechanical loading. This adaptive process of a tendon in response to applied loading is termed tendon adaptation.

The aim of tendon rehabilitation is to initiate the correct tendon adaption process with controlled loading. Remodelling and re-maturing are involved in this process to re-align the pathological fibres, increase the stiffness, and reduce the thickness of the Achilles tendon (Arampatzis et al., 2007a; Arampatzis et al., 2010).

### **2.3.2 Rehabilitation protocol I: Eccentric loading training**

The rehabilitation protocol includes 3 sets of 15 repetitions of a heel-drop exercise on the edge of a stair with both a straight and flexed knee (Alfredson et al., 1998)(Figure 2.10). The exercise is performed twice a day, 7 days a week, for 12 consecutive weeks. The load can be gradually added using a backpack as the training proceeds. The patient should feel discomfort, but not disabling pain, during the training process. For each repetition, the eccentric loading phase should last three seconds. Between each set, there should be a two minute rest period.

The eccentric loading training is a high-frequency exercise. With the recommendations above, the training sessions come to 308 minutes every week. The benefits of this regimen are that no additional equipment is required, and the exercise can be done at home. Only a simple step and a backpack for extra loading are required.

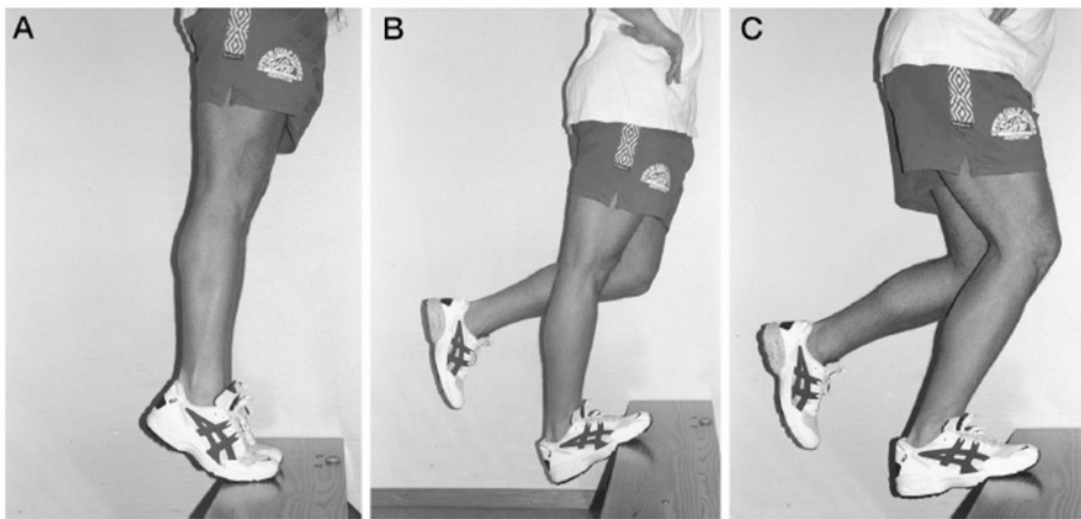


**Figure 2.10 – The eccentric loading training for midportion Achilles tendinopathy.**

Reproduced with permission from Alfredson et al. (1998).

---

### **2.3.3 Rehabilitation protocol II: Heavy slow resistance training**

The heavy slow resistance regimen was adapted from the training regimen for patella tendinopathy (Gaida and Cook, 2011; Kongsgaard et al., 2009; Kongsgaard et al., 2010). The training requires a rather high load and is only be feasible with gym equipment (Figure 2.11). The load required is 65-85% of the maximum weight that can be lifted once with good technique, also known as the repetition maximum (RM). It is worth noting that it is difficult to determine one RM, especially in patients. Therefore, the RM is usually estimated clinically, using the assumption that the load that can be lifted 8 times is equal to 80% of the RM (Brzycki, 1998). In this rehabilitation protocol, in the first week, the patients are instructed to perform 15RM gradually stepping up to 6RM, which correspond to 65% and 85% of the maximum weight they can carry, respectively.

In the clinical setting, the maximum weight each patient can perform will also be affected by the severity of the tendinopathy and the strength of the patient.

The regimen is performed three times per week with resistance equipment, including three exercises: heel rise and drop with a seated calf raise machine, heel rise and drop in a leg press machine, and heel rise and drop bearing a barbell on the shoulders. Patients were asked to perform three exercises with the loading shown in Table 2.1. A 2-minute rest between each set and a 5-minute rest between each exercise is recommended.



**Figure 2.11 – The heavy slow resistance training includes three exercises: seated calf-raise, ankle push in a leg press machine and standing heel rise bearing a barbell.**

Reproduced with permission from Beyer et al. (2015).

Week No.	Sets	Reps/Loads
Week1	3 sets	15 RM
Week 2 to 3	4 sets	12 RM
Week 4 to 5	4 sets	10 RM
Week 6 to 8	4 sets	8 RM
Week 9 to 12	4 sets	6 RM

**Table 2.1 – Heavy slow resistance protocol suggested by Beyer et al. (2015)**

Repetition maximum (RM) refers to the maximum loading that the patients can perform smoothly.

The heavy slow resistance training is more time efficient than eccentric loading, with only 107 minutes required per week, but the one-year outcome is not significantly different from that of the traditional eccentric loading regimen (Beyer et al., 2015). The heavy slow resistance regimen requires access to resistance equipment and instructions

from a physiotherapist, and therefore it is arguably more suitable for athletes than the general population.

## **2.4 Biomechanical methodologies for investigating Achilles tendon and midportion Achilles tendinopathy**

Although non-invasive *in vivo* measurement of muscle and tendon force is not feasible, the biomechanics of midportion Achilles tendinopathy can be investigated in different ways. This section will review the methodologies used in the literature to investigate midportion Achilles tendinopathy. As the tendon consistently experiences a cyclic force, the tendon mechanical properties such as stiffness, Young's modulus, and hysteresis can be measured using cadaveric specimens (Guney et al., 2015; Lintz et al., 2011; Wren et al., 2003; Wren et al., 2001). Mechanical loading rigs have also been designed and employed to simulate dynamic conditions (Stephen et al., 2018).

For *in vivo* evaluation, 'buckle' transducers have been used to measure the Achilles tendon force. Unsurprisingly, due to the invasiveness of the procedure, it is not a commonly employed approach. Non-invasive measures, such as dynamometers and force platforms, have been applied to measure the joint torque and external forces that enable a simple mechanical quantification of the tendon force. However, because of the agonist and antagonist muscle activity, the measured force and torque are the summation of the effects of all muscles crossing the joint.

Clinically available imaging modalities, such as ultrasound and MRI, have been used to assess tendon fibre displacement, tendon morphology, and pathological features.

Ultrasound allows dynamic testing *in vivo*, while MRI provides excellent static three-dimensional (3D) information.

Computer modelling techniques also play a role in estimating the forces of muscles and tendons. Finite element modelling can be used to simulate the tendon compression and shear force under different loading conditions and with different tendon morphology, while musculoskeletal modelling can quantify the muscle and tendon forces for different participants *in vivo*.

#### **2.4.1 Mechanical testing with cadaveric specimens**

The mechanical properties of tendons can be tested with a tensile test, where the tendons are stretched until they break and the force applied and the elongation history are recorded (Butler et al., 1978; Winter, 2009). A typical force-elongation curve for tendons includes 4 distinctive regions: i) Region I ('toe region'): the wavy collagen fibre within the tendon is straightened by the non-damaging loading, but not stretched. ii) Region II ('linear region'): the loading stretches the aligned fibres and the tendon fibre is not broken by the loading. iii) Region III ('plateau region'): the fibres started to break. The tendon still elongates, but the loading reaches a plateau. iv) Region IV: complete failure of the collagen fibres, the external loading drops (Winter, 2009). Mechanical properties such as stiffness, elastic modulus, stress at failure, and strain at failure can be calculated from the force-elongation curve. When a tendon is stretched, it does not behave purely elastically (Cohen et al., 1976; Hooley et al., 1980). The strain and stress seen by the tendon are also time-dependent. Such behaviour can be tested by applying a constant force on the tendon and measuring the strain over time (creep), maintaining constant elongation while measuring the change in force (stress-relaxation), and measuring stress and strain under cyclic loading and unloading (hysteresis).

The source of a tendon, preparation of the specimen, and the experimental protocol could largely affect the results of these tests. The preservation of the tendon could affect the properties of the tendons (Matthews and Ellis, 1968; Smith et al., 1996). To represent the tendon condition in vivo, fresh-frozen tendons are preferred over embalmed ones (Verstraete et al., 2015). In a tensile test, the specimens are trimmed into a dumbbell shape to ensure maximum stress occurs in the centre region. However, in tendons, such a process may damage the integrity of the collagen fibres and affect the results. The clamping of the specimen is may also damage the tendon fibres (Ker, 1992). Before testing, the tendon should be ‘conditioned’ by several stretch-recoil cycles to obtain stable measurement. This is due to the physical properties of the tendon that are associated with creep behaviour (Maganaris et al., 2008).

Besides mechanical properties, the Achilles and plantaris tendons have also been tested with mechanical loading rigs to simulate ankle motion (Stephen et al., 2018). In the study by Stephen et al. (2018), the Achilles and plantaris tendons were loaded with a fixed force. A differential motion of the tendons was identified when the plantaris tendon had a separate insertion anterior to the Achilles tendon, but not when the tendon inserted medially to the Achilles tendon. The compression between the tendons was the largest when the ankle was in maximum plantarflexion.

The Achilles and plantaris tendons have also been tested with mechanical loading rigs to simulate ankle motion (Stephen et al., 2018). In the study by Stephen et al. (2018), the Achilles and plantaris tendons were loaded with a fixed force. A differential motion of the tendons was identified when the plantaris tendon had a separate insertion anterior to the Achilles tendon, but not when the tendon inserted medially to the Achilles tendon. The compression between the tendons was the largest when the ankle was in maximum plantarflexion.



## 2.4.2 Mechanical testing *in vivo*

Force sensing platforms and dynamometers can be used to measure the torque and force exerted during activities *in vivo*. These have often been used in combination with optical motion capture systems, which provide real-time 3D coordinates representing the kinematics of body segments. Such combinations can reliably calculate the joint torque *in vivo*. Medical imaging techniques, such as ultrasound, are incorporated to obtain the displacement of the muscle-tendon junction (Bohm et al., 2014; Lichtwark and Wilson, 2005; Rees et al., 2008).

Measurement *in vivo* has the advantage of testing in a physiological environment, but there are still some problems. Tendons derived from more than one muscle are likely to have non-homogenous stress across the tendon and intra-tendon shearing could exist (Bojsen-Moller et al., 2004; Maganaris et al., 2006). In addition, friction and heat loss between surfaces will be included in hysteresis. Finally, the force exerted *in vivo* may not exceed the toe region of the tendon. Therefore, care must be taken when comparing the values from *in vitro* and *in vivo* measurements (Maganaris et al., 2008).

## 2.4.3 Medical imaging

MRI and ultrasound have been standard clinical evaluation tools for midportion Achilles tendon injury. MRI provides excellent static 3D information for evaluating tendon cross-sectional area, morphology, tendon volume, and pathological features (Bohm et al., 2014; Gardin et al., 2006; Iwanuma et al., 2011; Khan et al., 2003; Syha et al., 2015). The MRI sequence will affect the resonance intensity obtained. Fundamentally, the T1-weighted sequence is widely used to study anatomical structure, while T2-weighted image sequence has been used to highlight the water content of

tissue that gives information on inflammation. Proton-density image sequence has been used to evaluation joint geometry. Therefore, selecting an appropriate sequence is key to successful MRI studies.

Ultrasound is also regarded as a primary imaging modality for diagnosing Achilles tendon injury (Kader et al., 2002). Besides the plain B-mode ultrasound, colour Doppler ultrasound can be used to evaluate the vascularity of the tendon, which provides important information about the tendon injury. For biomechanical research, ultrasound allows dynamic testing and can be combined with advanced ultrasound techniques such as ultrasound elastography. As mentioned in Section 2.2.2, plain B-mode ultrasound has been used evaluate tendon displacement and moment arm (Arampatzis et al., 2007a; Arampatzis et al., 2007b; Arampatzis et al., 2008; Arampatzis et al., 2010; Bohm et al., 2014). More recently, ultrasound elastography has been developed to measure the intra-tendinous fibre non-uniform displacement during walking (Chernak and Thelen, 2012; Chernak Slane and Thelen, 2014; Slane and Thelen, 2014, 2015). Ultrasound shearwave elastography enables the estimation of tissue stiffness and has been used to measure the stiffness of healthy and pathological Achilles tendons. Pathological tendons could be more compliant than healthy tendons (Arda et al., 2011; Chen et al., 2013). However, due to the high stiffness and anisotropy of tendon tissue, the measurement of Young's modulus for Achilles tendon using shear wave elastography may be inaccurate (DeWall et al., 2014).

#### **2.4.4 Electromyography**

Electromyography (EMG) is a technique to record the collective myoelectric activity of muscle fibre membranes, which can be measured by attaching electrodes to the skin's surface (also termed 'surface EMG') or by inserting needle electrodes into the muscles

(also termed ‘fine-wire EMG’). Surface EMG can only be used for muscles lying directly under the skin’s surface, while the activity of deep muscles can only be measured by fine-wire EMG.

EMG does not directly quantify the Achilles tendon force, but it reveals the activation level of muscles. In musculoskeletal modelling (described in Chapter 2.4.5), EMG has been widely used to validate muscle activation levels predicted by models.

One of the major disadvantages of EMG is inter-subject comparison. As an electrode is only able to sense the activity of a small portion of the muscle fibres, the comparison of raw EMG signals between muscles is inappropriate. One feasible way to compare EMG data across muscles and subjects is normalizing the raw signal to a reference value, which is typically obtained from a motion that fully activates the target muscle (Burden, 2010; Mathiassen et al., 1995). A common consensus for the normalization is that the activity should be repeatable, can be performed manually, and can produce a maximum activation of the muscle of interest.

It is generally accepted that surface EMG signals have some correlation to the muscle force; however, it is not clear whether the relationship is linear, curvilinear, or non-linear (Bilodeau et al., 2003; Gregor et al., 2002; Herzog et al., 1998; Karlsson and Gerdle, 2001; Lawrence and De Luca, 1983; Madeleine et al., 2001; Moritani and Muro, 1987; Onishi et al., 2000). The correlation may be affected by the processing technique, examined muscle, and the performed exercise.

## **2.4.5 Computational modelling**

There are two major modelling methods for studying midportion Achilles tendinopathy: finite element modelling and musculoskeletal modelling. Finite element models have been based upon 3D models segmented from MRI (Handsfield et al., 2017)

and have been used to estimate displacement, stresses, and strains within the tendon. Finite element models provide an understanding of how the load is transmitted within the geometry of the structure, resulting in stresses and strains. The results are highly dependent on the boundary conditions (constraints and loads) as well as the material models used within the analysis.

Musculoskeletal modelling has also been used to study the Achilles tendon and midportion Achilles tendinopathy. Musculoskeletal modelling can be divided into two categories: forward dynamic models and inverse dynamic models. Forward dynamic models require prior knowledge of the muscle excitation (could be obtained from EMG) or joint torques to calculate a motion pattern. This could be useful for surgical planning and outcome prediction. However, an accurate measurement of muscle excitation and torque can be challenging, thus limiting the clinical use of forward dynamic models (Erdemir et al., 2007). On the other hand, inverse dynamics models have been frequently used for muscle force estimation. With kinematic marker data collected by an optical motion capture system, joint kinetic data can be calculated under the assumption of modelling the human as a chain of rigid body segments. The muscle forces are then decided using an optimization process. Inverse dynamic models provide a descriptive, rather than predictive, understanding of muscle forces (Erdemir et al., 2007).

There are many software packages available for musculoskeletal modelling. Three software packages are introduced here: AnyBody, OpenSim, and FreeBody. They can all perform biomechanical analysis using motion capture data with a predefined anatomical model or a custom-made model. Each software package contains predefined models. These software packages have similar workflows but different predefined anatomical model settings. In general, the model is scaled to the observed kinematic

data, and then the joint torque is calculated from inverse dynamic analysis; finally, a static optimization is used to calculate the muscle and joint reaction forces.

AnyBody is the most sophisticated commercial software package on the market. The AnyBody model contains models of different anatomical regions, such as the lower limb, shoulder, arm, lumbar spine, and a full body model. It analyses the human body as a series of rigid bodies and allows multibody analysis. The lower limb model contains 169 muscles and has 6 degrees of freedom (Carbone et al., 2015; De Pieri et al., 2018). The Anybody model uses inverse dynamics and an optimization method to solve muscle redundancy. AnyBody offers nine scaling methods (Benoit et al., 2015); the most advanced one takes into account the participant's fat percentage. The AnyBody also supports the input of STL files. With this feature, the environment can be simulated as well.

OpenSim is a freely available software package with a large associated community. Inverse and forward dynamics can be implemented in OpenSim. It also provides built-in algorithms (Residual Reduction Analysis) (Anderson et al., 2006) to minimize the kinematic errors and Computed Muscle Control (Thelen and Anderson, 2006) to drive the model to track the desired kinematics. OpenSim also includes the muscle dynamics, taking into consideration the force-velocity and force-length relationships between the muscle and the tendon, which is modelled as a spring (Millard et al., 2013). The most recently used model includes 80 muscles and 20 degrees of freedom for the lower body. The muscle force prediction was also achieved by inverse dynamics and static optimization.

The FreeBody model is a freely available software package developed by a research group at Imperial College (Cleather and Bull, 2015). It is a lower limb model containing a single right leg with 163 muscle elements 22 degrees of freedom. FreeBody has

several associated anatomical datasets that are accompanied by MRI images of the participant. This allows the visualization and manipulation of the anatomical model (Ding et al., 2016).

Previous musculoskeletal models of the Achilles tendon based on inverse dynamics have investigated Achilles tendon loading during eccentric exercise. The peak plantarflexion moment was reduced when the exercise was performed with the knee flexed compared with knee extended, and this reduced moment resulted in reduced Achilles tendon loading during knee-flexed eccentric exercise (Weinert-Aplin, 2014). Besides rehabilitation, the effect of intra-tendinous strain was also simulated with musculoskeletal modelling. The introduction of a coupled insertion site for gastrocnemius and soleus will result in decreased peak muscle forces (Franz and Thelen, 2016). The outputs of musculoskeletal modelling are frequently used as boundary conditions for finite element modelling. Using finite element analysis, it was found that the von Mises stress is the largest at the midportion (4.6-7.9 cm) and insertion site of the Achilles tendon. This stress was sensitive to tendon geometry (Hansen et al., 2017; Toumi et al., 2016). This modelling result also strengthens the mechanical hypothesis for midportion Achilles tendinopathy.

## **2.5 Mechanical properties of the Achilles tendon *in vitro* and *in vivo***

### **2.5.1 In vitro measurement of mechanical properties of the Achilles tendon and plantaris tendon**

Large variation is seen in the mechanical properties of the Achilles tendon. In tensile tests, the Achilles tendon has been shown to have a Young's modulus of  $819 \pm 208$  MPa, with an ultimate strength of  $79 \pm 22$  MPa (Wren et al., 2003; Wren et al., 2001). The Achilles tendon exhibits significant viscoelastic properties, meaning that the loading history will affect the strain response of the tendon. When tested using the same loading protocol, the plantaris tendon demonstrates three times higher stiffness (5.7 vs. 1.7 N/mm) and seven times higher stress at failure (1.4 vs. 0.2 N/mm<sup>2</sup>) (Lintz et al., 2011).

The value of stress at failure for Achilles tendon is much lower than the value reported by Wren et al. (2003) due to the specimen preparation, whereas the tendons from Lintz et al. were trimmed to standardized size. Such preparation is likely to destroy the integrity of the tendon fibre and result in lower stress at failure.

### **2.5.2 In vivo measurement of mechanical properties of the Achilles tendon**

The result of the *in vivo* measurement also varied. The elastic modulus was measured between 300 and 1400 MPa. The Achilles tendon was reported to experience stress and strain of 20-42 MPa and 5-8% (Arampatzis et al., 2005; Hansen et al., 2003; Kubo et al., 2000; Maganaris and Paul, 2002; Magnusson et al., 2001; Muramatsu et

al., 2001). Besides the variations in mechanical property in each individual Achilles tendon, the difference in each protocol and activities performed is also likely to affect the value reported. (Maganaris et al., 2008).

Any pathology of the tendon is likely to affect the mechanical properties. The Achilles tendon patients showed larger strains compared to the healthy controls (Child et al., 2010). To quantify the effect of rehabilitation on the tendon, Bohm et al. (2014) used a dynamometer and optical motion capture system in combination to quantify the torque about the ankle. This was then used in combination with the moment arm with respect to the ankle centre of rotation, measured with ultrasound, to calculate the force of the Achilles tendon. With the tendon cross-sectional area measured in MRI and the antagonistic muscle force estimated using normalized electromyography, the Achilles tendon Young's modulus in vivo was  $870 \pm 200$  MPa. Furthermore, a significant increase in tendon stiffness and Young's modulus was found after rehabilitation. Long strain duration training was more effective in increasing tendon stiffness than high strain rate training (Bohm et al., 2014).

## 2.6 Summary

Midportion Achilles tendinopathy is a painful condition and rehabilitation exercises can sometimes prove ineffective. One possible reason is that the exact aetiology of the condition is not fully understood. It is also possible that the cause is multi-factorial or the categorisation of 'midportion Achilles tendinopathy' should be further divided.

There are two major hypotheses regarding the aetiology of midportion Achilles tendinopathy: (i) intra-tendon differential loading and (ii) plantaris involvement. The



differential loading may result from uneven pulling from the triceps surae. However, it is not understood how the rotational fibre structure potentially affects the loading within the tendon.

The second hypothesis suggests that the plantaris tendon could be involved. It is proposed that because some types of plantaris tendon are tethered to the Achilles tendon, the anatomical adjacency and possible compression and friction between the two tendons may cause pathology. MRI and ultrasound of the plantaris and Achilles tendons may further elucidate the relationship between the two.

From the observation of injury prevalence and patient groups, it is likely that midportion Achilles tendinopathy has a biomechanical basis. However, it is difficult to investigate the mechanical effect *in vivo*. Musculoskeletal modelling provides an alternative approach to investigate the biomechanics of midportion Achilles tendinopathy by estimating the muscle forces during activity. The predicted values can then be correlated with EMG recorded during the same activity.

This chapter reviewed the fundamental aspects of midportion Achilles tendinopathy, from the biomechanics of normal anatomy to pathology and rehabilitation. As a first step, the anatomical variation of the plantaris tendon could be a starting point to understand the normal anatomical variation and it is also related to the mechanism of the tendon injury. Therefore, the following chapter will analyse the plantaris tendon geometry in healthy people.

## Chapter 3

### Plantaris tendon geometry *in vivo*

Chapter 2 showed the potential role of the plantaris tendon in developing midportion Achilles tendinopathy, therefore, in this chapter, the plantaris tendon geometry is investigated. Plantaris is a small muscle with high anatomical variation. Clinically, plantaris tendon involvement has been observed in patients with midportion Achilles tendinopathy. However, it is not fully understood how the risk of developing this pathology could be related to the different anatomical variants. In addition, due to the small size of the plantaris tendon, most plantaris tendon variations categorised in the literature are based on cadaveric dissection, restricting translation to a clinical setting. The aim of this study was to provide a clinical categorization and visualization of the plantaris tendon variation *in vivo* that could then be used for evaluating the potential risk of plantaris tendon involvement.

### 3.1 Introduction

Midportion Achilles tendinopathy is one of the most common foot and ankle sports injuries. Observational studies indicate that athletes involved in mid- to long-distance running or jumping have a high risk of Achilles tendinopathy (Pollock et al., 2016). Although the precise mechanism of midportion Achilles tendinopathy development is still elusive, the plantaris tendon has been suggested to be an important contributing factor (Alfredson, 2011, 2017; Bedi et al., 2016; Calder et al., 2015; Calder et al., 2016; Cook and Purdam, 2012; Cook and Purdam, 2014; Masci et al., 2015, 2016; Olewnik et al., 2017; Smith et al., 2017; Spang et al., 2016; van Sterkenburg et al., 2011a; van Sterkenburg et al., 2011b; van Sterkenburg and van Dijk, 2011).

As reviewed in Chapter 2, several biomechanical observations support the hypothesis of plantaris tendon involvement in the development of midportion Achilles tendinopathy. In mechanical testing of plantaris and Achilles tendons from fresh frozen cadaveric specimens, the plantaris tendon was found to have a higher stiffness than the Achilles tendon (Lintz et al., 2011). Furthermore, there is evidence of differential movement and compression between the plantaris and Achilles tendon during ankle motion (Smith et al., 2017; Stephen et al., 2018). Also, a local retinaculum-like structure has been reported following an anatomical dissection of plantaris tendon. This structure restricts the free gliding between the plantaris and Achilles tendons, which could lead to higher friction between them (van Sterkenburg et al., 2011a).

Clinical studies have also provided some evidence about plantaris involvement in Achilles tendinopathy. In 80% of surgery for Achilles tendinopathy, the plantaris tendon was found to be invaginated in the Achilles tendon (Alfredson, 2011). In patients

that are recalcitrant to conservative treatment, removal of the plantaris tendon resulted in good reduction in symptoms and high rates of return to play (Calder et al., 2015; Calder et al., 2016; Masci et al., 2015; Pearce et al., 2012; van Sterkenburg et al., 2011b).

As discussed in Chapter 2, the anatomical position of the plantaris tendon insertion has significant variation and has been categorized by dissection into up to 9 distinct types (Daseler and Anson, 1943; Joshi et al., 2014; van Sterkenburg et al., 2011a). Such a complex classification may not be clinically applicable, because imaging cannot distinguish different tissue to this extent. As dissection often affects local tissue integrity, the dynamics between the plantaris and Achilles tendons cannot be fully reconstructed. In addition, the pathophysiological role of each individual type has not been elucidated.

The morphology of the plantaris tendon and its relationship to the Achilles tendon may be clinically important, as it may stratify patient treatment (Alfredson, 2017). Although several studies have reported a thickened plantaris tendon before or during surgery for midportion Achilles tendinopathy, clinical evaluation is still very challenging, as there is still no consensus as to whether MRI or ultrasound is more sensitive in identifying the plantaris tendon and its anatomical relationship to the Achilles tendon.

The aim of this study was to investigate plantaris tendon geometry *in vivo* using two routine imaging examination modalities: MRI and ultrasound. To understand the change of distance between different types of plantaris tendon and Achilles tendon during activity, the complete range of ankle motion was examined. The hypothesis was that the changing pattern of the distances differs with different types of plantaris tendon.

Clarifying this relationship could facilitate the understanding the plantaris motion and its potential role in midportion Achilles tendinopathy.

## **3.2 Method**

### **3.2.1 Participants**

Thirty-four healthy participants (19 male, 15 female) were included in this study (Table 3.1). The exclusion criteria included previous lower limb surgery, recent lower limb injury, a history of Achilles tendinopathy and any medical history that would preclude MRI examination. These participants were recruited from a university population under the ethical approved of the local research ethics committee (Imperial Research Ethics Committee reference: 16IC3385, Appendix B). All participants gave written informed consent.

No.	Gender	Age (years)	Weight (kg)	Height (m)
S01	male	25	96	1.88
S02	female	36	73	1.60
S03	female	27	55	1.65
S04	male	28	73	1.78
S05	male	27	65	1.78
S06	male	26	96	1.85
S07	male	29	80	1.78
S08	male	36	80	1.90
S09	female	30	50	1.64
S10	male	26	67	1.80
S11	male	28	75	1.76
S12	male	31	61	1.62
S13	male	26	75	1.70
S14	female	32	53	1.60
S15	female	32	86	1.77
S16	male	28	63	1.73
S17	female	29	58	1.67
S18	male	33	72	1.70
S19	female	27	63	1.67
S20	male	32	95	1.92
S21	female	28	45	1.60
S22	male	30	85	1.75
S23	male	31	62	1.73
S24	female	28	51	1.53
S25	female	25	63	1.73
S26	female	25	65	1.69
S27	female	25	75	1.75
S28	female	22	65	1.63
S29	male	27	58	1.78
S30	male	32	82	1.70
S31	female	38	53	1.65
S32	male	24	65	1.67
S33	female	27	53	1.60
S34	male	28	63	1.70
Mean ± Std.		28.8 ± 3.7	68.4 ± 13.7	1.72 ± 0.09

**Table 3.1 – Participants’ anthropometric data**

### 3.2.2 MRI protocol

The MRI examination was performed with a 3T MAGNETOM Spectra (Siemens, Munich, Germany). To acquire fine resolution and contrast between the plantaris tendon and surrounding soft tissues, many protocols were tried during pilot testing. A T1-weighted protocol with isometric voxels ( $0.61 \times 0.61 \times 0.61$ mm) was initially tested in the pilot study. Isometric voxels are usually preferred if segmentation of the MRI will be performed. Unfortunately, this would have made the scanning protocol too long for each participant.

Instead, a proton density sequence with a voxel size of  $0.44 \times 0.44 \times 1$  mm was chosen to balance the scanning time and identification of the plantaris tendon. The protocol was chosen after discussing with a medical physicist and performing a series experimental scanning to ensure the quality of the image and shorten the scanning time. Although T1 has been the standard sequence for anatomy, it took more than 7 minutes to perform each scan in our pilot testing, whereas the sequence chosen for this study only took about 4 minutes. We had a restricted timeframe that was available to image the joint in different angles, both due to the ability of the participants to remain still, and availability of the equipment. The 1mm slice thickness is one-third of the thickness acquired using standard clinical protocols. The scanning sequence was characterized by a TR of 4220 ms, a TE of 23 ms, flip angle of  $150^\circ$ , matrix size of  $320 \times 260$ , a field of view of  $140 \times 140$  mm, and a 30% distance factor.

The participants were scanned in the supine position. The right ankle was scanned with axial slices at six fixed angles across the full range of motion to obtain the geometry of the tendons (Figure 3.1). Six fixed-angled wedges were used to hold the ankle at  $45^\circ$ ,  $30^\circ$  and  $15^\circ$  of plantarflexion, neutral and  $10^\circ$  and  $20^\circ$  of dorsiflexion. Commercially available foot insole orthotics (Express Orthotics, Foot Science

International, Christchurch, New Zealand) were attached to the wedge surface as the interface between the foot and wedge to ensure straight alignment. A hook and loop fastener was used to strap the forefoot to the wedge.

---

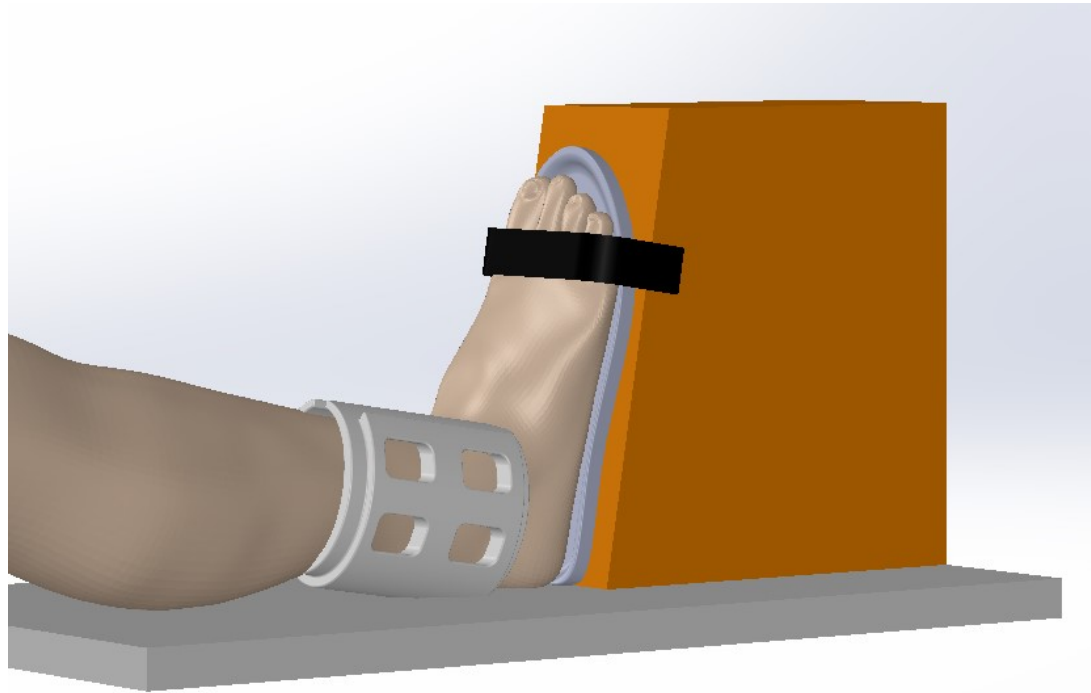


**Figure 3.1 – The wedge and coil setting for MRI scanning.**

---

The movement requirement meant that the regular ankle coil could not be used. Therefore, a four-channel small-sized flex coil (4-channel Flex Coil, Siemens, Munich, Germany) was wrapped around the Achilles tendon from the posterior side. The selection of the coil was based on the number of channels and the area of the coil. There are six-channel commercial coils available, but they are larger in size. This would have resulted in a larger area of coverage but a smaller magnetic field intensity within the covered space. Therefore, it was decided to reduce the coverage space but increase the magnetic field intensity on the hindfoot, where midportion Achilles tendinopathy occurs. Hence, the four-channel flex coil was chosen.



### **3.2.3 Ultrasonography protocol**

To confirm the plantaris tendon geometry, B-mode ultrasound (EPIQ 5G, Philips, Eindhoven, The Netherlands) was performed on a subset of 20 participants (3 participants from Type 1 and all the subject from the other Types), which included those for whom the plantaris tendon could not be identified on the MRI scan or those with atypical geometry, defined as the geometry other than medial insertion. The insertion pattern will be discussed in detail in Chapter 3.2.5.

The participants were scanned in a prone position. Only the right plantaris tendon geometry was examined. The ultrasound was performed by a single sports medicine consultant, who was trained in musculoskeletal ultrasound and regularly runs a musculoskeletal ultrasound clinic. The examiner was blind to the MRI results and the participants were allocated in random order to the examination session.

Plantaris tendon existence and geometry were confirmed by tracing the plantaris tendon alongside the medial aspect of the gastrocnemius aponeurosis and Achilles tendon down to the insertion.

### **3.2.4 Image segmentation protocol**

Manual MRI segmentation of the Achilles tendon, plantaris tendon, calcaneus and distal tibia and fibula were performed for each participant, at each joint angle and then reconstructed to form 3D models using the Mimics Innovation software package (v.19, Materialise, Belgium). To compare the Achilles tendon and plantaris tendon geometries across the range of motion, the 3D models constructed at different ankle joint angles were registered to the tibia and calcaneus, respectively, using the 3-Matic Research software package (v.12, Materialise, Belgium) and MATLAB (2017a, MathWorks, Massachusetts, USA).

The Achilles tendon was segmented along with the gastrocnemius aponeurosis, which can be identified as a hypo-resonant crescent-shaped area posterior to the gastrocnemius. The plantaris tendon was traced from the medial side of the gastrocnemius aponeurosis to the insertion. For some plantaris tendon geometries, the tendon formed a separated hypo-resonant area, apart from the gastrocnemius aponeurosis, and could be distinguished from the Achilles tendon. The segmentation of bone in MRI included the hypo-resonant cortex and the hyper-resonant marrow.

### **3.2.5 Plantaris tendon categorization**

The plantaris tendon geometries were categorized into five groups (Types 1 to 5). This classification was modified from the groups proposed by Daseler and Anson (Daseler and Anson, 1943). In this study, we aimed to distinguish the tendon geometry using both MRI and ultrasound, which could be less sensitive. The categorization from Daseler and Anson classifies the tendon based on the insertion site of the plantaris, which could be objectively seen in the MRI.

Type 1 plantaris tendons inserted onto the calcaneus medial to the Achilles tendon. Type 2 included tendons inserting 0.5-2.5 cm anterior to the Achilles tendon on the calcaneus and other tendons fanning into a thin structure or discontinuing. Type 3 tendons travelled from the medial to the dorsal aspect of the Achilles tendon. Type 4 tendons directly inserted into the medial border of the Achilles tendon at 1-16 cm above the calcaneus. Type 5 represented tendons that were not identifiable using either MRI or ultrasound.

To compare the prevalence of plantaris tendon types with those defined in the literature, the nine categorizations reported by van Sterkenburg et al. (2011) were down-categorized to five types: 'medial onto calcaneus', 'medial, fan-shaped onto

calcaneus', and 'medial with thin slips onto calcaneus' were categorized as Type 1; thus Type 1 tendons were present in 48.7% of their observed population. 'Anteromedial onto calcaneus', 'anteromedial, fan-shaped onto calcaneus', and 'anterior onto calcaneus' were categorized as Type 2 and accounted for 34.7% of their observed population. 'Posteromedial, fan-shaped onto calcaneus' was categorized as Type 3 and accounted for 15%. 'Medial onto the Achilles tendon' was categorized as Type 4 and accounted for 2.8%. The identification of plantaris tendon by van Sterkenburg et al. (2011) was 100%; therefore, the prevalence for Type 5 tendon was 0% (Figure 3.2).

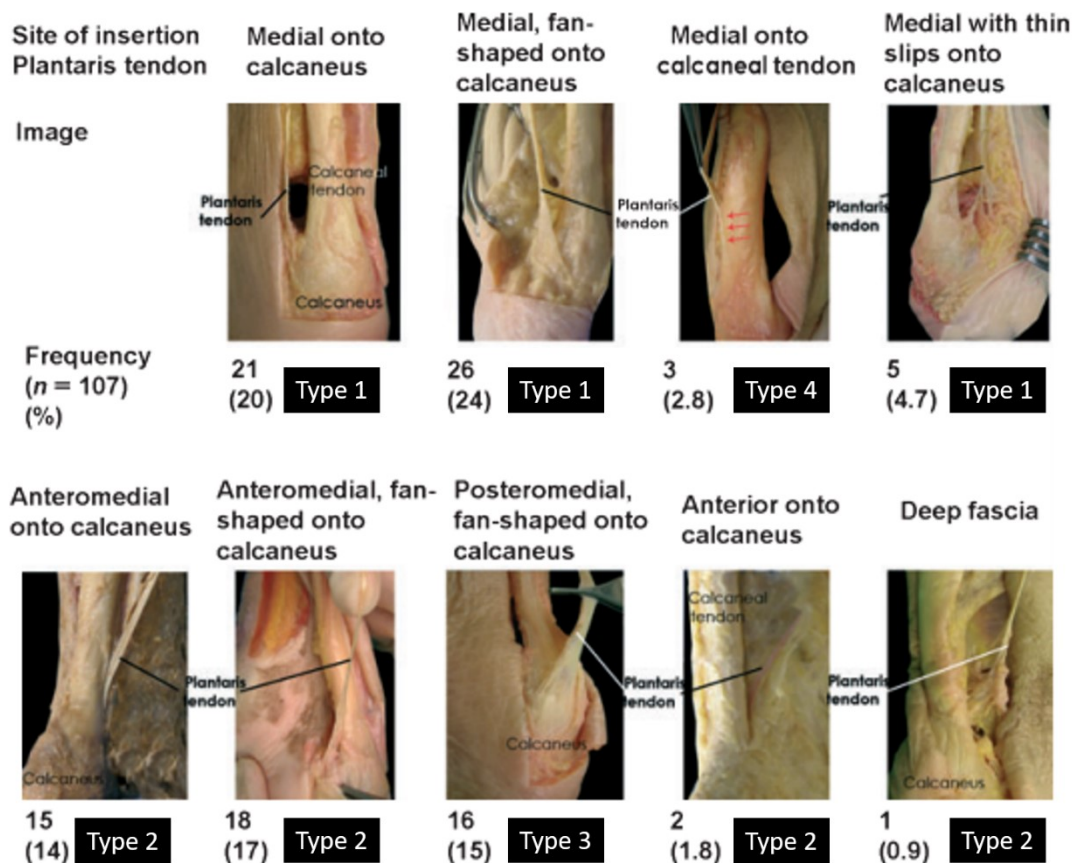


**Figure 3.2 – Down-categorization of the classification system proposed by van Sterkenberg et al. (2011).**

Reproduced and modified with permission from van Sterkenberg et al. (2011).

The gap size between the Achilles tendon and Type 1 plantaris tendon is quantified by summing up the minimal distance between the Achilles and plantaris tendons in each slice, multiplied by slice thickness. As the gap size is different in each individual, to compare the gap size change across people, the gap size at maximum dorsiflexion was set as reference point and the change in gap size with respect to maximum dorsiflexion was reported. The calculation of minimal distance in each slice was calculated in Matlab (2017a, MathWorks, Massachusetts, USA). Such a gap size analysis is not applicable to Types 2, 3, 4, 5. In Type 2 tendons, some tendon fanned into thin slices or inserted into local tissues. Types 3, 4, and 5 were either in close contact with the Achilles tendon or were non-identifiable.

### **3.2.6 Statistical analysis**

Descriptive measures were used to describe the proportion of different types of plantaris tendon. A post hoc power analysis based on a chi-square test was performed to confirm statistical power. A chi-square test was used to differentiate the distribution between the percentages of different categories. The statistical analysis was performed in SPSS (v.25, SPSS Inc., Chicago, IL).

## **3.3 Results**

The prevalence rates of the population in this study in comparison with those from the literature are summarized in Table 3.2. The geometries are illustrated in Figure 3.3. The percentage of each category in this study is not statistically different (Chi-square test, likelihood ratio: 0.11) with the percentages reported in the literature. A post-hoc power analysis revealed that on the basis of group proportion, this study had statistical power of 0.8 to identify an effect size of middle to large distance between the group ( $d=0.47$ ) (Cohen, 1992).

	This study Percentage [95% confidence interval]  (34 people)	Daseler and Anson (Daseler and Anson, 1943)  (161 specimens)	Joshi et al. (Joshi et al., 2014)  (84 specimens)	van Sterkenburg et al. (van Sterkenburg et al., 2011a)  (107 specimens)
Type 1	50.0% [33.2- 66.8%] (17/34)	45.6%	40.5%	48.7%
Type 2	23.5% [9.2-37.8%] (8/34)	29.8%	40.5%	34.7%
Type 3	5.9% [0-13.8%] (2/34)	14.2%	0%*	15%
Type 4	2.9% [0- 8%](1/34)	4.3%	9.5%	2.8%
Type 5	17.6% [4.8-30.4%] (6/34)	6.67%	9.5%	0%

**Table 3.2 – The plantaris tendon incidence of each type, compared with those from the literature.**

\*: Plantaris tendon with posterior insertion was not reported in this study.

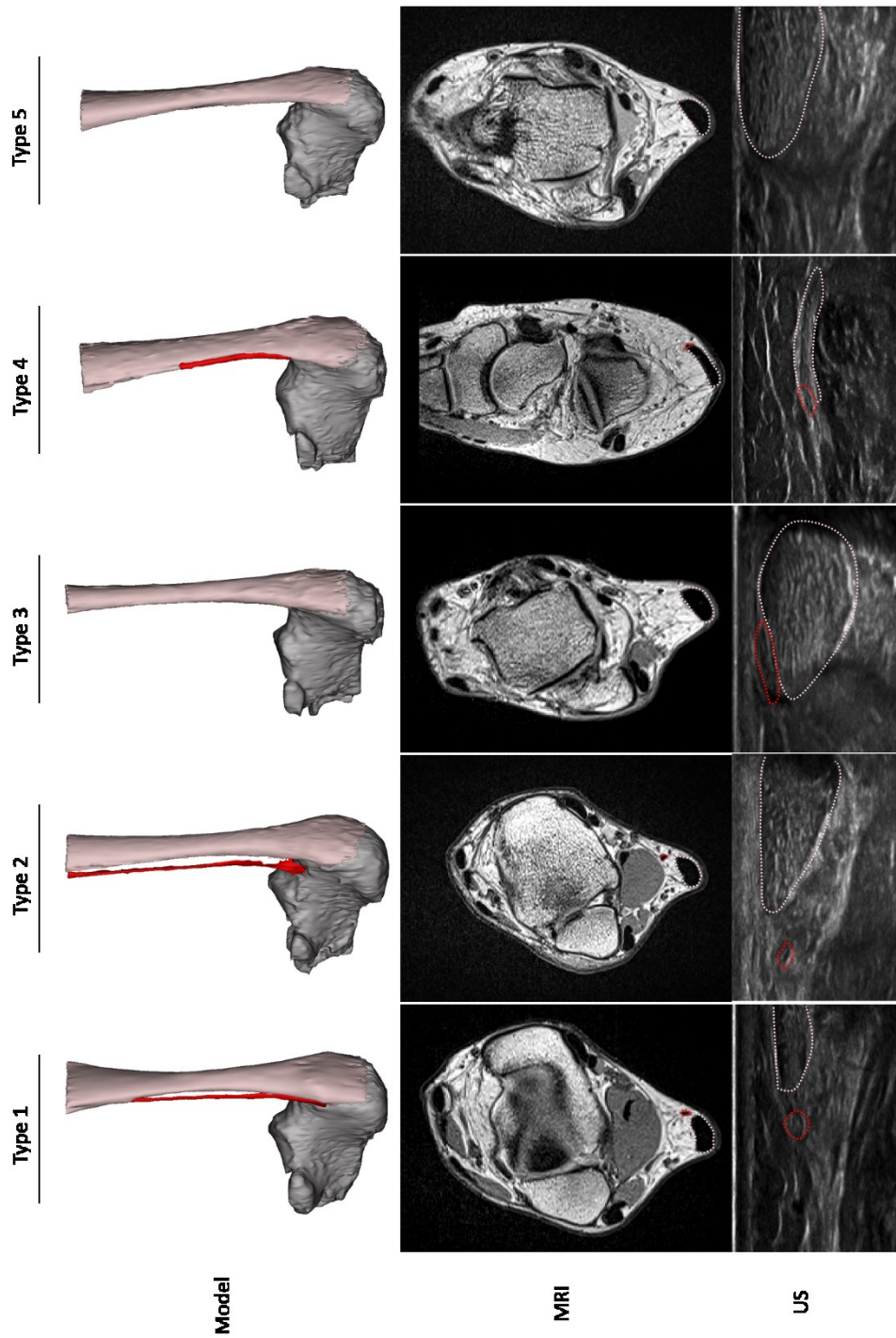


**Figure 3.3 – The types of plantaris tendon geometry and their presentation in MRI and ultrasound (US).**

The Achilles tendon (pink) and plantaris tendon were segmented from MRI. The contours of the Achilles (pink dotted line) and plantaris (red dotted line) were marked on the MRI and US.

The Type 1 plantaris tendon, travelling medially to the Achilles tendon, was the most common geometry. Twelve out of seventeen Type 1 tendons were separated from the Achilles tendon with a gap up to 2 mm wide. The location of this gap was between  $6.5 \pm 9.9$  mm and  $89.3 \pm 15.2$  mm (mean  $\pm$  standard deviation) measured from the Achilles tendon insertion. However, the other five had a plantaris tendon that travelled close to the Achilles tendon (Figure 3.4).



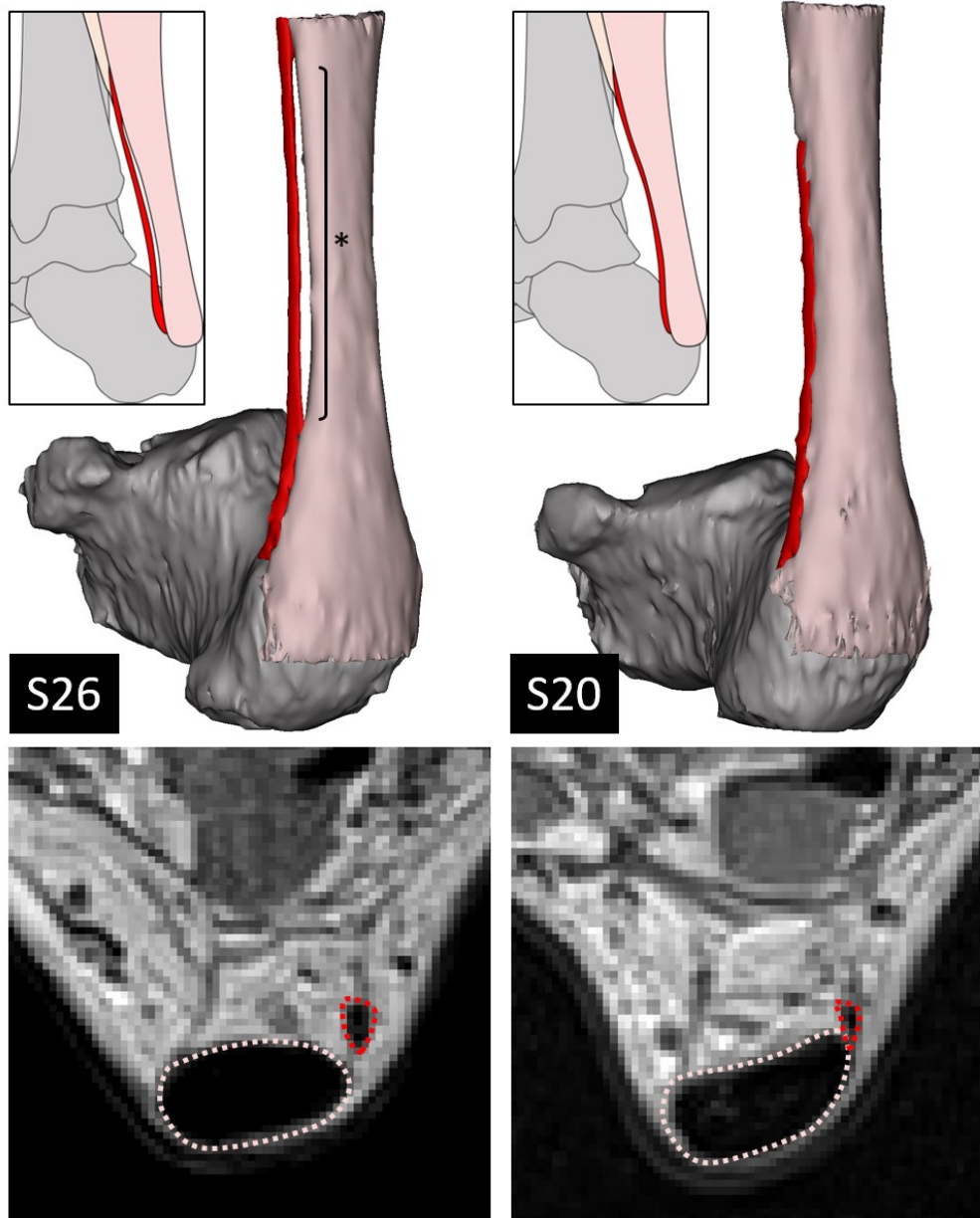


**Figure 3.4 – The variation within Type 1 plantaris tendons, illustrated by images of participants S26 and S20. Some Type 1 geometries have a gap (\*) between the Achilles and Plantaris tendons.**

Different interactions between the Achilles tendon and the plantaris tendon were noticed in Type 1 tendons. From dorsiflexion to plantarflexion, the gap between the Achilles and plantaris tendons increased for some participants while it decreased for others. The gap was filled by the Kager's fat pad (Figure 3.5). Although the compression force could not be measured using imaging, such changes in gap size indicate the

compression during plantarflexion and dorsiflexion. The change in gap size from dorsiflexion to plantarflexion of all 17 Type 1 tendons is shown. Three tendons have increased gap size, nine are fluctuating around the reference line (20°), and five have decreased gap size.

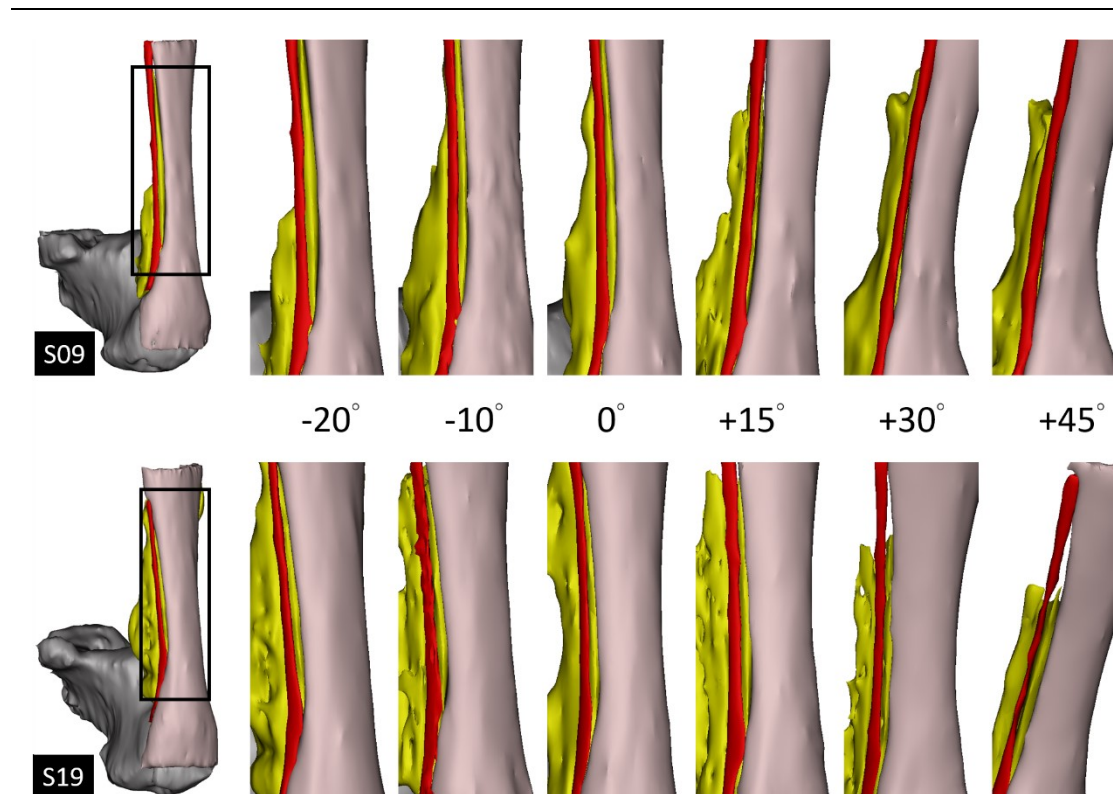


**Figure 3.5 – Different gap changes from dorsiflexion (-) to plantarflexion (+).**

The top row represents cases where the gap decreases from dorsiflexion to plantarflexion, while the bottom row represents the opposite. The gap was filled by Kager's fat pad (yellow).

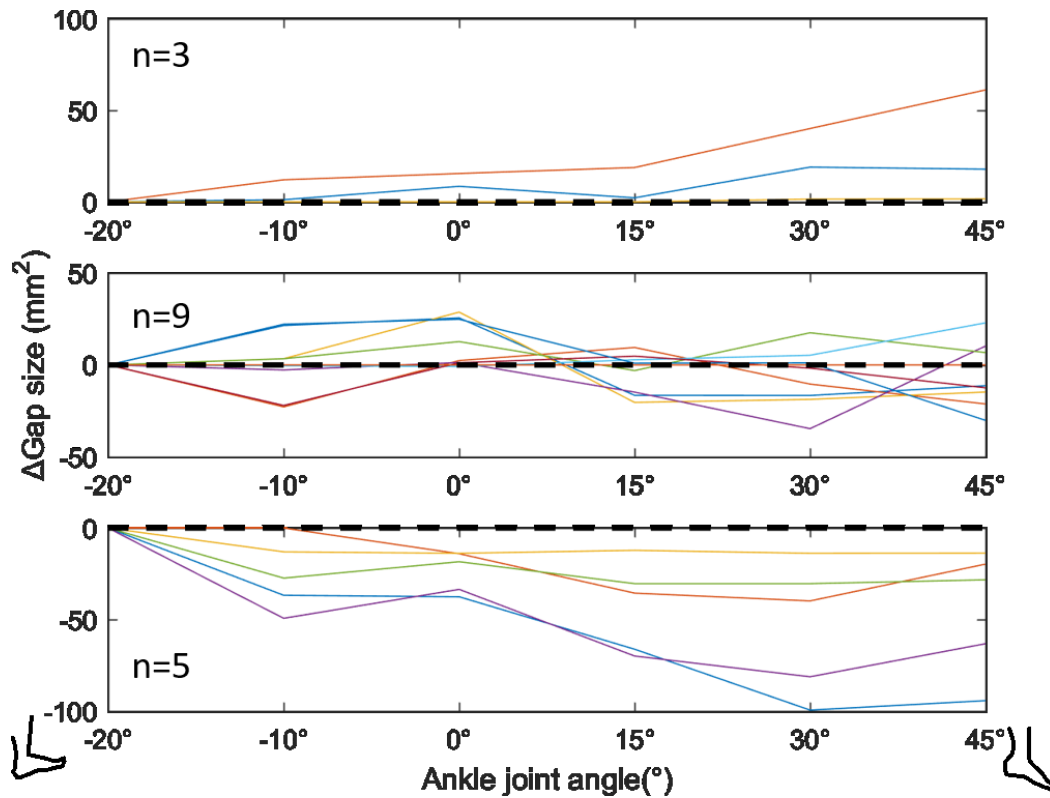


**Figure 3.6 - Change of the gap size from dorsiflexion to plantarflexion in Type 1 tendons**

In two of the Type 1 tendons, a segment was observed to be attached to the Achilles tendon throughout the range of motion. This segment remained the same length and was measured as  $28.0 \pm 0.5$  mm and  $20.4 \pm 1.8$  mm in these two tendons. The plantaris and Achilles tendons of these two participants were registered to the calcaneus and distal tibia to visualize the tendon movement. This segment moved with respect to the tibia but remained in the same position with respect to the two tendons, suggesting that this segment was an adhesion between the tendons (Figure 3.6).

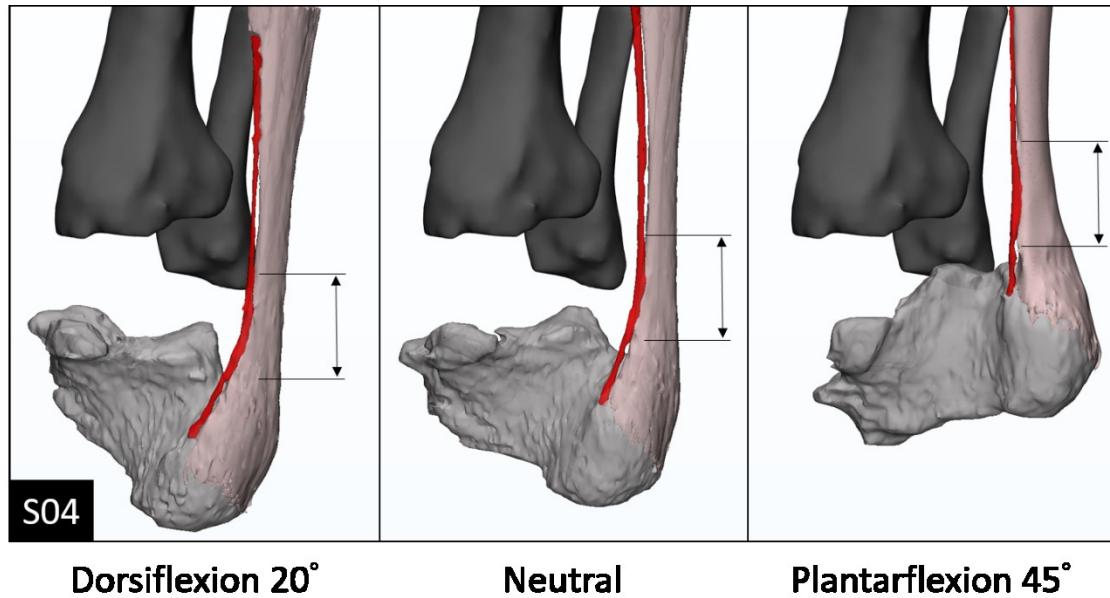


**Figure 3.7 – The attached segment (arrow) between the Achilles tendon and plantaris tendon for participant S04.**

Type 2 tendons tended to travel further from the Achilles tendon than Type 1 tendons, with the Kager's fat pad separating the two tendons. Type 2 tendons had a variety of insertions, three out of eight inserted anteriorly/medial-anteriorly to the Achilles tendon, while the others became a thin tissue that was not traceable on either MRI or ultrasound (Figure 3.7). Furthermore, from dorsiflexion to plantarflexion, the plantaris was separated from the Achilles tendon (Figure 3.8). Therefore, compression between the Achilles and plantaris tendons was unlikely to occur.

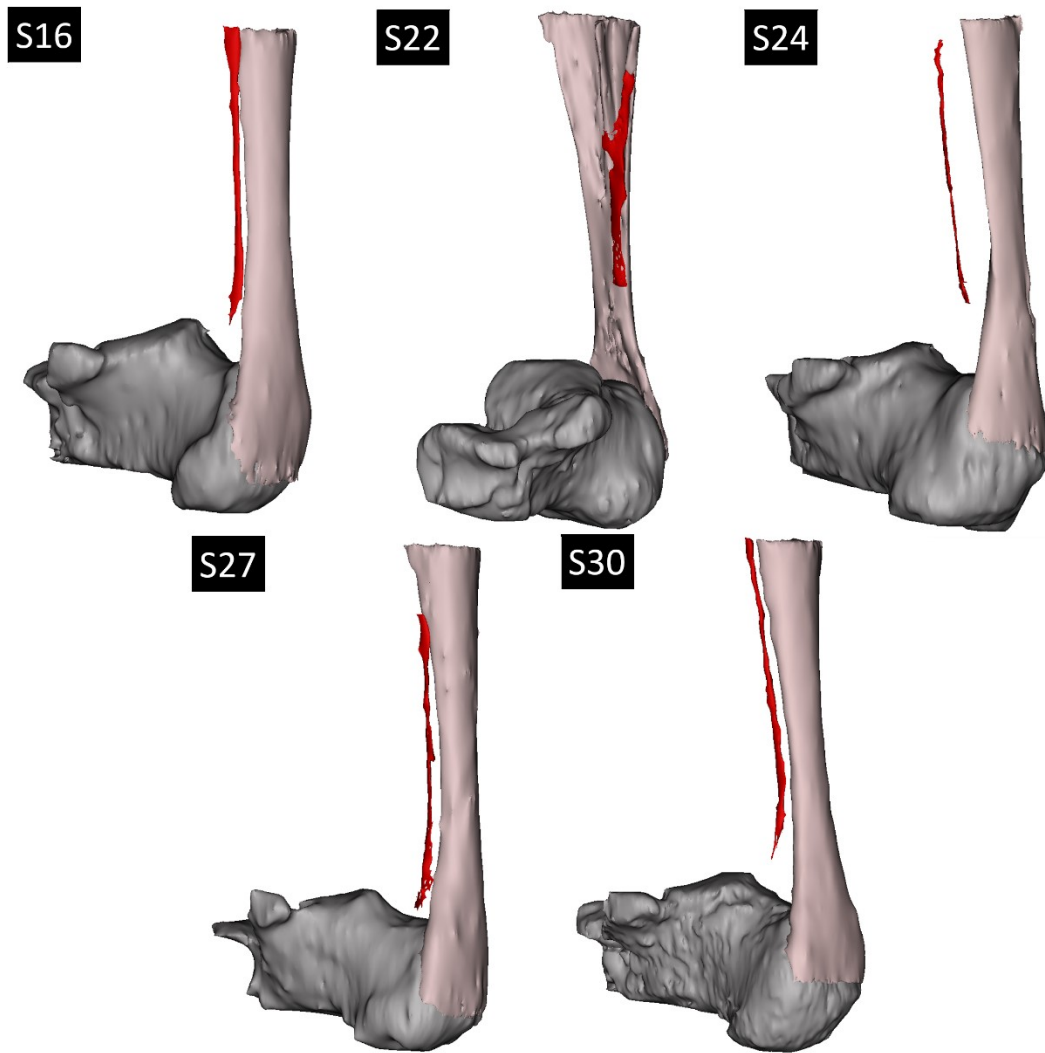


**Figure 3.8 – Fanning Type 2 plantaris tendon becoming untraceable.**

---

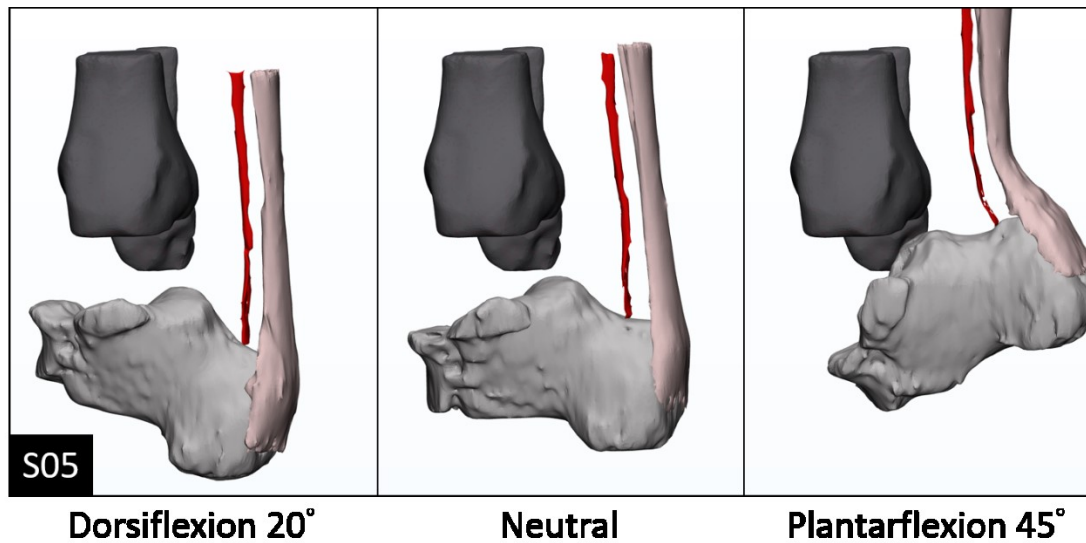


**Figure 3.9 – The Type 2 plantaris tendon and Achilles tendon of representative participant S05 during motion.**

Type 3 tendons stayed close to the Achilles tendon and inserted posteriorly to the Achilles tendon. This close relationship with the Achilles tendon made it non-identifiable from the MRI but it could be identified using ultrasound. In this study, only two Type 3 tendons were identified solely using ultrasound (Figure 3.3).

One Type 4 tendon was recognized, which travelled medially to the Achilles tendon before merging with it at 1.5 cm above the Achilles tendon insertion (Figure 3.3).

Using MRI, the plantaris tendon was not identifiable in seven participants. In two of the seven, the plantaris tendon was subsequently identified in the ultrasound scan, inserting posteriorly to the Achilles tendon. The others were non-identifiable in the ultrasound images.

### 3.4 Discussion

This is the first study to investigate plantaris tendon geometry *in vivo* across a range of ankle motion. The key findings of this study include: (i) adhesions may be present between the plantaris and Achilles tendons in asymptomatic people; (ii) Type 2 tendons have no contact with the Achilles tendon throughout ankle range of motion; (iii) ultrasound is more sensitive than MRI in identifying Type 3 plantaris tendons.

The plantaris and Achilles tendon geometries were modelled across the ankle joint range of motion, simulating the motion during running. The reconstructed 3D models allowed the visualization and comparison of tendon geometries between different joint angles. Type 2 tendons consistently remained separated from the Achilles tendon, from dorsiflexion to plantarflexion. The space between the tendons was filled by the Kager's fat pad (Figure 3.5). This finding suggests that athletes with a Type 2 tendon could have a lower risk of plantaris-related midportion Achilles tendinopathy. This is in contrast with Type 1, 3 and 4 tendons, which are positioned more closely to the Achilles tendon. Furthermore, the adhesive segment identified in two cases of Type 1 geometry would ensure the tethering of the two tendons, making compression and friction occur at the same location. Athletes with this morphology may be at risk of developing plantaris-related midportion Achilles tendinopathy.

The use of MRI and ultrasound to compare geometries of the plantaris tendon between individuals has enabled the identification of those individuals who may be at risk of developing plantaris-related Achilles tendinopathy. Type 3 tendons were not identified in any of the MRI series across the full range of motion, but by using ultrasound a clear border to the Achilles tendon could be easily identified. Admittedly,

a criticism of this study is that the sensitivity of ultrasound in identifying such a small tendon may be affected by the operator's skill. Therefore, cross-comparison between imaging techniques is suggested to achieve accurate identification.

### **3.4.1 Plantaris tendon geometry**

In the literature, the plantaris tendon insertion has previously been differentiated into nine groups and identification has been achieved in 100% of cases (van Sterkenburg et al., 2011a). Such detailed classification can only be achieved by cadaveric dissection. The identification rate of the plantaris tendon tends to be higher by dissection than by medical imaging (Spang et al., 2016). Also, the clinical importance of nine different categories of plantaris tendon has not been explored.

A spectrum of proximity to the Achilles tendon was observed within Type 1 tendons. Five of them had a gap of less than 2 mm and the remainder were greater. Once a minor injury of the tendon occurs, a swollen Achilles tendon could encourage contact between the two tendons and propagate the tendinopathic process (Figure 3.4).

The compression between the Achilles and plantaris tendons has been measured in cadaveric studies. However, the results were diverse. Smith et al. (2017) measured an increasing plantaris compression when the ankle was in dorsiflexion, while the experiment of Stephen et al. (2017) showed an increased compression force in plantarflexion. Differences in the experimental setting, specimen integrity and loading conditions could lead to such different findings, but so could anatomical variability. In the study presented here, the imaging protocol controlled these factors and observed both situations (Figure 3.5), suggesting that it is an anatomical effect. Although the compression force was not quantified, it could be estimated using other techniques,



such as finite element analysis using the deformation and geometry of Kager's fat pad as an input.

Type 2 plantaris tendons theoretically reduce the risk of any mechanical compression or friction (Figure 3.8). Therefore, stratifying treatment based on morphology could be used to develop targeted rehabilitation protocols and imaging-guided interventions, such as a personalized rehabilitation regimen and local injection to mitigate the irritation between the two tendons. Patients with midportion Achilles tendinopathy should be evaluated for plantaris involvement before treatment and rehabilitation. It is reasonable that patients with Types 1, 3, and 4 plantaris tendons adopt different rehabilitation strategies, such as isometric exercise, to avoid plantaris interaction caused by extreme joint ranges of motion (Rio et al., 2016).

### **3.4.2 The attachment between the Achilles and plantaris tendons**

In the literature, tissue connections between the Achilles and plantaris tendons have been identified in cadaveric studies. A retinacular-like structure tethering the plantaris and Achilles tendons has been found to restrict the gliding between the two tendons (van Sterkenburg et al., 2011a). However, this structure has never been reported in vivo. In another study, a fibro-fatty tissue was identified between the Achilles and plantaris and was associated with neo-innervation (Smith et al., 2017; Spang et al., 2015), which could cause pain. This fibrofatty tissue deforms to various degrees during motion. In two Type 1 tendons in this study, a fixed length of plantaris was attached to the Achilles tendon throughout the range of motion, where the plantaris was separated from the proximal Achilles tendon, attached to the Achilles tendon at approximately 5 cm above the insertion, and then re-separated from the Achilles at 2 cm, before inserting onto the calcaneus, medial to the Achilles tendon (Figure 3.6). This 'split-attach-re-split-insert'

pattern is different from other Type 1 geometries. When the segmented plantaris and Achilles tendon geometries from different joint angles were registered to the tibia, this attached segment was fixed relative to the tendons but moved with respect to the tibia (Figure 3.6). This suggests that the attachment stayed between the tendons and was not connected to any bony structure. This attachment meant that contact between the two tendons was maintained and this could lead to shear force at the attachment site.

Evidence has been found in previous investigations that pathological changes in the tendon precede clinical symptoms (Emerson et al., 2010; Haims et al., 2000; Kannus and Jozsa, 1991; Khan et al., 2003). Adhesions are also indicative of tendon pathology (van Sterkenburg et al., 2011a). It has been reported that 22% of elite sprinters could develop plantaris-related midportion Achilles tendinopathy (Pollock et al., 2016). The method developed in this study can be used to identify the geometry predisposing midportion Achilles tendinopathy, allowing early detection of tendon injury and preventing further deterioration.

### **3.4.3 The absence rate of plantaris**

The proportions of each geometry were similar to those found in previous studies (Table 3.2); however, the absence rate was higher when compared to cadaveric studies. This trend is also seen in the literature. The absence rates based on medical imaging tended to be higher compared to cadaveric dissection (Aragao et al., 2010; Delgado et al., 2002; Freeman et al., 2008; Haims et al., 2000; Harvey et al., 1983; Jackson et al., 2014; Jakubietz et al., 2011; Jianmongkol et al., 2002; Kose et al., 2014; LaPrade et al., 2007; Mackay and McCulloch, 1990; Moss, 1988; Nayak et al., 2010; Saxena and Bareither, 2000; Schlicht and Morrison, 1992; Sharma et al., 2015; Vanderhooft, 1996; Wehbe, 1992; Wening et al., 1996; White, 1960). Only two studies used MRI to identify

the existence of plantaris and they reported absence rates of 14.8% (Kose et al., 2014) and 37.2% (Saxena and Bareither, 2000). Absence rates are not the only difference, as the relative prevalence of each type of plantaris tendon indicates that Type 2 and Type 3 tendons are possibly missed when using both MRI and ultrasound, as the prevalence of these types is lower in this study than in the dissection literature (Table 3.2). This is reasonable because the plantaris tendon is thin in Type 2, and the tendon lies on the Achilles for the whole pathway in Type 3. Those tendon geometries that are thin or closely attached to the Achilles tendon make the identification from MRI and ultrasound difficult.

#### **3.4.4 Limitation**

The major limitation of this study is that only healthy volunteers were included. In addition, it is impossible to validate the results of tendon categorisation. One feasible way to validate this result is to perform the same scanning protocol on cadaveric specimens and dissect them. An attempt was made to integrate geometry identification using both MRI and ultrasound. Such cross comparisons help to improve the sensitivity of plantaris tendon identification and to identify the gap between MRI and ultrasound interpretation. In addition, all of the MRIs were conducted using a single imaging protocol. It is possible that Type 3 tendons could be identified with another MRI protocol. Although the MRI slice thickness of this study was 1 mm, which is thinner than the thickness of the clinical routine (3 mm), thinner slices would likely result in better models for geometry categorization.

### 3.5 Conclusion

Differences in plantaris tendon geometry may generate variable interactions with the Achilles tendon. The adhesion of Type 1 tendons was identified and appeared to tether the tendons. This could cause mechanical interaction between the Achilles and plantaris tendons and may be relevant to the development of mid-portion Achilles tendinopathy. Type 2 tendons have a lower risk of compression and friction against the Achilles tendon because the plantaris tendons are separate from the Achilles throughout the range of motion, although the effect of the fat pad should be further explored. Type 3 plantaris tendons could be missed from MRI alone and therefore cross-comparison with ultrasound is recommended. The categorization of the plantaris tendon geometry proposed in this study can be implemented in a clinical setting and could lead to personalized treatment strategies or preventive measures.

Patients with plantaris-involved midportion Achilles tendon pain were not included in this study. To date, there is no evidence suggesting a particular plantaris tendon geometry would lead to midportion Achilles tendinopathy. One approach is to categorize plantaris tendon geometry in a patient cohort and compare the prevalence of the plantaris tendon types. This will be investigated in the next chapter.

## **Chapter 4**

# **Plantaris tendon geometry in patients with plantaris-involved midportion Achilles tendinopathy**

The last chapter laid the groundwork for identification of the plantaris tendon using MRI and ultrasound. In healthy subjects, five different plantaris tendon geometries were identified and compared with results from cadaveric dissections in the literature. From multiple static scans, the geometries were visualised during movement. In this chapter, plantaris tendon geometry will be evaluated in individuals diagnosed with midportion Achilles tendinopathy with plantaris tendon involvement in order to develop hypotheses regarding anatomical and biomechanical effects implicated with tendinopathy, such as the involvement of compression and friction.

## 4.1 Introduction

The plantaris tendon has been observed to be associated with midportion Achilles tendinopathy, where, in surgery for midportion Achilles tendinopathy, the stiff plantaris tendon is frequently observed to cause an indentation on the soft, swollen Achilles (Alfredson, 2011). It is possible that compression and friction between these tendons could cause local injury to the Achilles tendon. Clinically, the removal of the plantaris tendon can shorten the time of return to sport when compared to traditional open debridement surgery (Bohu et al., 2009; Calder et al., 2015; Calder et al., 2016), and improve Achilles tendon healing (Masci et al., 2015).

As there is high anatomical variability, the risk of plantaris tendon involvement in midportion Achilles tendinopathy may be a function of this varying anatomy and so the effect may vary between different types of tendon geometry. Mechanical simulations using cadaveric specimens have demonstrated that if the plantaris tendon inserts on the calcaneus anteriorly (Type 2) or medially (Type 1) to the Achilles tendon, it could have larger differential displacements along the tendon pathway than one that inserts directly onto the Achilles tendon (Stephen et al., 2018). This increased axial differential motion could result in a predisposition to midportion Achilles tendinopathy with plantaris tendon involvement. However, as shown in Chapter 3, some Type 1 and Type 2 tendons do not contact the Achilles tendon throughout the range of motion at the level of 4-8 cm above insertion, which is the region where midportion Achilles tendinopathy often occurs. This absence of contact would suggest lower (or absent) compression and friction between the two tendons. Therefore, to reconcile these contradictory observations, it would be beneficial to investigate the geometry of the plantaris tendon

in midportion Achilles tendinopathy patients where there has been a diagnosis of plantaris tendon involvement.

Although it has been reported during surgery for midportion Achilles tendinopathy that the plantaris tendon was invaginated or adherent to the Achilles tendon (Alfredson, 2011; Calder et al., 2015; Masci et al., 2016), fine categorization of the plantaris tendon geometry in midportion Achilles tendinopathy patients has not been reported previously. Therefore, it is not understood if there is a correlation between plantaris tendon geometry and midportion Achilles tendinopathy. Considering the high anatomical variation of the plantaris tendon, categorizing the plantaris tendon geometry in patients could help to clarify the mechanism of plantaris tendon involvement.

The aim of this study was to apply the categorization system proposed in Chapter 3 to the plantaris tendon in a cohort of those diagnosed with plantaris-tendon involved midportion Achilles tendinopathy. The hypothesis is that the distribution over different types (excluding Type 5) in patients with plantaris-involved midportion Achilles tendinopathy will be different than the healthy groups. Only patients with plantaris-involvement are included, as the focus of this work is on the role of plantaris in midportion tendinopathy. This retrospective observation could further elucidate the role of the plantaris tendon in the development of midportion Achilles tendinopathy.

## 4.2 Methods

### 4.2.1 Participants

A retrospective data analysis of the medical imaging database of the Fortius Clinic taken between December 2015 and June 2018 was conducted. The anonymized MRI and ultrasound images of patients diagnosed with midportion Achilles tendinopathy with plantaris tendon involvement were analysed. Diagnostic criteria included: i) clinical symptoms of medial-based Achilles tendon swelling/pain/flickering sensation, ii) plantaris identified on MRI or ultrasound with focal inflammatory response around this region, iii) relevant clinical history, such as recent changing of activity level (distance, speed, duration), footwear, or surface the patient exercises on. Only patients with both MRI and ultrasound scan records were included. A total of 36 MRIs (left: 20, right: 14) and ultrasound images and reports from 29 patients were collected. The study was approved by the local medical ethics committee (Appendix B). The control group was a healthy control cohort (n=34, 19 male, 15 female, age:  $28.8 \pm 3.7$  years) collected from university environment.

### 4.2.2 Image segmentation and categorization

To obtain accurate geometry, only MRI scans that were obtained using an imaging sequence of T1 weighted or proton-density weighted axial views were included, as these sequences are used routinely for evaluating anatomical structures of the musculoskeletal system (Shapiro et al., 2012). To compare with the geometry reported in Chapter 3, the Achilles tendon and plantaris tendons from the tendinopathic patient were segmented. The segmentation protocol and categorization criteria were described



in Chapter 3. Due to the retrospective nature of this study, the scans were performed in slice thicknesses of 3, 3.5, or 4 mm with various pixel sizes.

### **4.2.3 Statistical analysis**

The incidences of different types of plantaris tendon geometry were compared with the incidence from the healthy cohort reported in Chapter 3. Some patients had bilateral tendinopathy, but different geometry was presented in each leg, so each plantaris tendon was reported independently. A chi-squared analysis was used to analyse the frequency difference with a post-hoc analysis of adjusted residuals, and the p-value was adjusted using Bonferroni correction and the significance level after correction was 0.05. Due to the small number (<5) of tendons in some types, the p-value of the likelihood ratio was reported, rather than the p-value of the Pearson's chi-squared test. With the sample number, the post hoc statistical power analysis showed power of 0.8 to detect middle to large distances ( $d = 0.46$ ) (Cohen et al., 1976).

The statistics were processed with SPSS software (v.25, SPSS Inc., Chicago, IL).

## **4.3 Results**

The incidence of each type of plantaris tendon geometry in the tendinopathy and healthy groups are summarized in Figure 4.1. A representative segmented model of each plantaris tendon type, with corresponding MRI and ultrasound images, are shown in Figure 4.2.

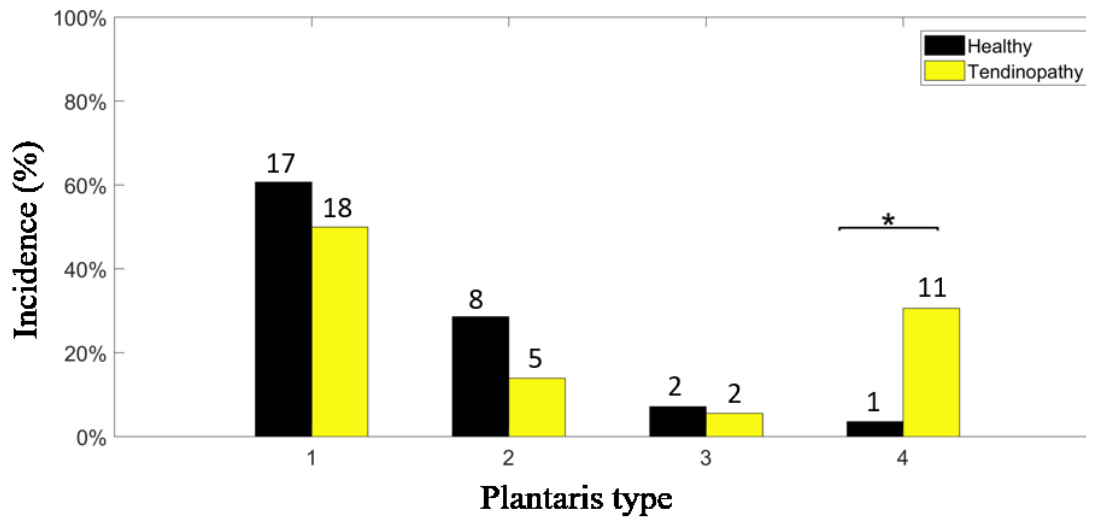


**Figure 4.1 – Frequency of plantaris tendon anatomical variants (number of tendons) for the tendinopathy group and a healthy control group.**

The incidences of Type 4 were significantly different between the healthy and tendinopathy cohorts \*: adjusted  $p < 0.05$

---

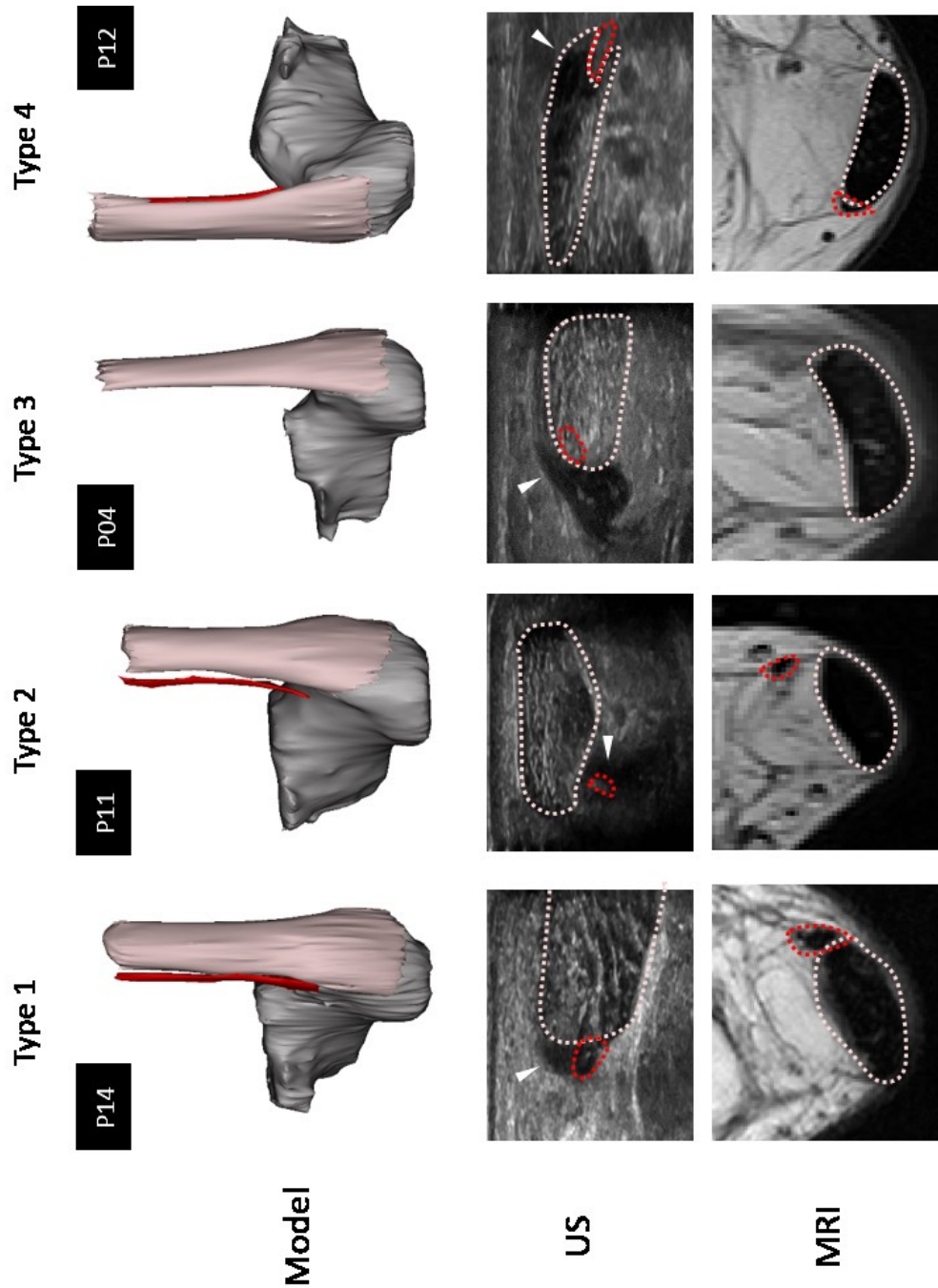


**Figure 4.2 – Representative segmented models and corresponding ultrasound (US) images and MRI sections of the plantaris tendon geometry from a group of 36 tendons in 33 patients with plantaris tendon involved midportion Achilles tendinopathy.**

The identification numbers of the participants are shown in the black boxes. The Achilles tendon is encircled by the pink dotted line, while the plantaris tendon is encircled by the red dotted line. The inflammation area is marked by the white arrowhead.

There was a significant difference between the healthy and tendinopathy groups in plantaris geometry distribution ( $p = 0.001$ , likelihood ratio of chi-squared test). Post-hoc analysis showed significant differences in the incidence of Type 4 and 5 tendons after Bonferroni correction (adj.  $p = 0.015$  and  $0.03$ , respectively).

In Type 1 tendons, the interaction between the Achilles and plantaris tendons was not consistent. Contact between the tendons occurred at different positions on the plantaris tendon (Figure 4.3), and the centre of inflammation was measured as  $62.9 \pm 14.7$  mm ( $n=18$ ) above the Achilles tendon insertion.

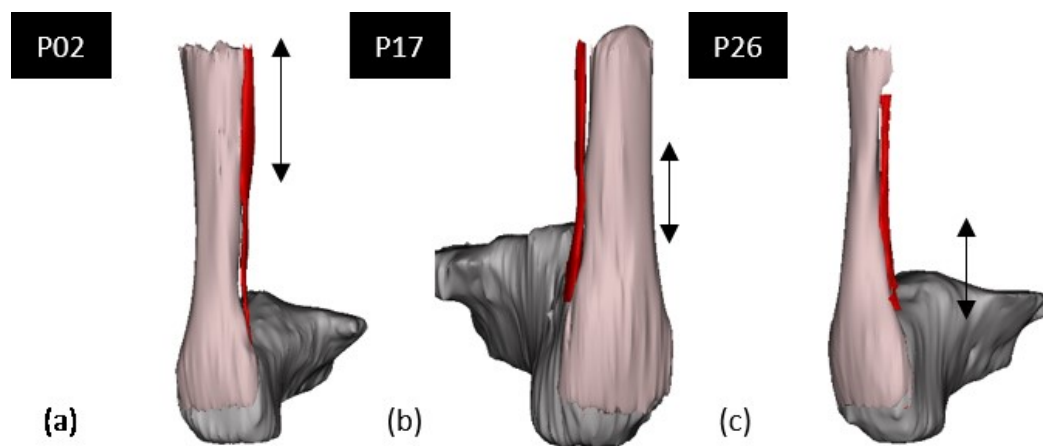


**Figure 4.3 – Representative Type 1 plantaris tendon geometry variants from a group of 18 tendons in 17 patients with plantaris-involved midportion Achilles tendinopathy.**

The identification numbers of the participants are shown in the black boxes. The representative locations of inflammation and contact between the Achilles and plantaris tendon are indicated by the double-headed arrows. (a) The plantaris inflammation and contact occur at the level of gastrocnemius aponeurosis expansion, and then no contact was observed until insertion. (b) The plantaris inflammation and contact only occur at the midportion, and then no contact was observed until insertion. (c) The inflammation and contact were observed from midportion to insertion.

---

In the five Type 2 plantaris tendons, all tendons inserted close ( $1.83 \pm 1.15$  mm) to the anterior surface of the Achilles tendon (Figure 4.4). However, tendinopathy was noticed in Type 2 tendons even when the only contact was with the distal gastrocnemius aponeurosis (Figure 4.4c), or there was no contact with the Achilles tendon (Figure 4.4a).

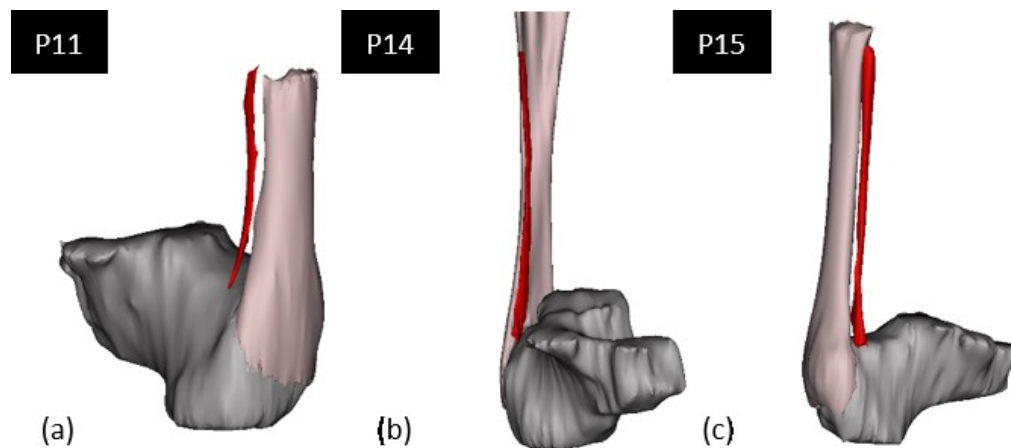


**Figure 4.4 – Representative Type 2 plantaris tendon geometry variants from a group of 5 tendons in 4 patients with plantaris-involved midportion Achilles tendinopathy.**

The identification numbers of the participants are shown in the black boxes. (a) No contact of the plantaris tendon with the Achilles tendon. (b) Plantaris tendon travels closely anterior to the Achilles tendon. (c) Thickened plantaris tendon seen at the level where no contact occurred with the plantaris tendon.

---

Only two Type 3 tendons were observed, and increased inflammation could be seen in these on the dorsal-medial surfaces in ultrasound (Figure 4.2). In Type 4 tendons, often only a small segment in the MRI could be identified due to the close relationship of the plantaris with the Achilles, while in the ultrasound the plantaris tendon could often be seen running closely by the Achilles tendon and eventually merging with it (Figure 4.5).

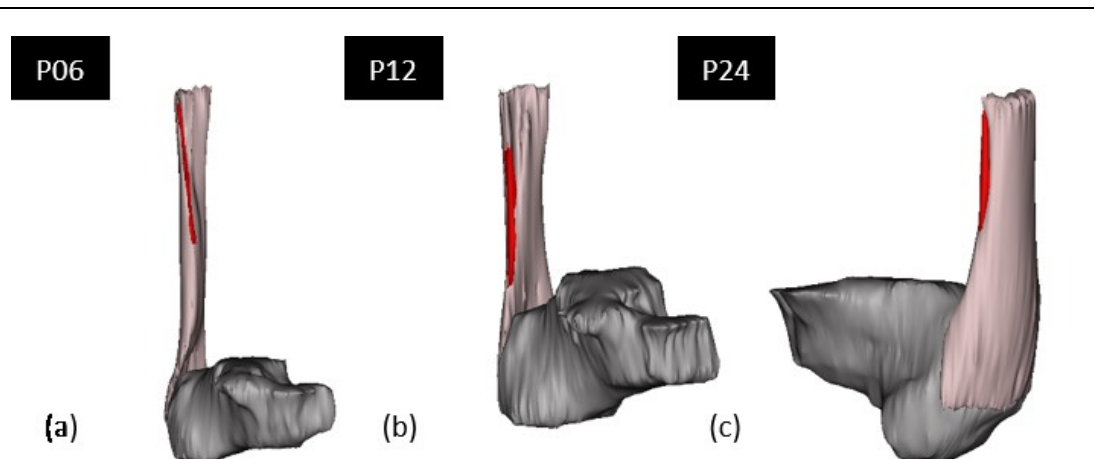


**Figure 4.5 – Representative Type 4 plantaris tendon geometry in a group of 11 tendons in 9 patients with plantaris-involved midportion Achilles tendinopathy**

Plantaris tendons insert directly to the Achilles tendon and only a small segment can be identified before inserting to the Achilles tendon.

---

#### 4.4 Discussion

This is the first study to categorize plantaris tendon geometry in patients with plantaris-involved midportion Achilles tendinopathy. Although different hypotheses about the mechanical role of the plantaris tendon in midportion Achilles tendinopathy have been proposed (Alfredson, 2011; Calder et al., 2016; Masci et al., 2015; Stephen et al., 2018; van Sterkenburg et al., 2011a), the validation of these hypotheses is challenging due to the difficulties inherent in identifying the tendon and the infeasibility of *in vivo* compression or shear force measurement. This study attempts to clarify the role of the plantaris tendon in midportion Achilles tendinopathy by categorizing the tendon geometry using routine imaging techniques for plantaris tendon evaluation, aiming to maintain clinical utility.

The key finding of this study is the significantly greater incidence of plantaris tendons inserting directly into the Achilles tendon (Type 4) in the tendinopathy cohort, while the incidences of other types were not different from the healthy cohort. In addition, a variety of the plantaris tendon geometries observed within the tendinopathy group are presented in this study.

It is not understood as to whether the plantaris tendon was a primary cause of the midportion Achilles tendinopathy or it is just an innocent tendon being compressed by the swollen Achilles tendon. From the differences observed between the distributions in plantaris tendon type between the tendinopathy and healthy cohorts, it may be that both scenarios may occur.

As Types 1, 2, and 3 showed no difference in the prevalence compared to the normal population, it is possible that the plantaris tendon involvement is irrelevant to the geometry of the plantaris. Therefore, the high incidence of Type 1 tendons is likely due to its high incidence in the general population as Type 1 tendons account for 50% of the population in the healthy cohort. To the contrary, Type 4 tendons may initiate midportion Achilles tendinopathy due to the close contact and merging of the two tendons. In the mechanical simulation reported by Stephen et al. (2018), this type of geometry has a minimal differential axial displacement between the Achilles and plantaris tendons during motion. From the results of the simulation and the incidence in the tendinopathy group, it is possible the effect of direct insertion to the Achilles outweighs the effect of differential axial movement or strain of the tendons.

A smaller proportion of Type 2 tendons were observed to have fewer contacts with the Achilles tendon during motion than the other types, as shown in Chapter 3, but they still were implicated in some of the pathological cases, even if no contact was observed in the static MRI. There are several possible explanations for this observation. First, it

is possible that the compression could be propagated through the fat pad between the tendons. It has been shown that when the plantaris is involved in midportion Achilles tendinopathy, the Kager's fat pad that is localized around the tendons also showed an increased inflammatory response (Calder et al., 2016). Secondly, it is possible that the tendon-to-tendon contact occurs during exercise, where there is valgus hindfoot motion. In Chapter 3, the ankle was scanned in a neutral position without varus/valgus, and only dorsiflexion and plantarflexion were investigated. In mechanical simulations described in the literature, the compression force between the Achilles and plantaris tendon increased when the hindfoot was placed in a valgus position (Stephen et al., 2018).

Two Type 3 tendons were identified in this study but only in the ultrasound. As discussed in Chapter 3, the evaluation of plantaris tendon geometry using the MRI alone could introduce false negatives in this category.

The main limitation of this study is its retrospective nature. The selection bias over the patient population was acknowledged by the authors. As only people who had MRI scans were included, it is possible that patients with only mild symptoms that did not require an MRI were not included. However, in clinical practice, the examination modality selected for a patient depends largely on the preference and speciality training of the clinician. For this study, it was necessary to include patients with both MRI and ultrasound imaging. Analysing plantaris tendon geometry solely based upon ultrasound reports would increase the operator-dependency and subjectivity and decrease the repeatability of the study. Secondly, patients were included if they had a diagnosis of midportion Achilles tendinopathy with plantaris tendon involvement. The existence of the plantaris tendon on either MRI or ultrasound is necessary to achieve this diagnosis. This could also mean that patients with a plantaris tendon that was non-identifiable on ultrasound and MRI were not included because they were not be diagnosed with



plantaris tendon involvement. This is a limitation not just in this study, but also reflects the detection limit of the current imaging examination modalities. Finally, due to variation in the clinical routine, the sequence parameters of the scans varied. This is a common issue in retrospective studies involving quantification of signals, such as volume or signal intensity. This problem was mitigated by the fact that this study only involved tendon categorization based on the insertion location.

## 4.5 Conclusion

The categorization of the plantaris tendon in patients with plantaris-involved midportion Achilles tendinopathy could help to clarify the injury mechanism of the tendons. The population with Type 4 tendons was higher in the affected cohort, while the incidence of Types 1, 2 and 3 did not differ. The mechanism of tendinopathy could be multifactorial, as tendinopathy was also observed at levels where no contact between the tendons occurred. More prospective studies are needed to clarify the potential interaction between the tendons.

In this chapter, the hypothesis regarding the link between plantaris tendon and midportion Achilles tendinopathy was analysed. The differences in the distribution of plantaris tendon geometry type between tendinopathy and healthy cohorts showed that the plantaris tendon plays an important role in midportion Achilles tendinopathy. In the next chapter, the focus will be brought to the differential loading of the Achilles tendon.

## **Chapter 5**

### **Effect of the twisted fibre structure of the Achilles tendon on loading**

This chapter investigates the mechanical hypothesis that the twisted fibre structure of the Achilles tendon causes differential loading within the tendon itself. This was identified in Chapter 2 and is addressed in this chapter using subject-specific musculoskeletal modelling. The selection of different Achilles tendon variants is based on cadaveric studies from the literature and lower limb MRI scans. In order to properly model the insertion of twisted fibres, a semi-automated algorithm is implemented to divide the segmented Achilles tendon area. The results are then compared with commonly used approaches of modelling the Achilles tendon insertion. Finally, this is discussed in the context of the mechanical hypothesis.

## 5.1 Introduction

As described in Chapter 2, the fibre bundles that make up the Achilles tendon have a twisted structure. The twist originates from the origin of the Achilles tendon, where the gastrocnemius aponeurosis and soleus fibres converge. At the insertion, the soleus fibres are often reported to be on the medial side, while the gastrocnemius lateralis fibres are on the lateral side. The fibre configuration at the insertion has been reported to have many different patterns.

Cummins et al. (1946) reported the tendon fibre configuration in 100 specimens and first reported a degree of fibre rotation in the population. In their study, the rotation was categorized according to the fibre composition at the posterior aspect of the Achilles tendon at the level of 1cm above insertion. The least rotation was defined as the proportion of soleus fibres being less than a third, moderate rotation was defined as the proportion of soleus fibres on the posterior aspect being approximately one half, while extreme rotation was defined as the proportion being more than two thirds (Figure 5.1). The prevalence rate of these three types was 52%, 35%, and 13%, respectively.

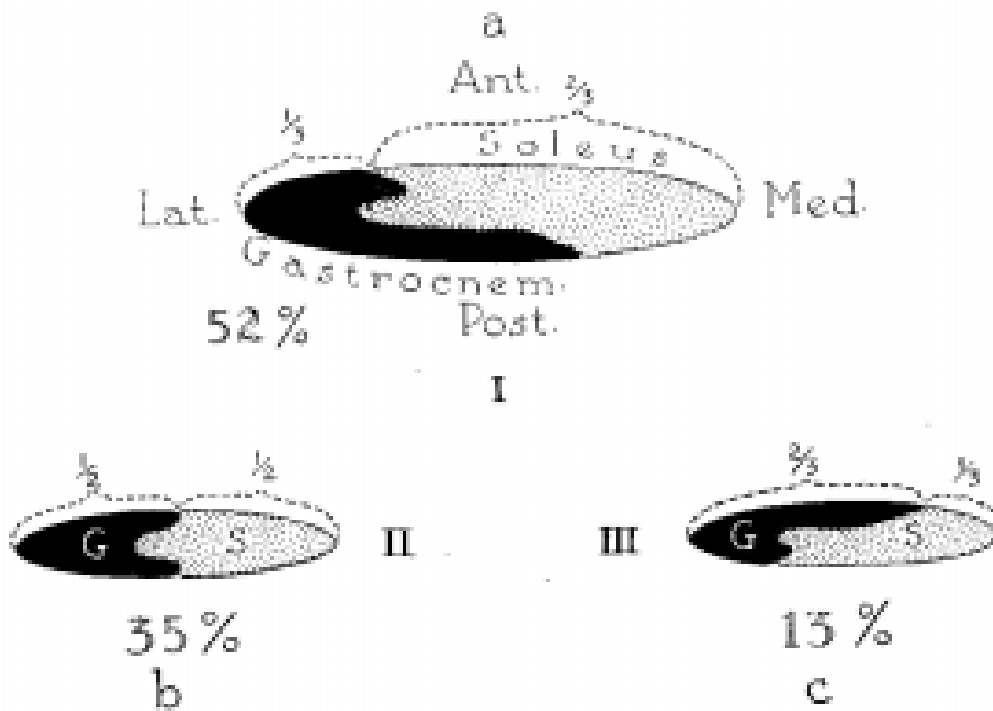


**Figure 5.1 – Categorisation of Achilles tendon fibre rotation into (a) least, (b) moderate, and (c) extreme rotation.**

Reproduced with permission of Cummins et al. (1946).

Many years later, Szaro et al. (2009) reported a more complex configuration as a result of dissecting 20 specimens (Figure 5.2). The configuration pattern of gastrocnemius fibres was described as resembling the Eiffel Tower and ‘sitting like a rider on a horse’ (Szaro et al., 2009). In this study, the gastrocnemius fibres were further separated into gastrocnemius medialis and lateralis.

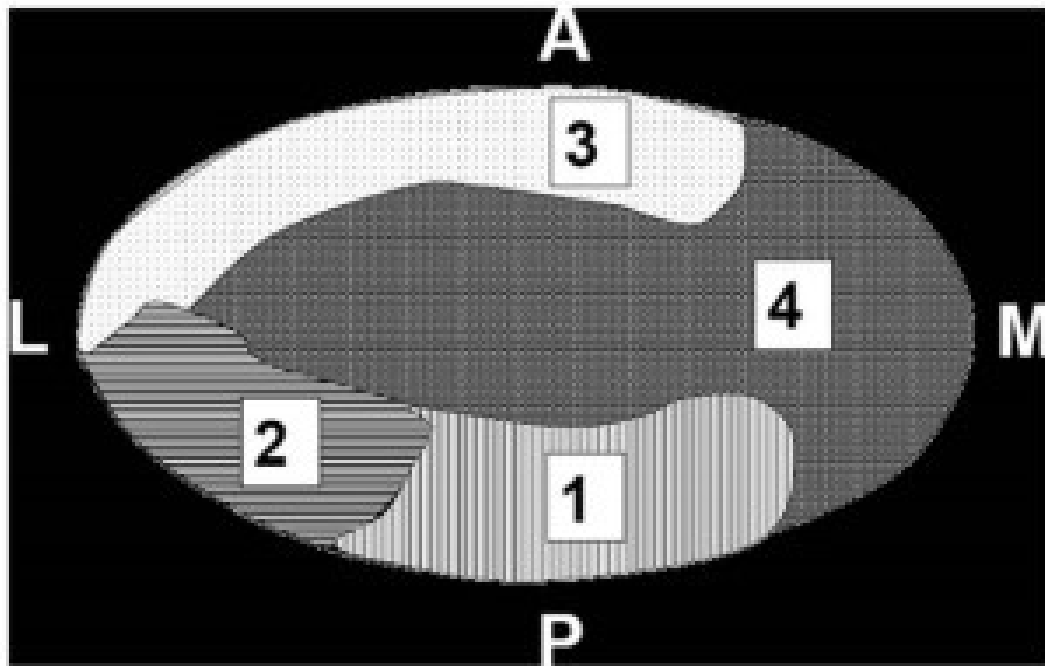


**Figure 5.2 – Achilles tendon fibre configuration reported by Szaro et al. (2009).**

1: medial segment of medial gastrocnemius muscle fibres, 2: lateral segment of the medial gastrocnemius muscle fibres, 3: lateral gastrocnemius muscle fibre, 4: soleus muscle fibres, A: anterior side, P: posterior side, M: medial side, L: lateral side. Reproduced with permission of Szaro et al. (2009).

---

Edama et al. (2015) further identified the fibre bundle paths for each muscle in the Achilles tendon. In his dissection of 110 legs, the muscle fibre bundles from gastrocnemius lateralis, medialis and soleus were separated, and the insertion of each fibre bundle was identified (Figure 5.3). A similar prevalence rate was reported for least (50%), moderate (43%) and extreme (7%) rotations (Edama et al., 2015).

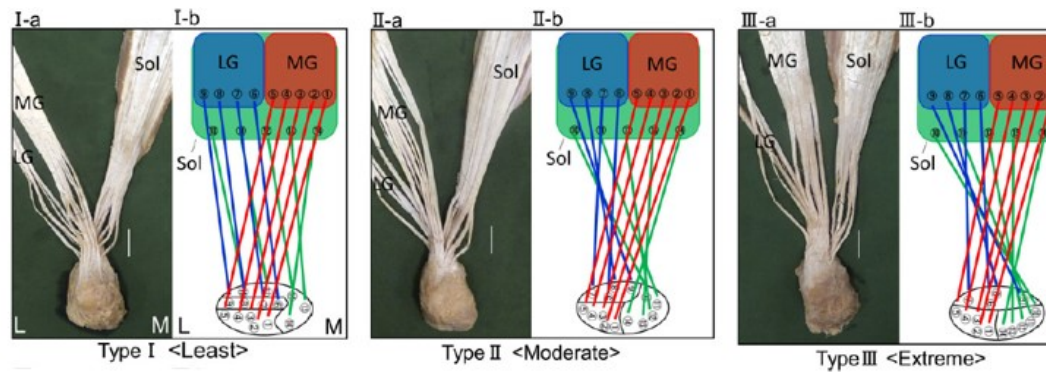


**Figure 5.3 – Achilles tendon fibre configurations reported by Edama et al. (2015). Reproduced with permission of Edama et al. (2015).**

The rotation of Achilles tendon in (a) dissection (b) schematic illustration. Fibre bundles from the lateral gastrocnemius (LG), medial gastrocnemius (MG) and soleus (Sol) converge with varied degrees of rotation in the Achilles tendon

As described in Chapter 2, the Achilles tendon transmits a significant force to drive locomotion. From a mechanical perspective, different degrees of rotation will affect the moment arm of each muscle about the joint centre of rotation. Furthermore, in lower limb musculoskeletal modelling, when the Achilles tendon insertion has been modelled as a single point (Figure 5.4). It has been identified as the parameter that has the largest effect on the resultant muscle forces (Carbone et al., 2012), which suggest that changing the insertion site of the Achilles tendon will affect the overall muscle force prediction the most. The effect of changing Achilles tendon insertion is three times larger than the effect of changing the second most sensitive element, gluteus medius anterior (Carbone et al., 2012). The sensitivity analysis was done by perturbation of the insertions and origins of all the muscles in the lower limb model with the aim to identify the key element that will affect the force prediction the most. The Achilles tendon insertion was perturbed as a whole in their study. This finding makes physiological sense, as triceps

surae has large force-generating capacity and is the prime mover in the walking movement.

---

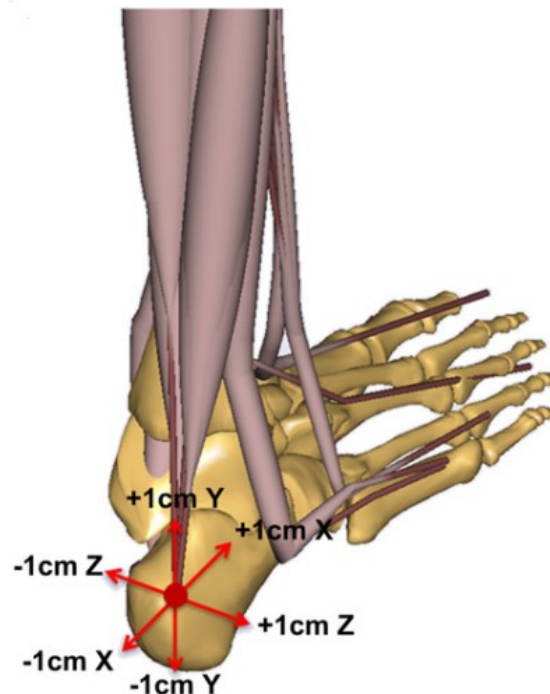


**Figure 5.4 – Perturbation of the Achilles tendon insertion modelled as a single point.**

Perturbation in each direction (X-axis – pointing forward, Y-axis – pointing upward, Z-axis – pointing laterally) changes the overall muscle force prediction of the model. Reproduced with permission of Carbone et al. (2012).

---

As discussed in Chapter 2, the rotational structure of the fibre bundles could be associated with midportion Achilles tendinopathy, as the twisting fibres bundles could affect the intra-tendinous differential displacement and cause microtrauma (Edama et al., 2015; Kader et al., 2002; Lersch et al., 2012; Toumi et al., 2016). To understand the aetiology of midportion Achilles tendinopathy, it is critical to analyse the loading conditions of every muscle contributing to the Achilles tendon and having a model that could represent the actual geometry of the Achilles tendon insertion.

To analyse the rotational effect on each of the muscles of the Achilles tendon, the methodology of musculoskeletal modelling was chosen as it allows the simulation of different insertional types. The rotation of the fibre would likely alter the moment arm of the gastrocnemius and soleus and therefore could be associated with differential loading in these muscles, possibly leading to midportion Achilles tendinopathy. This rotational feature has not previously been considered in lower limb musculoskeletal modelling. Specifically, the insertion site of the Achilles tendon is often modelled as a single insertion at the centroid (Anderson and Pandy, 1999; Carbone et al., 2015; Carbone et al., 2012) or bilateral insertions, on the medial and lateral border of the Achilles tendon (Ding et al., 2016; Klein Horsman et al., 2007).

The aim of this study is to investigate the effect of these Achilles tendon rotational variants in musculoskeletal modelling, with the goal of bridging the gap between cadaveric findings and modelled anatomical muscle parameters. It is hypothesised that different degrees of rotation (least, moderate, and extreme rotation, as described in Edama et al. (2014)) will result in different peak force magnitudes within the triceps surae and different force distributions with different Achilles tendon insertion patterns, which could enable improved understanding of the role of the Achilles tendon rotational structure in midportion Achilles tendinopathy.



## 5.2 Methods

### 5.2.1 Anatomical datasets

Subject-specific anatomical parameters of nine persons from an open-source anatomical musculoskeletal model dataset were used (Ding et al., 2018). This dataset includes the 3D coordinates of muscle lines of action, bony landmarks, via points and wrapping objects for the right leg. These parameters were obtained from manual segmentation of lower limb MRI scans.

The muscles are split into 163 muscle elements based on a template from the literature (Klein Horsman et al., 2007). In this muscle architecture, the Achilles tendon is composed of six muscle elements for soleus, one for gastrocnemius medialis, and one for gastrocnemius lateralis. Each muscle element has its own muscle line of action and maximum muscle force. The activations of each element are independent.

### 5.2.2 Rotational tendon fibre structure

In the original dataset, the Achilles tendon insertion was presented as two points on the medial and lateral tips of the tendon, where gastrocnemius medialis and the medial soleus insert on the medial side, and where gastrocnemius lateralis and the lateral soleus insert on the lateral side. This approach to modelling the insertion represents a parallel fibre pattern that maximises the inversion/eversion moment arm.

To decide the insertion for the other anatomical variants, the MRI of each subject was analysed. The Achilles tendon was identified and segmented at 1 cm above the insertion on the calcaneus using Mimics (v.19 Materialise, Leuven, Belgium). According to the illustrations presented in the literature, this segmented cross-sectional

area was divided into eight different subareas using MATLAB (The Mathworks Inc., Natick, MA). Each subject was modelled with three types of anatomical insertion (least, moderate and extreme rotation reported in Edama et al. (2014)), representing different degrees of rotation. The centroid of each subarea was projected onto the calcaneal surface. These projected points were assigned as the insertions for corresponding muscle elements (Figure 5.5) as it was not possible to distinguish between these insertions at the calcaneal level on the MRI scans. Besides the anatomical insertions, common modelling insertions were also calculated. The centroid of the Achilles tendon cross-sectional area was also projected to the calcaneus and used for the single insertion modelling (Figure 5.5, M2).

For ease of communication, in this thesis, the anatomical insertional variants of ‘least rotation’, ‘moderate rotation’, and ‘extreme rotation’ are named A1, A2, and A3, respectively, while the single and bilateral modelling insertions are named M1 and M2, respectively (Table 5.1).

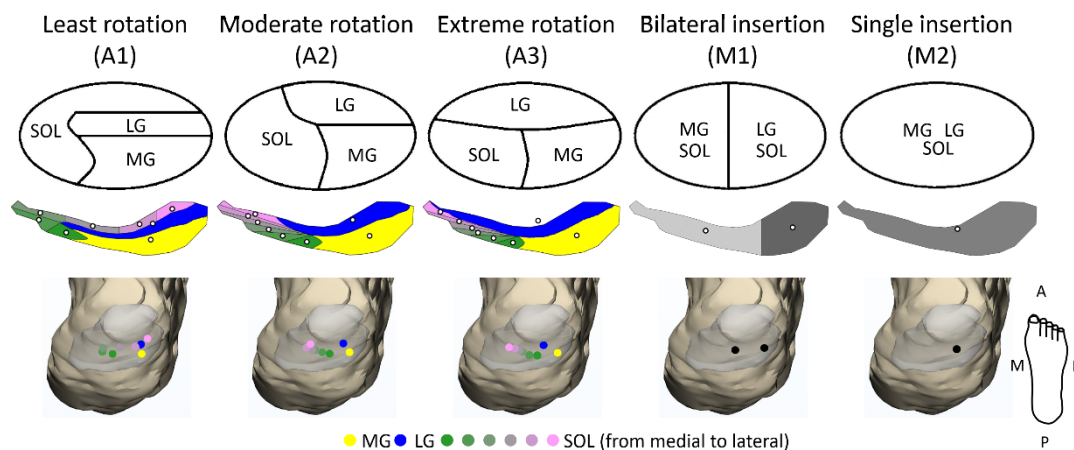


**Figure 5.5 – Representation of different degrees of rotation of the Achilles tendon insertion in a musculoskeletal model.**

LG: gastrocnemius lateralis, MG: gastrocnemius medialis, GAS: overall gastrocnemius, SOL: soleus, ACH: Achilles tendon. A: anterior, P: posterior, M: medial, L: lateral.

Nomenclature	Insertion type description
A1	Least rotation of the fibre bundles.
A2	Moderate rotation of the fibre bundles.
A3	Extreme rotation of the fibre bundles.
M1	Bilateral insertion points on the centroid of medial and lateral halves of the Achilles tendon insertion.
M2	A single insertion point at the centroid of the Achilles tendon insertion.

**Table 5.1 – The nomenclature of the insertional types.**

### 5.2.3 Kinematic marker datasets

The kinematic and kinetic data of each subject during level walking were available from a previous study (Ding et al., 2018) along with the anatomical dataset. The kinematic and kinetic data were recorded by a ten-camera optical motion capture system (Vicon Motion Systems, Oxford, UK) at 100 Hz and a force plate platform (Kistler Instrument Corp., Winterthur, Switzerland) at 1000Hz.

A randomly selected single walking trial of each subject was analysed. The force plate and marker data were processed with a 4th degree Butterworth low pass filter with a cut off frequency of 4 Hz (Winter, 2009) to remove unwanted high-frequency noise.

The force plate data were downsampled by a ratio of 10:1 to synchronize with the kinematic marker data.

#### **5.2.4 Musculoskeletal model**

The maximum muscle forces were calculated by multiplying the PCSAs by a constant value representing maximum muscle stress. The PCSA of each muscle was decided according to a regression equation based on the height and weight of the participant on which the model was based, to account for possible muscle capacity variation of each individual (Handsfield et al., 2014). The maximum muscle stress was 61 N/cm<sup>2</sup> (Wickiewicz et al., 1983). The maximum muscle stress will directly affect the maximum capacity of all muscles. In literature, there has been a huge variation about the maximum muscle stress, ranging from 11 N/cm<sup>2</sup> (Fukunaga et al., 1996) to 137 N/cm<sup>2</sup> (Pruim et al., 1980). A muscle stress of 61 N/cm<sup>2</sup> was used extensively in lower limb modelling to provide enough strength to the muscles in the lower limb (Anderson and Pandy, 1999).

The muscle-tendon unit was modelled as a simple line of action; the force-length and force-velocity characteristics were not modelled. The maximum force of each muscle equals the muscle PCSA (scaled from height and weight according to the Handsfield et al. (2014)) multiplied by the maximum muscle stress.

The FreeBody musculoskeletal model (Cleather and Bull, 2015) was used to analyse the effect of employing anatomical and commonly used simplifications of the Achilles tendon insertion. The FreeBody model calculates muscle forces by inverse dynamics and constrained optimization. As described in Chapter 2, the model first calculates the joint torques and the intersegmental forces using inverse dynamics. As the muscles crossing the same joint can have overlapping functions, the muscle forces required to

achieve a certain joint torque and intersegmental force are an underdetermined system. Thus, the constrained optimization serves to solve the underdetermined muscle forces by minimizing a predefined objective function. For gait analysis, the objective function is defined as Equation 5.1, as proposed by Crowninshield et al.

$$F(\mathbf{x}) = \sum_i \left( \frac{x_i}{f_i} \right)^3, \quad i = 1, \dots, 163 \quad \text{Equation 5.1}$$

where

$\mathbf{x}_i$  represents the muscle force to be solved;

$f_i$  represents the maximum muscle force of the muscle;

The power of three was chosen to be in line with the objective function used in Carbone et al. (2012). In the literature, powers from 2 to 5 and to infinity (min/max) have been used. Such objective functions could slightly change the co-activation of the muscles, but the peak force should remain the same (Rasmussen et al., 2001). To date, there has not been consensus as to which objective function best represents the actual control strategy of human motion.

As there were no elements representing tendons or ligaments in the model, the Achilles tendon force was represented by the summation of soleus, gastrocnemius medialis, and gastrocnemius lateralis muscle forces.

### 5.2.5 Statistical analysis

The triceps surae muscle forces during gait were investigated. All forces were normalized to the participant's body weight. The median muscle forces and interquartile range (IQR) are presented, as the data were not normally distributed. The peak forces were compared using non-parametric Friedman's test followed by a post hoc analysis with Bonferroni correction for multiple comparisons. The similarity between the muscle force patterns was compared using the coefficient of multiple correlations (CMC) (Ferrari et al., 2010; Garofalo et al., 2009; Kadaba et al., 1989). The criteria for assessment of the coefficient of multiple correlations are specified below:

$CMC < 0.65$  poor

$0.65 < CMC < 0.75$  moderate

$0.75 < CMC < 0.85$  good

$0.85 < CMC < 0.95$  very good

$0.95 < CMC < 1$  excellent

## 5.3 Results

Gait cycles were analysed from heel strike to heel strike. The median timing of the toe-off event occurred at 61.3% (IQR: 61.0-62.6%) of the cycle. The median and IQR of the triceps surae muscle forces are shown in Figure 5.6. A boxplot showing the distribution of peak forces for the different insertional types is presented in Figure 5.7.

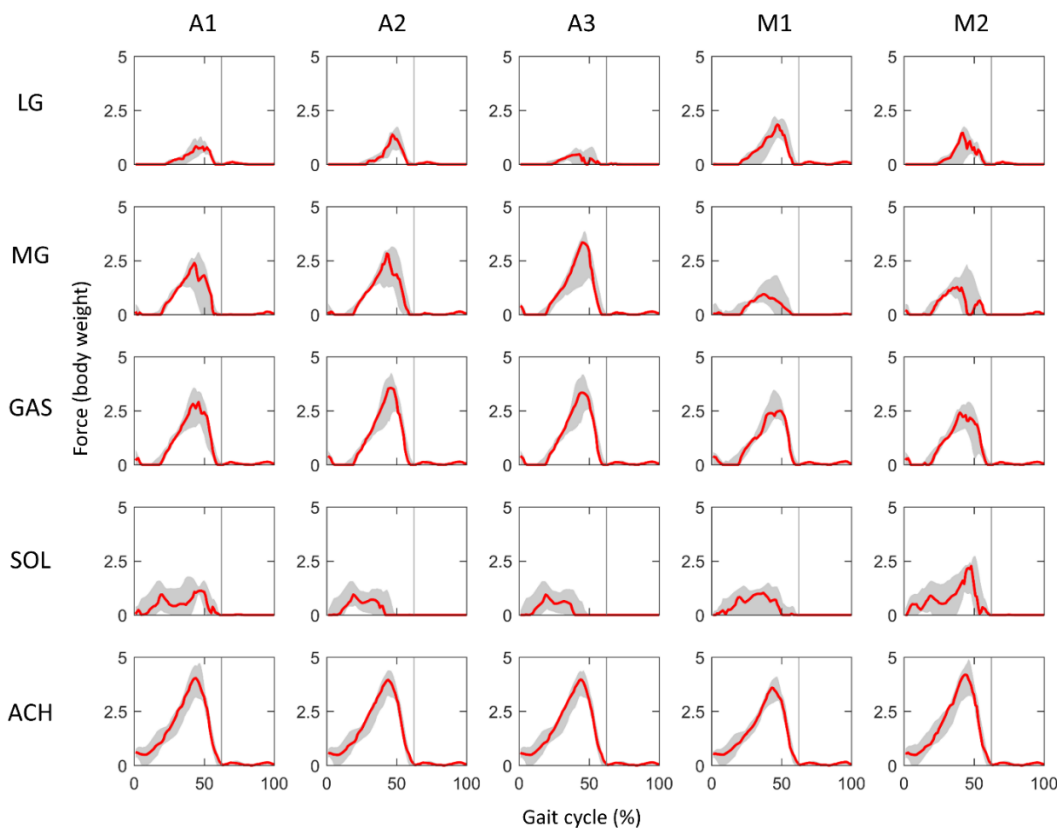


**Figure 5.6 – The median and interquartile range of the triceps surae muscle forces and the Achilles tendon force (n=9)**

LG: gastrocnemius lateralis, MG: gastrocnemius medialis, GAS: total gastrocnemius (the sum of LG and MG), SOL: soleus, ACH: Achilles tendon (the sum of GAS and SOL). The toe-off event is marked by the grey vertical line. A1: least rotation of the fibre bundles. A2: moderate rotation of the fibre bundles. A3: extreme rotation of the fibre bundles. M1: bilateral insertion points on the medial and lateral aspects of the Achilles tendon insertion. M2: a single insertion point at the centroid of the Achilles tendon insertion.

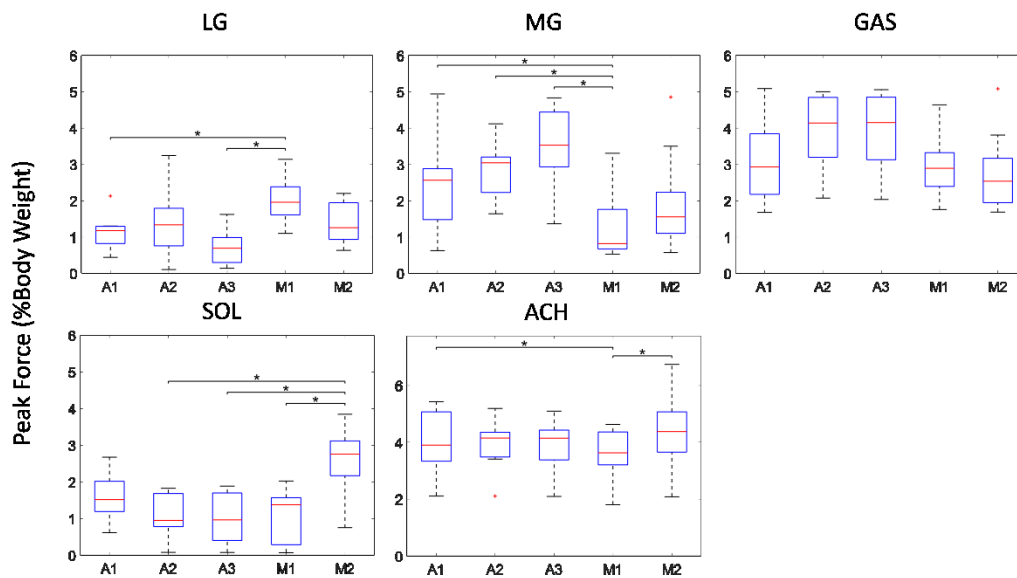


**Figure 5.7 – Box plots of the peak forces of medial gastrocnemius, lateral gastrocnemius, overall gastrocnemius, soleus and Achilles tendon force (n=9) for different insertion types.**

LG: gastrocnemius lateralis, MG: gastrocnemius medialis, GAS: total gastrocnemius (the sum of LG and MG), SOL: soleus, ACH: Achilles tendon (the sum of GAS and SOL). A1: the least rotation fibre bundle pattern. A2: the moderate rotation fibre bundle pattern. A3: the extreme rotation fibre bundle pattern. M1: bilateral insertion points on the medial and lateral aspects of the Achilles tendon insertion. M2: a single insertion point at the centroid of the Achilles tendon insertion. The toe-off event is marked by the grey vertical line. \* represents a comparison with a statistically significant difference (adj.  $p < 0.05$ ).

The peak forces of LG were higher in M1 than A1 and A3, and the peak force of MG was lower in M1 than A1, A2 and A3. No statistically significant differences were observed at the peak of the total gastrocnemius force. In summary, the force distribution differed only between anatomical rotational variants and the simplified model insertion, M1.

A significant increase in the soleus peak force was observed in M2 compared to A2, A3 and M1. This increase was observed to occur before the toe-off event and seemed



to result in a sharing of the force from MG (Figure 5.6). For the peak Achilles tendon forces, the only differences were a lower force for M1 compared with that for A1 and M2. No significant differences in these forces were noted between other insertion types (Figure 5.7).

The muscle force pattern similarities are shown in Table 5.2. Excellent similarities were noticed in the Achilles tendon force, good to excellent similarities were seen in overall gastrocnemius force. For the soleus, there was a good similarity between A2 and A3, the remainder showed moderate to poor similarity.

Lateral head of gastrocnemius				
	A1	A2	A3	M1
A2	0.8189	--	--	--
A3	0.4733	0.5467	--	--
M1	0.7978	0.8178	0.4633	--
M2	0.8800	0.7656	0.4122	0.8211
Medial head of gastrocnemius				
	A1	A2	A3	M1
A2	0.9222	--	--	--
A3	0.7756	0.8944	--	--
M1	0.7767	0.6333	0.3756	--
M2	0.8700	0.7278	0.4867	0.8900
Gastrocnemius				
	A1	A2	A3	M1
A2	0.9544	--	--	--
A3	0.9589	1.0000	--	--
M1	0.9367	0.9422	0.9411	--
M2	0.9644	0.8878	0.8911	0.9456
Soleus				
	A1	A2	A3	M1
A2	0.5744	--	--	--
A3	0.6778	0.8711	--	--
M1	0.4911	0.4267	0.4778	--
M2	0.7400	0.2878	0.3911	0.6111
Achilles tendon				
	A1	A2	A3	M1
A2	0.9989	--	--	--
A3	0.9956	0.9978	--	--
M1	0.9911	0.9911	0.9878	--
M2	0.9956	0.9944	0.9956	0.9811

**Table 5.2 – The coefficient of multiple correlations of the activation pattern during a gait cycle (n=9) between different insertional variants.**

For Achilles tendon forces in all insertional types, excellent similarities (CMC > 0.95) were noted.

## 5.4 Discussion

This is the first study to include the rotational fibre bundle structure of the Achilles tendon in musculoskeletal modelling. Since the Achilles tendon insertion is the most sensitive parameter in overall muscle prediction, the inclusion of appropriate anatomy is important to achieve accurate muscle force prediction. The anatomical variants (A1, A2, and A3) showed different force distribution patterns in LG and MG compared with modelled insertions (M1, M2). However, the overall Achilles tendon forces remained the same.

### 5.4.1 Rotational insertions vs. simplified insertions

In the peak Achilles tendon force, there were no differences between M2 and other anatomical variants, but M1 had a lower peak force than A1. This suggests that a simplified, single insertion on the calcaneus for triceps surae could achieve the same results as the anatomical insertions, but a bilateral insertion will result in a lower predicted Achilles tendon force. This was expected, as a bilateral insertion will have an increased moment arm for inversion and eversion. This demonstrates that the use of a single insertion point is appropriate (particularly for overall tendon force), as has been done in previously published musculoskeletal models (Carbone et al., 2012). However, using a single insertion will lead to a higher calculated soleus force than that obtained from the anatomical variants.

The muscle activation patterns of soleus and gastrocnemius for rotational insertions (A1, A2, A3) were consistent with the normalized electromyography reported in the literature (Huang and Ferris, 2012; Pourmoghaddam et al., 2016) (Figure 5.8). As in a normal gait cycle, the MG activates more than LG (Huang and Ferris, 2012). The

comparison also showed a higher activation in the LG, whereas it showed a lower activation in the soleus.

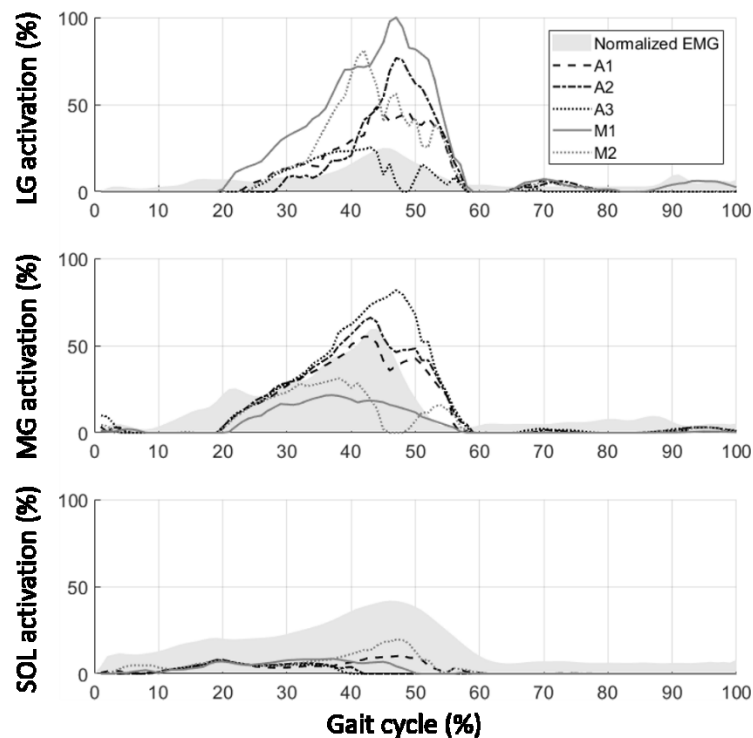


**Figure 5.8 – The median muscle activation (n = 9) of the different insertional variants of the Achilles tendon compared with normalized EMG from the literature.**

The medial and lateral gastrocnemius EMG signal during walking at 1.0m/s, normalized by walking 1.6m/s (Huang and Ferris, 2012), and the soleus EMG signal during walking at 1.1 m/s, normalized by 3.3 m/s (Pourmoghaddam et al., 2016).

In addition, the peak force magnitude of the Achilles tendon during gait has been measured *in vivo* using a buckle transducer as 2600 N (Komi et al., 1992), while the model calculated a median peak force of 2720 N (total range: 1848 - 3596 N) in this study. Furthermore, several studies have reported the use of ultrasound elastography to evaluate the differential displacement and elongation between superficial and deep fibres of the Achilles tendon, in which the superficial tendon fibres showed 16%-29% greater peak elongation than the deep tendon fibres. As the superficial fibres derive

from MG and deep fibres from soleus (Edama et al., 2015; Szaro et al., 2009), an increased MG force could increase the elongation of the superficial part of the tendon.

From the muscle force predictions, across different rotations for each subject, similar patterns of overall gastrocnemius and Achilles tendon force were observed. The model seems to predict the Achilles and overall gastrocnemius force, and then distribute the force among triceps surae. The soleus plays the role of making up the difference between the Achilles tendon force and the gastrocnemius; therefore, low activation and hence high variation was observed in the soleus force.

#### **5.4.2 The effect of rotation on modelling output**

In the rotational variants, it was observed that the MG force in the midstance phase of the gait cycle gradually increased as the degree of rotation increased (Figure 5.7). An increased MG force could increase differential loading within the Achilles tendon. Such differential loading could potentially increase the risk of microtrauma between the tendon fibres and lead to midportion Achilles tendinopathy.

After mapping the Achilles fibre components from the literature onto the insertional areas segmented from MRI scans, it was observed that although the degree of rotation varied, the centroid of MG remained at a similar location. The LG and soleus insertions changed to a greater extent (Figure 5.9).

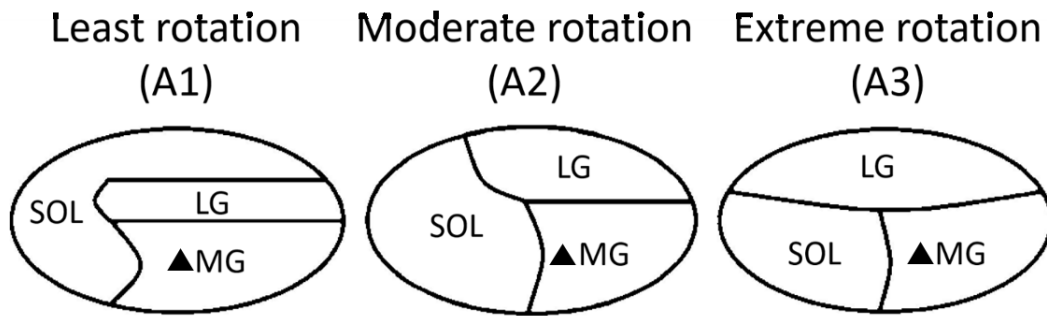


**Figure 5.9 – The difference between of medial gastrocnemius insertion locations (triangles) in different Achilles tendon insertion patterns.**

---

In A1, a second peak in the soleus force during the midstance phase was noticed (Figure 5.6); in A2 and A3, this peak appeared in the MG force. This observed peak in A1 corresponded to the peak activity in the normalized soleus EMG (Figure 5.8). This peak in soleus force was contributed by the soleus muscle fibres located at the anterior aspect of the Achilles tendon insertion. As the degree of rotation increased and the anterior soleus fibre bundles migrated to the medial side, the activation decreased. As a result, a very good similarity in soleus force pattern was noted between A2 and A3 (CMC = 0.87), but a poor similarity was noted between A1 and A2 (CMC = 0.57).

This work investigated changes in the moment arm as a result of different degrees of rotation. Although the location of the joint centre is also another potentially important factor, this study sought to control this factor. In the anatomical datasets of the FreeBody model, the ankle joint centre is predefined based on the midpoint of the medial and lateral malleoli. Changing the ankle joint centre would not only change the moment arm in the optimization process but also change the joint torque estimation in the inverse dynamics analysis.

There are several limitations to this study. First, the muscles presented in the FreeBody model are simply muscle lines of action and activation does not take into account the velocity and lengthening/shortening status of the muscle. As the motions performed did not involve significant flexion/extension of the joint, and the muscles do not become lengthened/shortened too much to compromise the force-generating capacity, this limitation is mitigated. Second, there is no information regarding the actual rotational geometry of the Achilles tendons of these subjects, as it is not possible to detect the rotation pattern *in vivo* through imaging or other methods. Therefore, although this study identifies the effect of anatomical variants, it does not provide a means to relate this to an individual's own anatomy. Finally, the possible differences in tendon mechanical properties caused by the rotation were not considered in this model. In other musculoskeletal models that include the elastic properties of the tendon, the force prediction of the muscle could be affected. However, as tendons are not modelled in FreeBody, the possible change in tendon property caused by the different degrees of tendon rotation will not affect the muscle force predictions in this study.

## 5.5 Conclusion

The introduction of rotational variants of the Achilles tendon changed the force distribution within triceps surae, but the overall Achilles tendon force was not changed. Modelling the Achilles tendon with a single insertion is justified only when targeting the overall Achilles tendon force, as higher soleus peak force and lower MG forces were observed, compared with more anatomical geometries.

As the degree of rotation increases, the MG force increases. The differential loading within in the Achilles tendon could be affected by the rotational fibre structure and could increase the risk of microtrauma and lead to midportion Achilles tendinopathy.

In this chapter, differences in the force distribution between MG, LG and soleus were observed. The model tends to activate LG more than soleus during a gait cycle. In the model, soleus is a stronger muscle than gastrocnemius as the PCSA of soleus is six times greater. Therefore, it seems counter-intuitive that a muscle with a smaller cross-sectional area will be activated more than a significantly stronger muscle. It is worth exploring, therefore how the model is distributing the force and how it optimizes the muscle forces. These points are addressed in the subsequent chapter.



## **Chapter 6**

# **A biomechanical comparison of rehabilitation protocols for midportion Achilles tendinopathy: eccentric loading and heavy slow resistance training**

The last two chapters addressed the quantification of Achilles tendon forces using musculoskeletal modelling. This chapter pulls together the prior work in the thesis to quantify Achilles tendon forces during two standard rehabilitation exercises for Achilles tendinopathy. As described in Chapter 2, there are two protocols that are commonly used for midportion Achilles tendinopathy: eccentric loading and heavy slow resistance training. In this chapter, the forces experienced by the Achilles tendon during these rehabilitation exercises will be calculated. This could facilitate a better understanding of the mechanism of tendon healing and propose improvements in the rehabilitation protocol.

## 6.1 Introduction

As discussed in Chapter 2, the Achilles tendon is frequently affected by tendinopathy. It has been reported that it accounts for 50% of Achilles tendon disorders and, amongst these, two-thirds are midportion Achilles tendinopathy (Jarvinen et al., 2001).

Rehabilitation exercises have played an important role in the treatment of midportion Achilles tendinopathy. Over recent decades, the eccentric loading protocol proposed by Alfredson et al. (1998) has become the mainstream choice for rehabilitation. The protocol emphasizes applying loading to the Achilles tendon at a controlled speed using an eccentric (heel drop) motion. The rationale for eccentric exercise is that the tendon may be loaded to a greater extent during eccentric motion, as compared to concentric motion, and thus the activity could stretch the tendon more. As described in Chapter 2, stretching or loading within the tendon could be a stimulus for tendon healing. However, a study that used ultrasound and motion capture to estimate Achilles tendon moment arm and quantified loading of the Achilles tendon during eccentric and concentric motions showed that there is no significant difference in the force-displacement behaviour of the tendon between the concentric and eccentric phases of motion (Chaudhry et al., 2015). Despite a clinical randomized control study showing better outcomes for eccentric than concentric rehabilitation (Mafi et al., 2001), systemic reviews conclude there is no convincing mechanical evidence to support the eccentric component (Malliaras et al., 2013).

Recently, a heavy slow resistance protocol for Achilles tendinopathy has been proposed, based on a similar protocol for patellar tendinopathy (Beyer et al., 2015; Kongsgaard et al., 2009). A randomized controlled trial comparing heavy slow

resistance training to traditional eccentric loading in patients with midportion Achilles tendinopathy reported only a borderline more favourable outcome at 12 weeks ( $p = 0.052$ ) and no difference at 52 weeks for the heavy slow resistance group, but that time taken for these participants to perform this protocol was one-third of the time taken for the eccentric loading protocol (Beyer et al., 2015).

However, the biomechanical mechanisms that achieve such efficient training have not been elucidated. It is also still not clear whether the eccentric or concentric protocol is more effective for Achilles tendon rehabilitation.

The modelling techniques described in the previous chapters can be used to quantify Achilles tendon loading. We hypothesized Achilles tendon force will be the same in eccentric and concentric phase. The aim of this study was to quantify the change of the Achilles tendon force in response to the external loading and different postures in the two commonly used rehabilitation activities. Through the analysis of the tendon force, the mechanism of the tendon loading, and efficiency of the heavy slow resistance protocol can be further understood. This can be used to further optimize rehabilitation protocols to increase the loading of the Achilles tendon during the rehabilitation exercises.

## **6.2 Methods**

### **6.2.1 Participants**

Eighteen healthy volunteers (11 male, 7 female, age:  $29.6 \pm 3.8$  years) from the imaging study presented in Chapter 3 were recruited. Participants were included if they

had no recent lower limb musculoskeletal injury or any other physical condition that would prevent them from performing the rehabilitation exercises. This study was approved by the Imperial College Research Ethics Committee (18IC4371, Appendix B).

## **6.2.2 Experimental protocol**

Participants were instructed to perform the exercises for both the eccentric loading protocol and the heavy slow resistance protocol, as described in Chapter 2. For the eccentric program, heel drop was performed both with knees flexed and knees straight. For the heavy slow resistance protocol (Figure 2.11), only the seated calf-raise and standing heel rise with the knee extended, as described in Chapter 2, were performed. The ankle push-off activity in a seated leg press machine with the knees extended was not performed, as the required knee and ankle angles were the same as those for the standing heel rise with knee extended activity. Participants were instructed to perform the exercises in both standing and seated positions with the toes of the right leg on the edge of a step and the heel unsupported. Participants were then instructed to perform three seconds of heel rise, from maximum dorsiflexion to maximum plantarflexion, followed by three seconds of heel drop, back to maximum dorsiflexion. Timings for each cycle were read out to the participants during the experiment.

As described in Chapter 2, the standard eccentric loading exercise uses a backpack for patients to apply extra loading at home, whereas the heavy slow resistance training requires gym equipment. In the original protocol, the patients are instructed to perform the activity to complete the exercise with tolerable pain. Therefore, each patient is likely to carry a different load according to their strength and severity of the tendinopathy. However, this study sought to quantify the loading of the Achilles tendon under

different loading conditions and rehabilitation postures. Therefore, the external loading applied was scaled to patient body weight. To control the loading conditions, a commercially available Smith machine (Marcy, Pomona, CA, U.S.) was used (Figure 6.1). This machine allows the same loading direction and the same range of motion as the standing heel rise with knee extended to be applied. A sponge cushion was wrapped in the centre of the bar to ensure a comfortable contact. To standardize the bar position between participants in the heavy slow resistance exercise, in the standing position, the bar was held on the shoulders with two hands and the bar was aligned vertically with respect to the posterior edge of the right heel. In the seated position, the bar was aligned with the right big toe, whilst the knee was in a flexed position, enabling the bar to rest on the thigh (Figure 6.1)

---

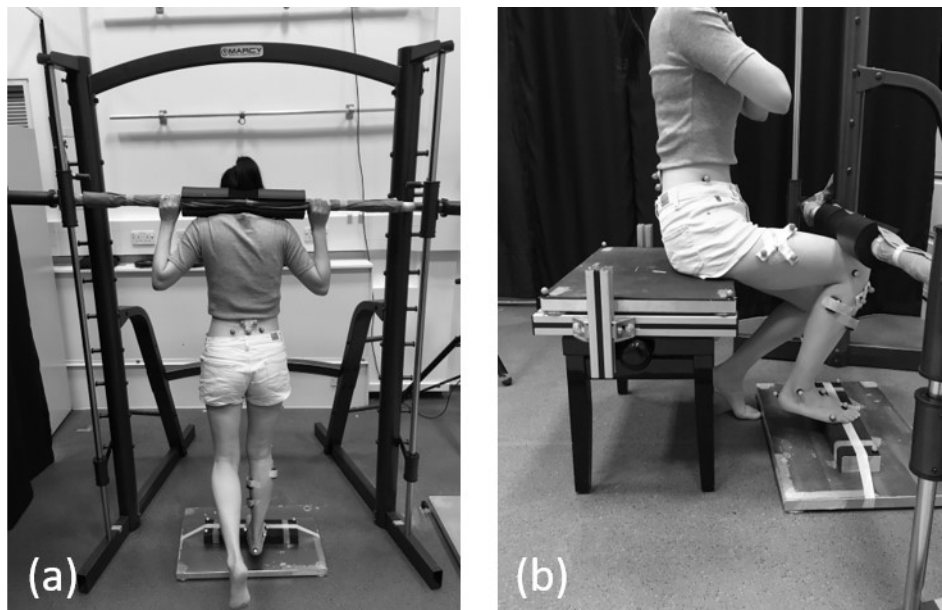


**Figure 6.1 – The (a) standing heel rise and (b) seated calf-raising performed with a Smith machine.**

---

For the eccentric loading exercise, only one loading condition was tested. The participants were asked to lift a bar (8 kg) without added weight and perform the heel

rise and heel drop exercise. No additional loading was added, because some participants could not lift any additional weight during the knee bent heel rise and drop exercise in the pilot study. For the heavy slow resistance, four loading conditions were performed: with no extra mass, with a bar (8 kg, or approximately 8%-16% body weight, BW) without additional added weight, with 25% BW including the bar, and with 50% BW including the bar. Three cycles were performed for each loading condition. A resting period of 2 minutes was administered between each loading condition. The combinations of the loading condition and posture are summarized in Table 6.1.

Order	Loading condition
1.	HSR -- Standing knee straight heel rise and drop with additional 25% BW (x 3 reps)
2	HSR -- Standing knee straight heel rise and drop with additional 50% BW (x 3 reps)
3	HSR & ECC -- Standing knee straight heel rise and drop with a bar of 79 N (x 3 reps)
4	HSR -- Standing knee straight heel rise and drop without bar (x 3 reps)
5	ECC -- Standing knee bent heel rise and drop with a bar of 79 N (x 3 reps)
6	HSR -- Seated calf-raise and drop with additional 25% BW (x 3 reps)
7	HSR -- Seated calf-raise and drop with additional 50% BW (x 3 reps)
8	HSR -- Seated calf-raise and drop with a bar of 79 N (x 3 reps)
9	HSR -- Seated calf-raise and drop without bar (x 3 reps)

**Table 6.1 – The loading condition and the activity performed**

Activities are listed in the order in which they were performed. Each loading condition was separated by a rest period of 2 minutes. HSR: the activity belongs to the heavy slow resistance protocol. ECC: the activity belongs to the eccentric loading protocol.

The order of the activities was the same for every participant. No randomization of the protocol was performed in this study as the pilot testing found that some participants were not able to perform the standing 50% BW when it was performed at the end of the

series of trials. Therefore, the trials with standing knee straight heel rise and drop with additional 25% BW and 50% BW were performed first.

### 6.2.3 Kinematic and kinetic data collection

Twenty-three reflective markers were attached to the skin of each participant to enable the measurement of lower limb kinematics. The markers and their locations are shown in Figure 7.2. The marker positions were measured with a 10-camera optical motion capture system (Vicon Motion Systems, Oxford, UK). An additional two markers were attached to the ends of the bar to measure the bar displacement.

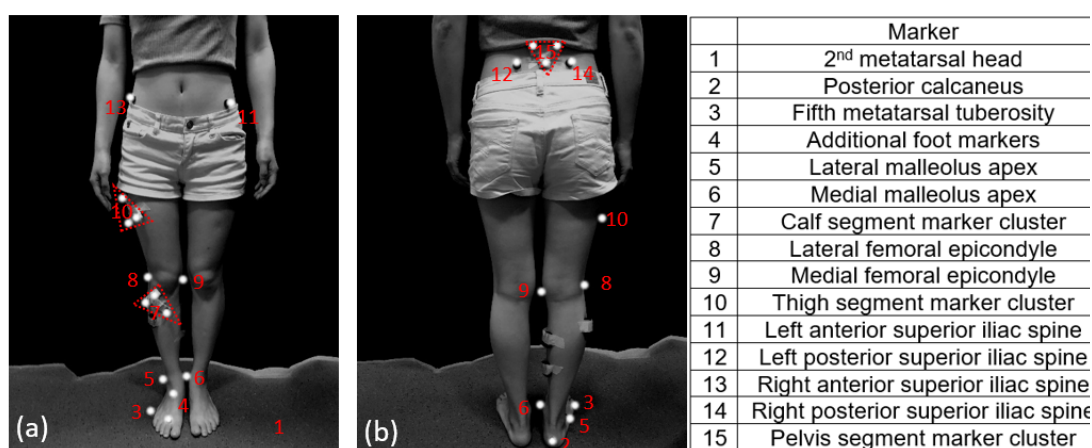


**Figure 6.2 – (a) Anterior and (b) posterior views of the twenty-three reflective markers used in the trial, consisting of 12 single markers and 9 clusters, each of three markers**

Two force platforms (Kistler Instrument Corp., Winterthur, Switzerland) were used to quantify the forces between the participants and their surroundings. One was placed on the ground to measure the ground reaction force and the other was placed on an adjustable chair to record the force on the seat. A step of dimensions



91 mm × 410 mm × 57 mm (l × w × h) was attached to the middle of the force plate on the ground. Participants were asked to perform heel rise and drop with only the forefoot on the step to mimic the motion performed during rehabilitation (Figure 7.1).

The kinematic marker data were collected at 120 Hz and the ground reaction forces at 2160 Hz. The recorded ground reaction forces were filtered through a 4<sup>th</sup> degree Butterworth low pass filter with a cut-off frequency of 4 Hz (Winter, 2009) followed by a down-sampling to 120 Hz.

## **6.2.4 Musculoskeletal modelling**

The FreeBody model, described in Chapter 5, was used to calculate the torque around the joints and the muscle forces during the motion. Within FreeBody, the joint torque was calculated based on inverse dynamics with the mass, centre of mass, and inertial parameters of the body segments derived from published anthropometric data (de Leva, 1996).

To allow subject-specific representations of muscle capacity, physiological cross-sectional areas of the muscles were estimated based on regression equations of muscle volume in the literature (Handsfield et al., 2014; Ward et al., 2009). This was achieved by estimating the overall lower limb muscle volume using the participant's height and weight, and then dividing the total muscle volume based on the proportions reported by Handsfield et al. (2014). Each individual muscle volume was then divided by the muscle fibre length reported by Ward et al. (2009) to obtain the physiological cross-sectional area. In this way, the maximum force capacities of each participant were different.

There are nine sets of muscle lines of action, segmented from nine different individuals, in the anatomical dataset that is associated with FreeBody. For each participant, the muscle lines were chosen based on the dataset with the same gender and closest body mass. This was found in a previous study to be the scaling that most accurately quantifies ankle joint forces (Ding et al., 2018). The Achilles tendon insertion was modelled with the least rotation, as it accounts for 50% of the population and, as shown in Chapter 3, use of this model did not result in any difference in the total Achilles tendon force when compared with the force predicted using the other anatomical insertions.

### **6.2.5 Achilles tendon force estimation**

The muscle force calculation based on the optimization process will account for the co-activation of multiple muscles to achieve a motion. However, it is difficult to validate the level of co-activation. The co-activation presented in the model might be ‘mathematical’ but not physiological. An alternative way to estimate the Achilles tendon force is to estimate the tendon moment arm based on ultrasound (Manal et al., 2013), MRI (Maganaris et al., 1998), or bony landmarks, and then the tendon force can be calculated by dividing the ankle torque by the estimated moment arm. This assumes the Achilles tendon provides all the torque for ankle motion and that the ankle joint has only one degree of freedom and, as such, accounts for zero co-activation. However, as described in Chapter 2, the Achilles tendon force was estimated to provide 90% of ankle plantarflexion torque. Therefore, such a simplified model can still be used to estimate the Achilles tendon force.

In this study, the tendon force was quantified using both methods. After the joint torque was calculated using inverse dynamics, the Achilles tendon force was calculated

using constrained optimization, as introduced in Chapters 5 and 6 (termed ‘FreeBody model’) and using subject-specific moment arms obtained from MRI (termed ‘subject-specific MRI model’).

In this study, the subject-specific moment arms were obtained from the static MRI scans acquired as described in Chapter 3 in which the ankle joint was scanned at 20° and 10° in dorsiflexion, 0°, 15°, 30°, and 45° in plantarflexion. In each joint position for each participant, a sphere was fitted to the talar dome using Mimics Innovation Suite (v.19, Materialise, Belgium). The centre of the sphere was defined as the centre of rotation of the joint (Figure 7.3). The Achilles tendon in each joint position was segmented and the line of action was determined by the centerline of the tendon, as calculated in MATLAB (2017a, MathWorks, Massachusetts, USA) (Figure 7.3).

Therefore, two modelling methods were performed in this study. Due to the infeasibility of validating the Achilles tendon force *in vivo*, there was no means to determine which modelling method was better or more accurate. These two modelling methods each have their own weaknesses. However, we could gain more confidence in the results if the two models showed the same trend in the Achilles tendon force pattern during the rehabilitation activity tested.

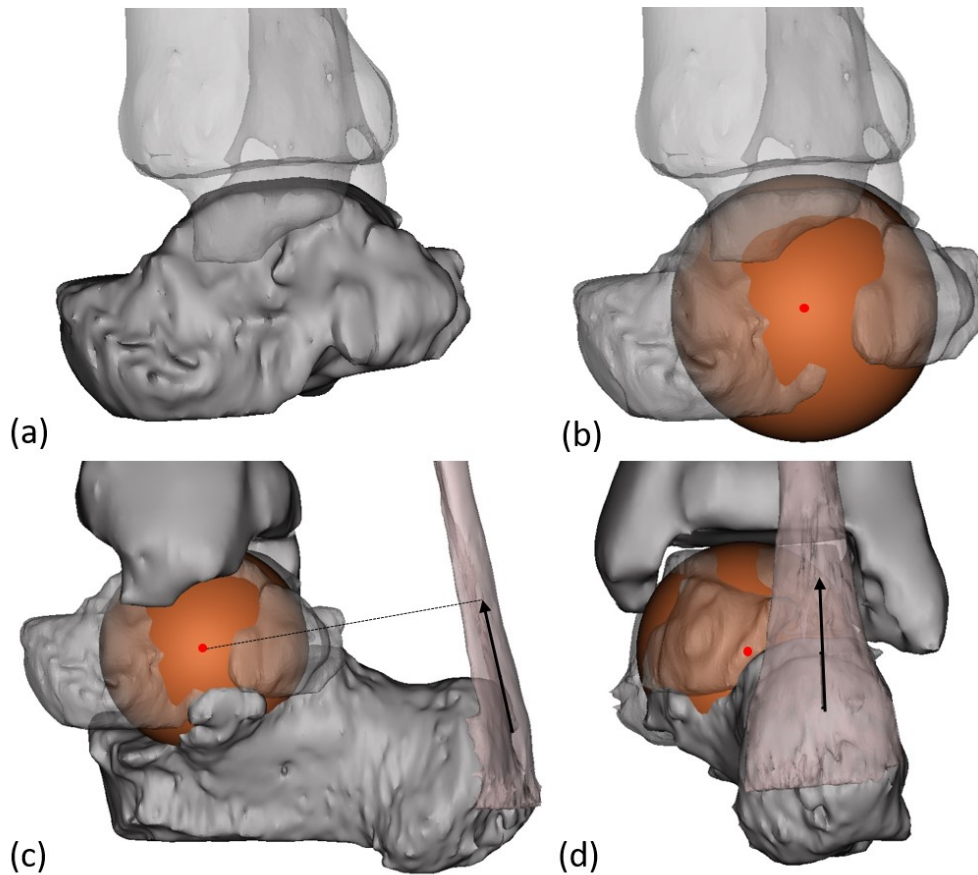


**Figure 6.3 – Determination of a subject-specific ankle centre of rotation of the ankle, and Achilles tendon line of action and moment arm.**

(a) The segmented tibia and fibula end and talus. (b) The sphere fit to the talar dome, the centre of the sphere is the estimated centre of rotation (red dot). (c) Lateral view of the Achilles tendon and force vector (black arrow) and effective moment arm (dotted line). (d) The posterior view of the Achilles tendon force vector (black arrow).

If the motion performed during the exercise went beyond the range of motion of the MRI scans ( $20^\circ$  dorsiflexion through  $45^\circ$  plantarflexion), the moment arm was linearly extrapolated from those in  $10^\circ$  and  $20^\circ$  dorsiflexion. Such extrapolation was based on the relationship between forefoot and hindfoot motion during dorsiflexion. The forefoot can bear a larger range of motion than the hind foot, but the movement of the two are proportional (Gatt et al., 2011).

### 6.2.6 Statistical analysis

The moment arm of the Achilles tendon calculated from MRI was compared with the moment arm estimated by the model using a Wilcoxon rank sum test, as participants' range of motion varied. In order to compare ankle torque and the Achilles tendon force across participants, the calculated torque and force were normalized by the participant's BW. The normalized torque during the motion in concentric (heel rise) and eccentric (heel drop) phases were compared using Wilcoxon signed ranked tests for paired data and the p-value was adjusted using Bonferroni correction with significant level defined as  $p < 0.05$ .

To assess possible predictors of normalized peak Achilles tendon force, stepwise multivariate regression analyses were carried out with five parameters, including external loading condition, weight, height, sex, and peak dorsiflexion angle. As the protocols were performed in standing and seated postures and the tendon forces were estimated using moment arms determined from MRI and musculoskeletal modelling, there were four regression models. The rate ratio, 95% confidence interval, and p-values of the significant predictors were reported. Computations were carried out using IBM SPSS software (v23.0, IBM Corp., Armonk, New York).

## 6.3 Results

### 6.3.1 The ankle torque and the Achilles tendon moment arm estimated during ECC and HSR

The normalized ankle torque over the joint range of motion during ECC and HSR are presented in Figure 6.4. The knee bent activity in ECC had the largest dorsiflexion angle amongst all the activities. In all the activities, the ankle torque increased with dorsiflexion. The peak ankle torque during knee straight and knee bent in ECC and eccentric and concentric phase in HSR are presented in Table 2.1. The concentric ankle torques were larger than eccentric in standing with additional 50% BW and 25% BW and in seated with 50% BW, 25% BW and the 8 kg bar.

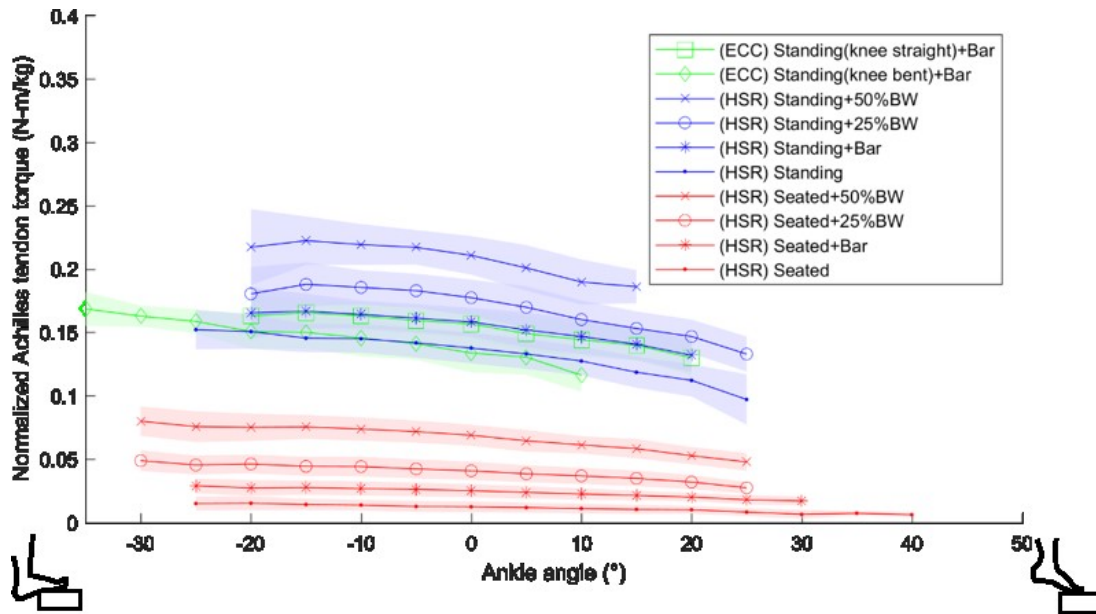


Figure 6.4 - Normalized ankle torque (mean  $\pm$  one standard deviation) for 18 participants over the range of motion for eccentric loading (ECC) and heavy slow resistance (HSR).

As participants had different ranges of motion, only the joint angle ranges that were achieved by more than half of the participants are shown.

ECC		
Peak normalized ankle torque (N-m/kg)	Knee straight	Knee bent
	0.171 ± 0.012	0.164 ± 0.013
HSR		
Peak normalized ankle torque (N-m/kg)	Concentric	Eccentric
Standing + 50% BW	0.230 ± 0.016	0.226 ± 0.015*
Standing + 25% BW	0.196 ± 0.015	0.191 ± 0.014*
Standing + 8kg bar	0.175 ± 0.010	0.171 ± 0.012
Standing	0.155 ± 0.013	0.153 ± 0.012
Seated + 50% BW	0.087 ± 0.009	0.077 ± 0.009**
Seated + 25% BW	0.053 ± 0.007	0.046 ± 0.008**
Seated + 8kg bar	0.034 ± 0.004	0.029 ± 0.005**
Seated	0.016 ± 0.004	0.017 ± 0.005

**Table 6.2 – The peak normalized torque in eccentric loading (ECC) and heavy slow resistance exercise (HSR). \*: p<0.05, \*\*: p<0.01, Wilcoxon signed rank test with Bonferroni correction.**



The Achilles tendon moment arm estimated from the FreeBody model and the subject-specific MRI are shown in Figure 6.5. The Achilles tendon moment arm measured from subject specific MRI scans was significantly larger than the moment arm predicted by the FreeBody model.

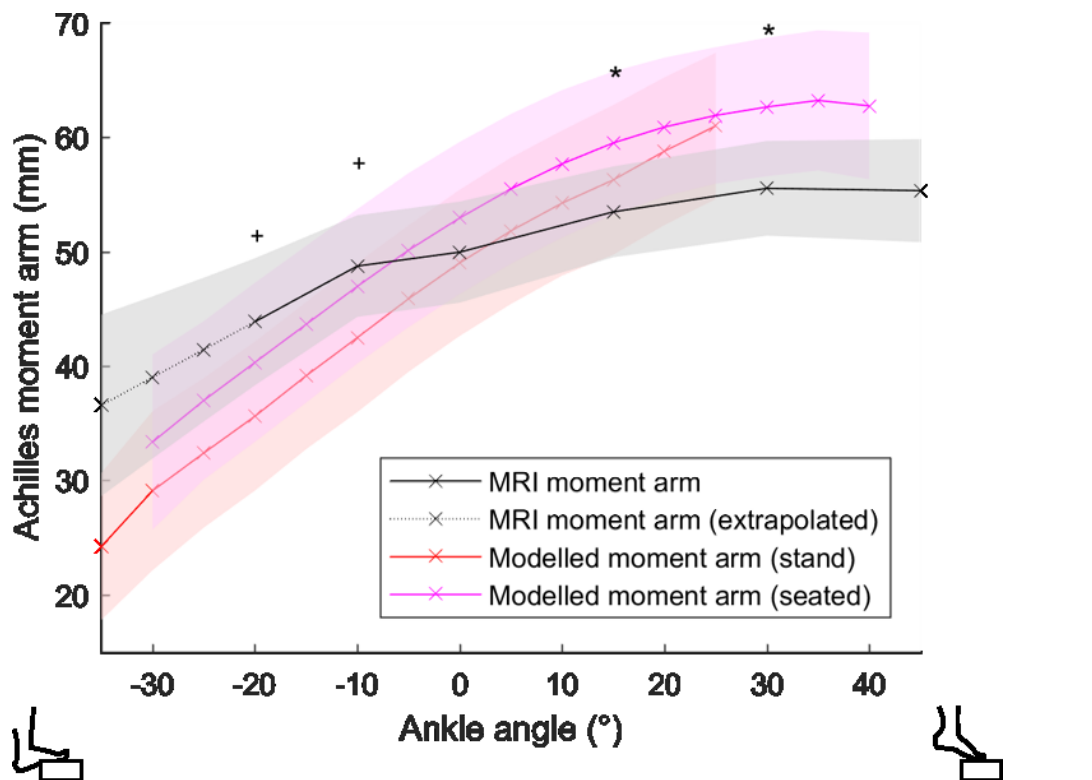


**Figure 6.5 - The Achilles tendon moment arm (mean  $\pm$  one standard deviation) from the scaled model and subject-specific MRI scans of 18 participants over a range of joint angles.**

As participants had different ranges of motion, only the joint angles that were achieved by more than half of the participants are shown. For dorsiflexion angles of less than  $-20^\circ$  obtained using MRI, the moment arms were extrapolated based upon the points at  $-10^\circ$  and  $-20^\circ$  (black dotted line). Statistical comparisons were performed using the Wilcoxon rank sum test. \*:  $p\text{-value} < 0.05$ , between MRI moment arm and modelled moment arm in the seated position. +:  $p\text{-value} < 0.05$ , between MRI moment arm and modelled moment arm in the standing position.

### 6.3.2 Achilles tendon force estimation from FreeBody model

The Achilles tendon forces over the ankle joint range of motion predicted by the FreeBody model are shown in Figure 6.6. The predicted Achilles tendon force increased as the ankle dorsiflexed. The peak Achilles tendon force seen in ECC and HSR were shown in Table 6.3. For ECC, the peak Achilles tendon force in knee bent is larger than knee straight. There were no significant differences in concentric force and eccentric in all exercises in HSR, except the Achilles tendon force in concentric is larger than eccentric in seated with bar.

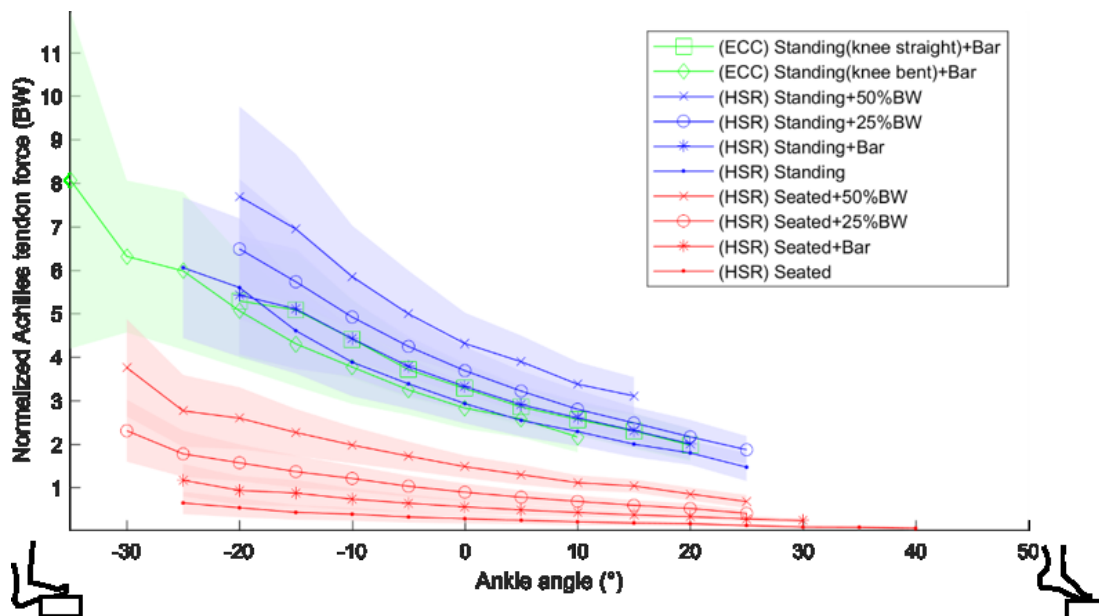


Figure 6.6 - Achilles tendon force (mean  $\pm$  one standard deviation) over ankle joint range of motion estimated by FreeBody for 18 participants, during the eccentric loading (ECC) and heavy slow resistance protocol (HSR) for different external loading conditions

ECC		
Peak Achilles force (BW)	Knee straight	Knee bent
	5.548 ± 1.586	7.678 ± 3.083**
HSR		
Peak Achilles force (BW)	Concentric	Eccentric
Standing + 50%BW	7.721 ± 2.603	7.878 ± 2.504
Standing + 25%BW	6.276 ± 1.832	6.486 ± 1.904
Standing + 8kg bar	5.503 ± 1.808	5.548 ± 1.586
Standing	5.650 ± 2.082	5.855 ± 2.116
Seated + 50%BW	3.916 ± 1.499	3.694 ± 1.930
Seated + 25%BW	2.475 ± 1.283	2.175 ± 1.190
Seated + 8kg bar	1.526 ± 0.717	1.365 ± 0.860*
Seated	0.687 ± 0.407	0.746 ± 0.460

**Table 6.3 - The peak Achilles tendon force predicted by FreeBody in eccentric loading (ECC) and heavy slow resistance (HSR) exercise. \*: p<0.05, \*\*: p<0.01, Wilcoxon signed rank test, with Bonferroni correction.**

### 6.3.3 Achilles tendon force estimation from the subject-specific MRI model

The Achilles tendon force predicted by subject-specific MRI model is shown in Figure 6.7. The same trend was found in the Achilles tendon force pattern. The maximum force predicted by the subject-specific MRI is shown in Table 6.4. The Achilles tendon force in the concentric phase is larger than eccentric phase in the seated position with external loading.

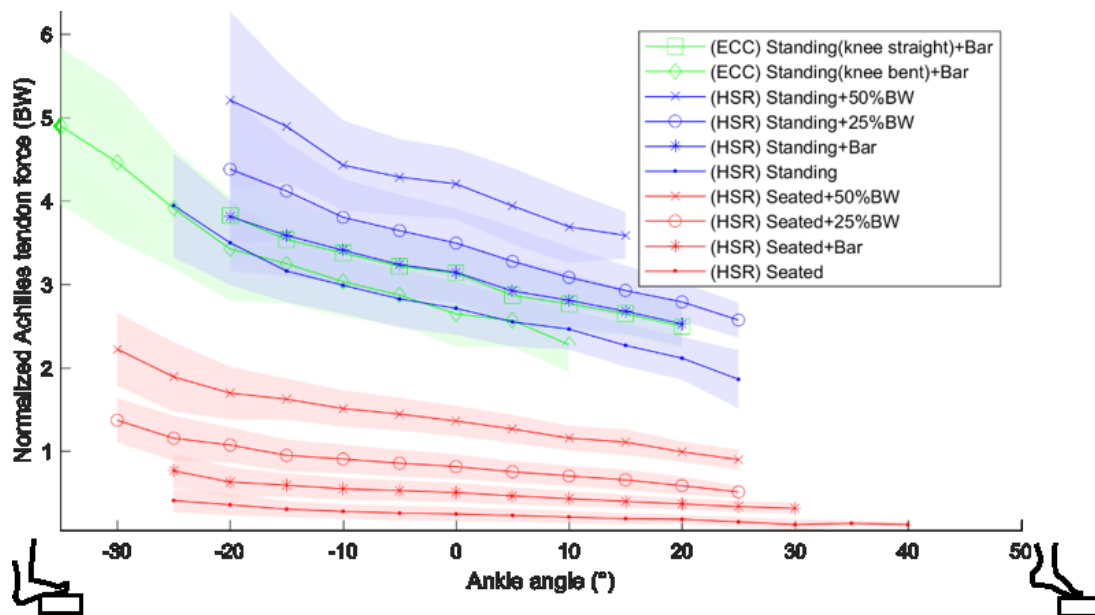


Figure 6.7 - Achilles tendon force (mean  $\pm$  one standard deviation) over ankle joint range of motion estimated by subject-specific MRI model for 18 participants, during the eccentric loading (ECC) and heavy slow resistance protocol (HSR) for different external loading conditions.

ECC		
Peak Achilles force (BW)	Knee straight	Knee bent
	3.775 ± 0.573	4.378 ± 1.158*
HSR		
Peak Achilles force (BW)	Concentric	Eccentric
Standing + 50%BW	5.053 ± 0.829	5.118 ± 1.032
Standing + 25%BW	4.320 ± 0.786	4.338 ± 0.910
Standing + 8kg bar	3.794 ± 0.544	3.775 ± 0.573
Standing	3.557 ± 0.662	3.607 ± 0.711
Seated + 50%BW	2.288 ± 0.635	2.041 ± 0.633**
Seated + 25%BW	1.388 ± 0.423	1.213 ± 0.455**
Seated + 8kg bar	0.892 ± 0.283	0.753 ± 0.288**
Seated	0.408 ± 0.173	0.430 ± 0.176

**Table 6.4 - The peak Achilles tendon force predicted by subject-specific MRI model in eccentric loading (ECC) and heavy slow resistance (HSR) exercise.**

**\*: p<0.05, \*\*: p<0.01, Wilcoxon signed rank test, with Bonferroni correction.**

### **6.3.4 Multivariate analysis**

A multivariate analysis of the normalized peak Achilles tendon force is shown in Table. The external loading and peak dorsiflexion angles were significant predictors of normalized peak Achilles tendon force during the heavy slow resistance cycle. The rate ratios for external loading were similar in standing and seated conditions, while the rate ratio for the peak dorsiflexion angle increased 50% in FreeBody model and 100% in simplified model in the standing position (Table 6.5).

Multivariate regression analysis of normalized peak Achilles tendon force				
Seated (FreeBody)			Adj. R <sup>2</sup> : 0.687	
Predictor	Rate ratio	Lower	Upper	p-value
Loading (N/BW) <sup>1</sup>	5.783	4.497	7.069	<0.001
Peak angle (°) <sup>2</sup>	-0.10	-0.129	-0.07	<0.001
Seated (MRI)			Adj. R <sup>2</sup> : 0.843	
Predictor	Rate ratio	Lower	Upper	p-value
Loading (N/BW)	3.394	2.98	3.808	<0.001
Peak angle (°)	-0.034	-0.043	-0.024	<0.001
Standing (FreeBody)			Adj. R <sup>2</sup> : 0.555	
Predictor	Rate ratio	Lower	Upper	p-value
Body mass (kg)	-0.960	-0.128	-0.061	<0.001
Loading (N/BW)	5.553	3.446	7.660	<0.001
Peak angle (°)	-0.155	-0.222	-0.088	<0.001
Female sex	-1.112	-1.935	-0.290	<0.01
Standing (MRI)			Adj. R <sup>2</sup> : 0.617	
Predictor	Rate ratio	Lower	Upper	p-value
Loading (N/BW)	3.353	2.725	4.342	<0.001
Peak angle (°)	0.072	0.047	0.098	<0.001
Body mass (kg)	-0.021	-0.033	-0.008	<0.01

**Table 6.5 – Multivariate regression analysis of the normalized peak Achilles tendon force during standing and seated motions in the heavy slow resistance protocol.**

<sup>1</sup> the additional loading applied; <sup>2</sup> the peak dorsiflexion achieved during the motion

## 6.4 Discussion

This study compared the magnitude of the Achilles tendon force during different rehabilitation exercises, to clarify the role of eccentric exercise compared with concentric exercise and to identify the significant factors that affect the peak force seen by the tendon. The key findings in this study include: (i) The Achilles tendon force is greater in dorsiflexion than in plantarflexion (ii) the peak Achilles tendon force in eccentric is not greater than concentric phase (iii) the range of motion of the ankle can be a critical predictive factor of normalized peak Achilles tendon force during motion.

The loading of the Achilles tendon could be an important factor affecting the effectiveness of rehabilitation. However, due to the infeasibility of direct force measurement *in vivo*, a musculoskeletal model was used to estimate the ankle torque, and then the tendon force was estimated using FreeBody and a simplified model with subject-specific Achilles moment arm. This parallel estimation of the force was to compare the predictions from the two models. The two modelling results showed similar trends but different magnitudes in the Achilles tendon force during the range of motion. Due to the infeasibility to measure the actual Achilles tendon force, it is challenging to determine which modelling method is better. Both methods were used in motion analysis and the relative trend is the same. The FreeBody model consistently predicted a significantly larger peak force than the simplified model did. This is likely due to the coactivation of other muscles and smaller moment arms estimated with the FreeBody in dorsiflexion angles. Since validation against the actual Achilles tendon force is impossible, the comparison here quantified the possible difference using different methodology.



### **6.4.1 Achilles tendon moment arm at extreme dorsiflexion**

As the maximum tendon forces occurred during dorsiflexion, the estimation of the tendon moment arm during extreme dorsiflexion positions is critical. The dorsiflexion angle quantified in the motion analysis lab was higher than that obtained while the foot was in the MRI scanner. This was likely due to external loading that further pushed the ankle into extreme ranges of motion, beyond the range that can be captured during MRI.

In this study, the MRI moment arm in dorsiflexion was extrapolated based on the relative forefoot and hindfoot kinematics reported in the literature (Gatt et al., 2011). The weakness of such extrapolation is acknowledged. In this study, the foot kinematics were evaluated as a combination of the forefoot and hindfoot motion. Therefore, the ankle joint angle measured was the angle between the calf and the whole foot. This joint angle is consistent with joint angles performed in the MRI. Gatt et al. (2011) investigated the kinematics of the forefoot and hindfoot during dorsiflexion using a motion capture system and revealed that the forefoot has a significantly larger range of motion than the hind foot. However, the forefoot and hindfoot motion were reported to be proportionate to one another. Therefore, for ankle angles beyond 20° dorsiflexion, the hind foot, where the Achilles tendon inserts, was assumed to keep rotating. Such extrapolation matched the trend of moment arms estimated by the model in extreme dorsiflexion (Figure 7.4).

More studies are needed to investigate the moment arm of the Achilles tendon at extreme dorsiflexion angles. As loading tendon within an MRI scanner can be challenging, ultrasound measurement techniques could be an alternative method to measure the moment arm in such extreme joint angles (Chaudhry et al., 2015).

## 6.4.2 Eccentric loading protocol vs. heavy slow resistance protocol

From the normalized peak Achilles tendon forces observed in this study, there was no evidence to show that eccentric motion could cause larger Achilles tendon loading under the same external loading conditions. Even in the seated calf-raising motion, larger tendon forces were seen in the concentric phase rather than the eccentric phase. In the literature, no difference was found in the estimated tendon force between concentric and eccentric exercise with the standing knee straight in a study with seven participants with the moment arm quantified using ultrasound (Rees et al., 2008). In the study in this chapter, different loading conditions and two rehabilitation exercises were tested and were shown to have the same result.

Besides the direction of motion, variation in ankle joint range of motion between different protocols was observed. The largest ankle dorsiflexion angle was seen in the standing knee bent and seated exercises. In the literature, the effectiveness of the knee bent activity largely focused on the differential activation patterns between the gastrocnemius and soleus (Alfredson et al., 1998). This could result in a different intra-tendon force distribution as the soleus becomes highly activated. However, in this study, large dorsiflexion angles were also observed in knee bent and seated positions. The moment arm change in such joint angles could cause a decisive effect on the overall normalized peak Achilles tendon force. Thus, the ankle dorsiflexion angle could be another important factor in the peak loading of the Achilles tendon and should be included when comparing rehabilitation protocols. From the regression analysis, the joint angle significantly predicts the normalized peak Achilles tendon forces. In the standing position, for each 5° increase in the peak dorsiflexion, peak tendon force increased by 35% BW (simplified model) to 75%BW (FreeBody model).

The external loading also significantly predicted the peak tendon force. Each additional BW loading could increase the tendon force by 3.3 N/BW to 5.5 N/BW. Therefore, the external loading applied during the rehabilitation process could be a determining factor for the success of rehabilitation. This could be one of the strengths of heavy slow resistance training, as gym equipment was used to apply the loads. In such a scenario, the loading can be adjusted to maximize the lifting capacity in standing and seated postures. In the knee bent protocol in this study, only 8 kg (a bar without added weight) was applied, as most participants found it difficult to do the activity when they were loaded more heavily. However, with the knee straight motion, all participants could lift an additional 50% BW. This could be one of the reasons why eccentric loading is less efficient than heavy slow resistance training, as most patients use one backpack to apply the loading at home and are not able to reach the appropriate loading for each posture.

In the regression analysis, the adjusted  $R^2$  values were lower in the standing than seated position (Table 6.5). This was possibly because exercises were more unstable in the standing than in the seated posture. This suggests that the kinematic differences from the relatively unstable standing posture could also affect the peak Achilles tendon force. Due to the larger variation of peak force predicted by the FreeBody model, the corresponding adjusted  $R^2$  were smaller; such variation is likely due to the anatomical variations of the muscle line datasets.

In both standing and seated postures, the Achilles tendon forces increased as the ankle dorsiflexed. Therefore, it is possible to increase the efficiency of the loading protocol by performing the motion from mid-range to dorsiflexion only, with emphasis on the extreme dorsiflexion angles, as this is the range in which the Achilles tendon

experiences peak loading. Further prospective studies on a patient group are needed to clarify the effect of the loading condition on tendon healing.

In this study, the order selected for the activities may have affected the results of the trials. To avoid the effect of fatigue on performance, the trials including heavy weight lifting were performed first and resting sessions were administered between activities. All the participants were able to finish the experiment smoothly. However, this pragmatic approach may have resulted in a bias and an alternative approach would have been to randomize the order and conduct the experiment across multiple sessions or days.

It is worth noting that the optimization algorithm used only optimizes the muscle force distribution to accomplish a certain motion. This is not related to whether the motion itself is perfectly stable/optimized. The optimization technique is used minimized the muscle activation to some extent to achieve the motion recorded. Physiologically, it is very possible the muscles does not follow an ‘optimized’ force-sharing strategy. Currently, the only way to validate the model prediction is to compare with the predicted joint force to outputs from instrumented implants. The model used in this study, FreeBody, has been validated against these types of data (Ding et al.2016)

A major limitation of this study was the lack of a tendinopathy patient population. The kinematics might change when asked to perform the exercise with tolerable pain in the Achilles tendon. The findings herein are based on the mechanical performance of the Achilles tendon, assuming tendon healing is stimulated by loading the tendon. Secondly, as subject-specific lower limb MRI anatomy was not used to define muscle lines of action and insertion, the actual muscle lines of action used were scaled from a previously obtained dataset. It is possible that the change in the lines of action could affect the Achilles tendon force prediction. This issue was mitigated by adopting the

regression equation proposed by Ding et al. to select a dataset with the same gender and closest weight (Ding et al., 2018).

## 6.5 Conclusion

During eccentric loading and heavy slow resistance rehabilitation, the Achilles tendon force and ankle joint torque increased as the ankle dorsiflexed. The peak force in the eccentric phase was not larger than that in the concentric phase in all the protocols. The major factors affecting peak Achilles tendon loading were external loading and peak dorsiflexion angle. This suggests that the standing knee bent position is the most effective way to load the Achilles tendon. Based on the observations of this study, the current protocols could be modified by performing mid-range to dorsiflexion motion only with an emphasis on reaching the extreme dorsiflexion angles. This study supports the clinical observation that concentric exercise protocols are as effective as eccentric exercise protocols but have the advantage of being more time-efficient. More studies are required to clarify the change in the moment arm in maximum dorsiflexion and investigate its effectiveness in a tendinopathy population.

## **Chapter 7**

### **Summary, discussion, and future work**

#### **7.1 Summary**

The plantaris tendon could play an important role in the development and progression of midportion Achilles tendinopathy. The static MRI series collected as part of this work enabled evaluation of the motion of the Achilles and plantaris tendons. Interestingly, plantaris tendons categorized as the same type could have different interactions with the Achilles tendon. This finding clarified the discrepancies reported in the cadaveric mechanical simulations discussed in Chapter 3 (Smith et al., 2017; Stephen et al., 2018). In addition, the potential for an attachment between the Achilles and plantaris tendons was identified. This is the first time such an adhesion has been reported with an imaging study. In addition to tendon interaction, it was discovered that Type 3 plantaris tendons cannot be identified by MRI alone. This is important for

clinical evaluation of patients being investigated for plantaris-related Achilles tendinopathy.

Although the connection between the anatomical findings described above and the development of demonstrable clinical symptoms remains unclear, this study is an important step in establishing the methodology to enable tendon geometry to be confidently investigated in patients.

From the observation of the plantaris geometry in tendinopathy patients, Type 4 tendons are more likely to be present than in a healthy population. This proves the hypothesis that tendon geometry plays an important role in plantaris-related Achilles tendinopathy. The fact that tendons of other types were also present in the tendinopathy group suggests that there might be other factors causing the plantaris tendon involvement.

Musculoskeletal models were used to investigate the forces on the Achilles tendon during motion, with a focus on the effect of the rotational structure of the tendon. Although no difference in the overall Achilles tendon force was found in the rotational variants, the distributions between the forces of the muscles that attach to the Achilles tendon varied. Among the rotational variants, the medial gastrocnemius muscle force increased as the tendon fibre bundle rotated. As the lateral Achilles tendon fibres were derived mainly from the medial gastrocnemius in this anatomical variant, the increasing force suggests that the lateral tendon fascicles could be more prone to injury with tendon fibre bundle rotation.

Finally, the musculoskeletal model was used to analyse the effectiveness eccentric loading and heavy slow resistance protocols. Although the experimental protocol did not load the Achilles tendon to the maximum capacity of each participant, the effect of different parameters can be analysed. The importance of the ankle flexion angle was

highlighted. As the ankle range of motion varied between different loading protocols, the peak force seen in the Achilles tendon was also affected. Therefore, there is potential that rehabilitation protocols could be further optimized by performing ankle flexion between neutral and dorsiflexion only. Performing the rehabilitation exercises in such a range of motion could maximize the tendon loading without inducing contact and possible compression and / or friction between the Achilles and plantaris tendons.

## **7.2 Discussion**

### **7.2.1 Mechanism of midportion Achilles tendinopathy**

A fundamental question raised within this thesis is, ‘What is midportion Achilles tendinopathy?’ The answer is that it is a large group of injuries that includes patients presenting with medial, central, and lateral tendon pain in the midportion (4-7 cm) of the tendon (van Dijk et al., 2011). It was not clear whether patients who present with different sites of pain have developed tendinopathy by the same mechanism.

Modelling of the Achilles tendon fibre structure indicates that the tendon force during in the lateral aspect of the Achilles tendon, which is primarily composed of fibres derived from the medial gastrocnemius, is likely to sustain larger forces as the tendon fibre bundle rotates. With increased forces seen during walking, it is possible that this portion of the tendon is prone to injury. This finding supports the mechanical theory of differential loading within the tendon and links with clinical studies identifying this as frequently the primary location of the injury.



It was not possible to detect the degree of rotation of the Achilles tendon fibre bundles and measure the individual muscle forces *in vivo*. Therefore, validation of the findings from the computational model is challenging. However, the results from the model indicated that one possible effect of this large medial gastrocnemius force is patients presenting with lateral-sided Achilles tendinopathy. More studies are needed to test this hypothesis. To clarify the relationship between medial gastrocnemius force and lateral Achilles tendinopathy it may be possible to investigate the proportion of each muscular component in the triceps surae in both healthy participants and patients with lateral Achilles tendinopathy. If the hypothesis is valid, it may be found that the medial gastrocnemius makes up a higher percentage of the triceps surae than the lateral gastrocnemius in Achilles tendinopathy patients.

Patients with plantaris tendon involvement frequently exhibit symptoms on the medial side of the Achilles tendon. This condition could be explained by the anatomical proximity between the Achilles and plantaris tendons. However, from the work presented here, it is not clear whether the plantaris tendon involvement is a primary injury or secondary to the midportion Achilles tendinopathy.

If it is the primary injury, it is possible that compression and / or friction between the plantaris and Achilles tendons causes midportion Achilles tendon injury. If it is secondary to midportion Achilles tendinopathy, the plantaris tendon is involved because the Achilles tendon was injured, causing it to swell, thereby making it touch the plantaris tendon. In both scenarios, the clinical symptoms could deteriorate as plantaris tendon involvement increases.

Observations from the healthy and tendinopathy groups suggest it is possible that the distribution between the various plantaris tendon types within the patient group is the result of both primary and secondary causes. A plantaris tendon involvement in

Achilles tendinopathy occurred in all types of geometry and the percentages of Types 1, 2, and 3 in patients were no different to those in the healthy cohort. It is possible that this indicates that the pathology originates from an Achilles tendon injury.

The large proportion of Type 4 tendons suggests the mechanism of injury of this group is different from that of the other plantaris types. Anatomical proximity can only explain part of the reason why more Type 4 tendons are likely to be involved. Type 3 plantaris tendons also have a close relationship to the Achilles tendon, but the prevalence of this type did not increase significantly in the tendinopathy group. This suggests that it is the effect of the direct insertion of Type 4 tendons, not anatomical adjacency, that is an important cause of plantaris involvement.

The plantaris tendon studies in Chapter 3 and 4 contributed to the understanding of the role of the plantaris tendon in the development of midportion Achilles tendinopathy. The plantaris categorization system can be used to evaluate the risk of plantaris tendon involvement. The plantaris tendon studies also facilitated the clinical evaluation of the plantaris tendon, determining that an ultrasound can be more sensitive than MRI in identifying Type 3 tendons.

Based on the findings presented in this thesis, it is possible that midportion Achilles tendinopathy can be divided into several subcategories due to different causes, such as plantaris-induced tendinopathy and medial gastrocnemius-related tendinopathy. A personalized treatment based on the individual cause of injury could improve the effectiveness of rehabilitation. This thesis has shown that the Achilles tendon force decreased from dorsiflexion to plantarflexion, while the contact between the two tendons increased as the patient moved towards plantarflexion. This suggests that patients with plantaris tendon involvement should reduce the plantarflexion angle during rehabilitation exercises, if contact between tendons is pathological. For patients

with Type 4 tendons, the traditional regimen, targeting the Achilles tendon, could have limited success, as the plantaris tendon geometry may be the root cause. Therefore, removal of plantaris tendon could be recommended as is commonly practiced (Calder et al., 2015; Masci et al., 2015). For patients presenting with lateral-sided symptoms, training with a bent-knee heel drop or seated calf-raise exercise could not only stimulate the healing of the Achilles tendon but also strengthen the soleus muscle that shares the loading with the medial gastrocnemius. More studies, including patient trials, are needed to test the effectiveness of the personalized treatment proposed above.

### **7.2.2 Limitations**

Only healthy participants were included in the sequential static MRI study and so there is no evidence that plantaris attachment will lead to an Achilles tendon injury. However, with the close contact between the Achilles and plantaris tendons throughout the range of motion, it is theoretically possible that these tendons bear a higher risk to be involved in midportion Achilles tendinopathy. Considering the low incidence rate of such attachments in the healthy population (2/34), performing a prospective cohort study would be challenging. In addition, shear and compression force was not directly measured in different plantaris types during motion, as in vivo measurement was not feasible. This is key to the understanding of the interaction between the two tendons.

There were 34 healthy volunteers in this sequential static MRI study. The anatomical investigation of plantaris type normally requires larger sample number. However, our study attempts to investigate the capacity of clinical imaging tools. The increased cost with methodology will inevitably decrease the sample size.

The selection bias in the tendinopathy plantaris tendon study is acknowledged. In this study, only patients with plantaris tendon involvement with both MRI and ultrasound scans were included. This study analysed plantaris geometry as an exposure to the plantaris involvement, so a causal relationship would not be able to be derived. A prospective study with all midportion Achilles tendinopathy patients could alleviate this problem.

For the musculoskeletal models used in Chapters 5 and 6, it is important to note that the FreeBody model is composed of only muscle lines of action. There are no ‘tendons’ in the model. The tendon forces estimated in this thesis were the summation of the triceps surae muscles and did not account for the tendon static length, stiffness, or viscoelastic properties. However, as only the tendon force was considered in this study, such simplifications are still representative of the force calculation. In addition, as addressed in Chapter 5, direction validation of muscle forces is challenging. It is also worth noting that lower limb musculoskeletal models’ force predictions are particularly sensitive to the location of the ankle joint centre. The ankle joint centre is empirically determined as the midpoint of the medial and lateral malleoli. However, due to the complicated ankle joint complex and soft tissue motion, the ankle joint centre could be mobile, in reality.

The modified rehabilitation motion proposed for Achilles tendinopathy was based on the hypothesis that tendon healing can be stimulated by loading the tendon in a controlled manner. The modified protocol could optimize the effectiveness of loading the Achilles tendon during motion.

### 7.3 Future work

To examine the plantaris tendon geometry, as described in the last section, a prospective study including MRI and ultrasound on all patients diagnosed with midportion Achilles tendinopathy, ideally from multiple clinicians, could better clarify the role of the plantaris tendon. This could also examine the inter-observer reliability of the categorization system. Including patients diagnosed of midportion Achilles tendinopathy, but no plantaris tendon involvement, could also facilitate understanding of role of the plantaris tendon.

Determining plantaris tendon geometry in the clinical environment may be improved by using ultrasound since this may more accurately differentiate closely adjacent tendon structures. Ultrasound could also be used to investigate the rotational fibre structure of the Achilles tendon. Cadaveric dissections with pre-dissection ultrasound scans could be used to establish the correlation between the Achilles tendon fibre bundle and ultrasound images. The results could be used as a parameter to improve the musculoskeletal modelling of triceps surae.

Finally, a prospective randomized controlled trial could clarify the role of mechanical loading on the Achilles tendon healing. By comparing the effectiveness of a modified protocol to original protocols in a patient group, the correlation between tendon loading and healing can be further revealed. Incorporating ultrasound to measure the change of tendon thickness may also enable comparison of the effectiveness of the loading protocol.

## 7.4 Conclusion

The cause of midportion Achilles tendinopathy appears multifactorial. From a biomechanical perspective, plantaris tendon involvement and intra-tendon differential loading could lead to the presentation of different symptoms. Thus, dividing midportion Achilles tendinopathy into sub-groups could be helpful to improve rehabilitation protocols. Current rehabilitation protocols could be further modified to increase their effectiveness. More studies are required to understand the pathophysiology of non-insertional Achilles tendinopathy and investigate the effect of potential modifications to rehabilitation protocols.

## References

- Abramowitch, S.D., Zhang, X., Curran, M., Kilger, R., 2010. A comparison of the quasi-static mechanical and non-linear viscoelastic properties of the human semitendinosus and gracilis tendons. *Clin Biomech (Bristol, Avon)* 25, 325-331.
- Ait-Haddou, R., Jinha, A., Herzog, W., Binding, P., 2004. Analysis of the force-sharing problem using an optimization model. *Mathematical Biosciences* 191, 111-122.
- Alfredson, H., 2011. Midportion Achilles tendinosis and the plantaris tendon. *Br J Sports Med* 45, 1023-1025.
- Alfredson, H., 2017. Persistent pain in the Achilles mid-portion? Consider the plantaris tendon as a possible culprit! *Br J Sports Med* 51, 833-834.
- Alfredson, H., Pietila, T., Jonsson, P., Lorentzon, R., 1998. Heavy-load eccentric calf muscle training for the treatment of chronic Achilles tendinosis. *Am J Sports Med* 26, 360-366.
- Almekinders, L.C., Temple, J.D., 1998. Etiology, diagnosis, and treatment of tendonitis: an analysis of the literature. *Med Sci Sports Exerc* 30, 1183-1190.
- Anderson, F.C., John, C.T., Guendelman, E., Arnold, A.S., Delp, S.L., Year SimTrack: Software for rapidly generating muscle-actuated simulations of long-duration movement. In *ISOBME*. Taipei.
- Anderson, F.C., Pandy, M.G., 1999. A Dynamic Optimization Solution for Vertical Jumping in Three Dimensions. *Comput Methods Biomech Biomed Engin* 2, 201-231.
- Aragao, J.A., Reis, F.P., Guerra, D.R., Cabral, R.H., 2010. The Occurrence of the Plantaris Muscle and its Muscle-Tendon Relationship in Adult Human Cadavers. *Int J Morphol* 28, 255-258.
- Arampatzis, A., Karamanidis, K., Albracht, K., 2007a. Adaptational responses of the human Achilles tendon by modulation of the applied cyclic strain magnitude. *J Exp Biol* 210, 2743-2753.
- Arampatzis, A., Karamanidis, K., Morey-Klapsing, G., De Monte, G., Stafilidis, S., 2007b. Mechanical properties of the triceps surae tendon and aponeurosis in relation to intensity of sport activity. *J Biomech* 40, 1946-1952.
- Arampatzis, A., Monte, G.D., Karamanidis, K., 2008. Effect of joint rotation correction when measuring elongation of the gastrocnemius medialis tendon and aponeurosis. *J Electromyogr Kinesiol* 18, 503-508.

- Arampatzis, A., Peper, A., Bierbaum, S., Albracht, K., 2010. Plasticity of human Achilles tendon mechanical and morphological properties in response to cyclic strain. *J Biomech* 43, 3073-3079.
- Arampatzis, A., Stafilidis, S., DeMonte, G., Karamanidis, K., Morey-Klapsing, G., Brüggemann, G., 2005. Strain and elongation of the human gastrocnemius tendon and aponeurosis during maximal plantarflexion effort. *Journal of biomechanics* 38, 833-841.
- Arda, K., Ciledag, N., Aktas, E., Aribas, B.K., Kose, K., 2011. Quantitative assessment of normal soft-tissue elasticity using shear-wave ultrasound elastography. *AJR Am J Roentgenol* 197, 532-536.
- Arndt, A.N., Komi, P.V., Brüggemann, G.P., Lukkariniemi, J., 1998a. Individual muscle contributions to the in vivo achilles tendon force. *Clin Biomech (Bristol, Avon)* 13, 532-541.
- Arndt, A.N., Komi, P.V., Brüggemann, G.P., Lukkariniemi, J., 1998b. Individual muscle contributions to the in vivo achilles tendon force. *Clinical Biomechanics* 13, 532-541.
- Astrom, M., Rausing, A., 1995. Chronic Achilles tendinopathy. A survey of surgical and histopathologic findings. *Clin Orthop Relat Res*, 151-164.
- Ballal, M.S., Walker, C.R., Molloy, A.P., 2014. The anatomical footprint of the Achilles tendon: a cadaveric study. *The bone & joint journal* 96-B, 1344-1348.
- Bedi, H.S., Jowett, C., Ristanis, S., Docking, S., Cook, J., 2016. Plantaris Excision and Ventral Paratendinous Scraping for Achilles Tendinopathy in an Athletic Population. *Foot Ankle Int* 37, 386-393.
- Benoit, D.L., Damsgaard, M., Andersen, M.S., 2015. Surface marker cluster translation, rotation, scaling and deformation: Their contribution to soft tissue artefact and impact on knee joint kinematics. *Journal of biomechanics* 48, 2124-2129.
- Beyer, R., Kongsgaard, M., Hougs Kjaer, B., Ohlenschlaeger, T., Kjaer, M., Magnusson, S.P., 2015. Heavy Slow Resistance Versus Eccentric Training as Treatment for Achilles Tendinopathy: A Randomized Controlled Trial. *Am J Sports Med* 43, 1704-1711.
- Bilodeau, M., Schindler-Ivens, S., Williams, D.M., Chandran, R., Sharma, S.S., 2003. EMG frequency content changes with increasing force and during fatigue in the quadriceps femoris muscle of men and women. *J Electromyogr Kinesiol* 13, 83-92.
- Birch, H.L., 2007. Tendon matrix composition and turnover in relation to functional requirements. *Int J Exp Pathol* 88, 241-248.



Bjur, D., Alfredson, H., Forsgren, S., 2005. The innervation pattern of the human Achilles tendon: studies of the normal and tendinosis tendon with markers for general and sensory innervation. *Cell and tissue research* 320, 201-206.

Bodine, S.C., Roy, R.R., Meadows, D.A., Zernicke, R.F., Sacks, R.D., Fournier, M., Edgerton, V.R., 1982. Architectural, histochemical, and contractile characteristics of a unique biarticular muscle: the cat semitendinosus. *J Neurophysiol* 48, 192-201.

Bohm, S., Mersmann, F., Tettke, M., Kraft, M., Arampatzis, A., 2014. Human Achilles tendon plasticity in response to cyclic strain: effect of rate and duration. *J Exp Biol* 217, 4010-4017.

Bohu, Y., Lefevre, N., Bauer, T., Laffenetre, O., Herman, S., Thauinat, M., Cucurulo, T., Franceschi, J.P., Cermolacce, C., Rolland, E., 2009. Surgical treatment of Achilles tendinopathies in athletes. Multicenter retrospective series of open surgery and endoscopic techniques. *Orthopaedics & traumatology, surgery & research : OTSR* 95, S72-77.

Bojsen-Moller, J., Hansen, P., Aagaard, P., Svantesson, U., Kjaer, M., Magnusson, S.P., 2004. Differential displacement of the human soleus and medial gastrocnemius aponeuroses during isometric plantar flexor contractions in vivo. *J Appl Physiol* 97, 1908-1914.

Brzycki, M., 1998. *A Practical Approach To Strength Training*. McGraw-Hill Contemporary.

Burden, A., 2010. How should we normalize electromyograms obtained from healthy participants? What we have learned from over 25 years of research. *J Electromyogr Kinesiol* 20, 1023-1035.

Butler, D., Grood, E., Noyes, F., Zernicke, R., 1978. Biomechanics of ligaments and tendons. *Exercise and sport sciences reviews* 6, 125-181.

Calder, J.D., Freeman, R., Pollock, N., 2015. Plantaris excision in the treatment of non-insertional Achilles tendinopathy in elite athletes. *Br J Sports Med* 49, 1532-1534.

Calder, J.D., Stephen, J.M., van Dijk, C.N., 2016. Plantaris Excision Reduces Pain in Midportion Achilles Tendinopathy Even in the Absence of Plantaris Tendinosis. *Orthop J Sports Med* 4, 2325967116673978.

Carbone, V., Fluit, R., Pellikaan, P., van der Krogt, M.M., Janssen, D., Damsgaard, M., Vigneron, L., Feilkas, T., Koopman, H.F., Verdonschot, N., 2015. TLEM 2.0 - a comprehensive musculoskeletal geometry dataset for subject-specific modeling of lower extremity. *J Biomech* 48, 734-741.

- Carbone, V., van der Krogt, M.M., Koopman, H.F., Verdonschot, N., 2012. Sensitivity of subject-specific models to errors in musculo-skeletal geometry. *J Biomech* 45, 2476-2480.
- Cavagna, G.A., Heglund, N.C., Taylor, C.R., 1977. Mechanical work in terrestrial locomotion: two basic mechanisms for minimizing energy expenditure. *The American journal of physiology* 233, R243-261.
- Chaudhry, S., Morrissey, D., Woledge, R.C., Bader, D.L., Screen, H.R., 2015. Eccentric and concentric loading of the triceps surae: an in vivo study of dynamic muscle and tendon biomechanical parameters. *Journal of applied biomechanics* 31, 69-78.
- Chen, X.M., Cui, L.G., He, P., Shen, W.W., Qian, Y.J., Wang, J.R., 2013. Shear wave elastographic characterization of normal and torn achilles tendons: a pilot study. *Journal of ultrasound in medicine : official journal of the American Institute of Ultrasound in Medicine* 32, 449-455.
- Chernak, L.A., Thelen, D.G., 2012. Tendon motion and strain patterns evaluated with two-dimensional ultrasound elastography. *J Biomech* 45, 2618-2623.
- Chernak Slane, L., Thelen, D.G., 2014. The use of 2D ultrasound elastography for measuring tendon motion and strain. *J Biomech* 47, 750-754.
- Child, S., Bryant, A.L., Clark, R.A., Crossley, K.M., 2010. Mechanical Properties of the Achilles Tendon Aponeurosis Are Altered in Athletes With Achilles Tendinopathy. *The American Journal of Sports Medicine* 38, 1885-1893.
- Cleather, D.J., Bull, A.M., 2015. The development of a segment-based musculoskeletal model of the lower limb: introducing FreeBody. *R Soc Open Sci* 2, 140449.
- Cohen, J.J.P.b., 1992. A power primer. 112, 155.
- Cohen, R., Hooley, C., McCrum, N., 1976. Viscoelastic creep of collagenous tissue. *Journal of biomechanics* 9, 175-184.
- Cook, J.L., Khan, K.M., Purdam, C., 2002. Achilles tendinopathy. *Man Ther* 7, 121-130.
- Cook, J.L., Purdam, C., 2012. Is compressive load a factor in the development of tendinopathy? *Br J Sports Med* 46, 163-168.
- Cook, J.L., Purdam, C.R., 2014. The challenge of managing tendinopathy in competing athletes. *Br J Sports Med* 48, 506-509.

- Cresswell, A.G., Loscher, W.N., Thorstensson, A., 1995. Influence of gastrocnemius muscle length on triceps surae torque development and electromyographic activity in man. *Exp Brain Res* 105, 283-290.
- Crowninshield, R.D., Brand, R.A., 1981. A physiologically based criterion of muscle force prediction in locomotion. *J Biomech* 14, 793-801.
- Cummins, E.J., Anson, B.J., et al., 1946. The structure of the calcaneal tendon (of Achilles) in relation to orthopedic surgery, with additional observations on the plantaris muscle. *Surgery, gynecology & obstetrics* 83, 107-116.
- Daseler, E.H., Anson, B.J., 1943. The plantaris muscle: An Anatomical Study of 750 Specimens. *J Bone Joint Surg* 25, 822-827.
- de Jonge, S., van den Berg, C., de Vos, R.J., van der Heide, H.J., Weir, A., Verhaar, J.A., Bierma-Zeinstra, S.M., Tol, J.L., 2011. Incidence of midportion Achilles tendinopathy in the general population. *Br J Sports Med* 45, 1026-1028.
- de Leva, P., 1996. Adjustments to Zatsiorsky-Seluyanov's segment inertia parameters. *J Biomech* 29, 1223-1230.
- De Pieri, E., Lund, M.E., Gopalakrishnan, A., Rasmussen, K.P., Lunn, D.E., Ferguson, S.J., 2018. Refining muscle geometry and wrapping in the TLEM 2 model for improved hip contact force prediction. *PloS one* 13, e0204109.
- de Vos, R.J., Weir, A., Cobben, L.P., Tol, J.L., 2007. The value of power Doppler ultrasonography in Achilles tendinopathy: a prospective study. *Am J Sports Med* 35, 1696-1701.
- Delgado, G.J., Chung, C.B., Lektrakul, N., Azocar, P., Botte, M.J., Coria, D., Bosch, E., Resnick, D., 2002. Tennis leg: clinical US study of 141 patients and anatomic investigation of four cadavers with MR imaging and US. *Radiology* 224, 112-119.
- Den Hartog, B.D., 2009. Insertional Achilles tendinosis: pathogenesis and treatment. *Foot Ankle Clin* 14, 639-650.
- DeWall, R.J., Slane, L.C., Lee, K.S., Thelen, D.G., 2014. Spatial variations in Achilles tendon shear wave speed. *J Biomech* 47, 2685-2692.
- Ding, Z., Kit Tsang, C., Nolte, D., Kedgley, A.E., Bull, A.M.J., 2018. Improving musculoskeletal model scaling using an anatomical atlas: the importance of gender and anthropometric similarity. *IEEE Trans Biomed Eng* (In submission).
- Ding, Z., Nolte, D., Kit Tsang, C., Cleather, D.J., Kedgley, A.E., Bull, A.M., 2016. In Vivo Knee Contact Force Prediction Using Patient-Specific Musculoskeletal Geometry in a Segment-Based Computational Model. *J Biomech Eng* 138, 021018.

- Dos Santos, M.A., Bertelli, J.A., Kechele, P.R., Duarte, H., 2009. Anatomical study of the plantaris tendon: reliability as a tendo-osseous graft. *Surg Radiol Anat* 31, 59-61.
- Drake, R.L.a., 2015. *Gray's anatomy for students*, Third ed.
- Edama, M., Kubo, M., Onishi, H., Takabayashi, T., Inai, T., Yokoyama, E., Hiroshi, W., Satoshi, N., Kageyama, I., 2015. The twisted structure of the human Achilles tendon. *Scand J Med Sci Sports* 25, e497-503.
- Edgerton, V.R., Smith, J.L., Simpson, D.R., 1975. Muscle fibre type populations of human leg muscles. *The Histochemical journal* 7, 259-266.
- Emerson, C., Morrissey, D., Perry, M., Jalan, R., 2010. Ultrasonographically detected changes in Achilles tendons and self reported symptoms in elite gymnasts compared with controls--an observational study. *Man Ther* 15, 37-42.
- Erdemir, A., McLean, S., Herzog, W., van den Bogert, A.J., 2007. Model-based estimation of muscle forces exerted during movements. *Clin Biomech (Bristol, Avon)* 22, 131-154.
- Ferrari, A., Cutti, A.G., Cappello, A., 2010. A new formulation of the coefficient of multiple correlation to assess the similarity of waveforms measured synchronously by different motion analysis protocols. *Gait Posture* 31, 540-542.
- Finni, T., Bernabei, M., Baan, G.C., Noort, W., Tijs, C., Maas, H., 2018. Non-uniform displacement and strain between the soleus and gastrocnemius subtendons of rat Achilles tendon. *Scand J Med Sci Sports* 28, 1009-1017.
- Franz, J.R., Slane, L.C., Rasske, K., Thelen, D.G., 2015. Non-uniform in vivo deformations of the human Achilles tendon during walking. *Gait Posture* 41, 192-197.
- Franz, J.R., Thelen, D.G., 2016. Imaging and simulation of Achilles tendon dynamics: Implications for walking performance in the elderly. *J Biomech* 49, 1403-1410.
- Fredberg, U., Stengaard-Pedersen, K., 2008. Chronic tendinopathy tissue pathology, pain mechanisms, and etiology with a special focus on inflammation. *Scand J Med Sci Sports* 18, 3-15.
- Freeman, A.J., Jacobson, N.A., Fogg, Q.A., 2008. Anatomical variations of the plantaris muscle and a potential role in patellofemoral pain syndrome. *Clin Anat* 21, 178-181.
- Fregly, B.J., Besier, T.F., Lloyd, D.G., Delp, S.L., Banks, S.A., Pandy, M.G., D'Lima, D.D., 2012. Grand challenge competition to predict in vivo knee loads. *J Orthop Res* 30, 503-513.

- Fukashiro, S., Komi, P.V., Jarvinen, M., Miyashita, M., 1995. In vivo Achilles tendon loading during jumping in humans. *European journal of applied physiology and occupational physiology* 71, 453-458.
- Fukunaga, T., Roy, R.R., Shellock, F.G., Hodgson, J.A., Edgerton, V.R., 1996. Specific tension of human plantar flexors and dorsiflexors. *J Appl Physiol* (1985) 80, 158-165.
- Gaida, J.E., Cook, J., 2011. Treatment options for patellar tendinopathy: critical review. *Current sports medicine reports* 10, 255-270.
- Galloway, M.T., Lalley, A.L., Shearn, J.T., 2013. The role of mechanical loading in tendon development, maintenance, injury, and repair. *J Bone Joint Surg Am* 95, 1620-1628.
- Gardin, A., Bruno, J., Movin, T., Kristoffersen-Wiberg, M., Shalabi, A., 2006. Magnetic resonance signal, rather than tendon volume, correlates to pain and functional impairment in chronic Achilles tendinopathy. *Acta Radiol* 47, 718-724.
- Garofalo, P., Cutti, A.G., Filippi, M.V., Cavazza, S., Ferrari, A., Cappello, A., Davalli, A., 2009. Inter-operator reliability and prediction bands of a novel protocol to measure the coordinated movements of shoulder-girdle and humerus in clinical settings. *Medical & biological engineering & computing* 47, 475-486.
- Gatt, A., Chockalingam, N., Chevalier, T.L., 2011. Sagittal plane kinematics of the foot during passive ankle dorsiflexion. *Prosthet Orthot Int* 35, 425-431.
- Gerus, P., Sartori, M., Besier, T.F., Fregly, B.J., Delp, S.L., Banks, S.A., Pandey, M.G., D'Lima, D.D., Lloyd, D.G., 2013. Subject-specific knee joint geometry improves predictions of medial tibiofemoral contact forces. *J Biomech* 46, 2778-2786.
- Gosline, J., Lillie, M., Carrington, E., Guerette, P., Ortlepp, C., Savage, K., 2002. Elastic proteins: biological roles and mechanical properties. *Philos Trans R Soc Lond B Biol Sci* 357, 121-132.
- Gregor, R.J., Komi, P.V., Jarvinen, M., 1987. Achilles tendon forces during cycling. *International journal of sports medicine* 8 Suppl 1, 9-14.
- Gregor, S.M., Perell, K.L., Rushatakankovit, S., Miyamoto, E., Muffoletto, R., Gregor, R.J., 2002. Lower extremity general muscle moment patterns in healthy individuals during recumbent cycling. *Clin Biomech (Bristol, Avon)* 17, 123-129.
- Guney, A., Vatansever, F., Karaman, I., Kafadar, I.H., Oner, M., Turk, C.Y., 2015. Biomechanical properties of Achilles tendon in diabetic vs. non-diabetic patients. *Exp Clin Endocrinol Diabetes* 123, 428-432.

- Haims, A.H., Schweitzer, M.E., Patel, R.S., Hecht, P., Wapner, K.L., 2000. MR imaging of the Achilles tendon: overlap of findings in symptomatic and asymptomatic individuals. *Skeletal Radiol* 29, 640-645.
- Hamner, S.R., Seth, A., Delp, S.L., 2010. Muscle contributions to propulsion and support during running. *J Biomech* 43, 2709-2716.
- Handsfield, G.G., Inouye, J.M., Slane, L.C., Thelen, D.G., Miller, G.W., Blemker, S.S., 2017. A 3D model of the Achilles tendon to determine the mechanisms underlying nonuniform tendon displacements. *J Biomech* 51, 17-25.
- Handsfield, G.G., Meyer, C.H., Hart, J.M., Abel, M.F., Blemker, S.S., 2014. Relationships of 35 lower limb muscles to height and body mass quantified using MRI. *J Biomech* 47, 631-638.
- Hanna, J.B., Schmitt, D., 2011. Comparative Triceps Surae Morphology in Primates: A Review. *Anatomy Research International* 2011, 22.
- Hansen, P., Aagaard, P., Kjaer, M., Larsson, B., Magnusson, S.P., 2003. Effect of habitual running on human Achilles tendon load-deformation properties and cross-sectional area. *Journal of applied physiology* 95, 2375-2380.
- Hansen, W., Shim, V.B., Obst, S., Lloyd, D.G., Newsham-West, R., Barrett, R.S., 2017. Achilles tendon stress is more sensitive to subject-specific geometry than subject-specific material properties: A finite element analysis. *J Biomech* 56, 26-31.
- Harvey, F.J., Chu, G., Harvey, P.M., 1983. Surgical availability of the plantaris tendon. *The Journal of hand surgery* 8, 243-247.
- Heinemeier, K.M., Kjaer, M., 2011. In vivo investigation of tendon responses to mechanical loading. *Journal of musculoskeletal & neuronal interactions* 11, 115-123.
- Herzog, W., Sokolosky, J., Zhang, Y.T., Guimaraes, A.C., 1998. EMG-force relation in dynamically contracting cat plantaris muscle. *J Electromyogr Kinesiol* 8, 147-155.
- Holmes, G.B., Lin, J., 2006. Etiologic factors associated with symptomatic achilles tendinopathy. *Foot Ankle Int* 27, 952-959.
- Hooley, C., McCrum, N., Cohen, R., 1980. The viscoelastic deformation of tendon. *Journal of Biomechanics* 13, 521-528.
- Huang, S., Ferris, D.P., 2012. Muscle activation patterns during walking from transtibial amputees recorded within the residual limb-prosthetic interface. *J Neuroeng Rehabil* 9, 55.

- Intriligator, M.D., 2002. Mathematical optimization and economic theory, in: Society for, I., Applied, M. (Eds.). Society for Industrial and Applied Mathematics (SIAM, 3600 Market Street, Floor 6, Philadelphia, PA 19104), Philadelphia, Pa.
- Iwanuma, S., Akagi, R., Kurihara, T., Ikegawa, S., Kanehisa, H., Fukunaga, T., Kawakami, Y., 2011. Longitudinal and transverse deformation of human Achilles tendon induced by isometric plantar flexion at different intensities. *J Appl Physiol* (1985) 110, 1615-1621.
- Jackson, J.B., 3rd, Philippi, M.T., Kolz, C.W., Suter, T., Henninger, H.B., 2014. Characterization of plantaris tendon constructs for ankle ligament reconstruction. *Foot Ankle Int* 35, 922-928.
- Jakubietz, M.G., Jakubietz, D.F., Gruenert, J.G., Zahn, R., Meffert, R.H., Jakubietz, R.G., 2011. Adequacy of palmaris longus and plantaris tendons for tendon grafting. *The Journal of hand surgery* 36, 695-698.
- Jarvinen, T.A., Kannus, P., Maffulli, N., Khan, K.M., 2005. Achilles tendon disorders: etiology and epidemiology. *Foot Ankle Clin* 10, 255-266.
- Jarvinen, T.A., Kannus, P., Paavola, M., Jarvinen, T.L., Jozsa, L., Jarvinen, M., 2001. Achilles tendon injuries. *Current opinion in rheumatology* 13, 150-155.
- Jianmongkol, S., Thumroj, E., Kosuwon, W., Kamanarong, K., 2002. Palmaris longus & Plantaris Tendon: Anatomical Variations & Relationship. [*Srinagarind Medical Journal*] 17, 160-163.
- Joshi, M.M., Joshi, S.D., Joshi, S.S., 2014. Morphological Variations of Muscle Plantaris: Anatomical and Clinical Insight. *Int J Anat Res* 2, 621-624.
- Kadaba, M.P., Ramakrishnan, H.K., Wootten, M.E., Gainey, J., Gorton, G., Cochran, G.V., 1989. Repeatability of kinematic, kinetic, and electromyographic data in normal adult gait. *J Orthop Res* 7, 849-860.
- Kader, D., Saxena, A., Movin, T., Maffulli, N., 2002. Achilles tendinopathy: some aspects of basic science and clinical management. *Br J Sports Med* 36, 239-249.
- Kannus, P., Jozsa, L., 1991. Histopathological changes preceding spontaneous rupture of a tendon. A controlled study of 891 patients. *J Bone Joint Surg Am* 73, 1507-1525.
- Karlsson, S., Gerdle, B., 2001. Mean frequency and signal amplitude of the surface EMG of the quadriceps muscles increase with increasing torque--a study using the continuous wavelet transform. *J Electromyogr Kinesiol* 11, 131-140.
- Ker, R., 1992. Tensile fibres: strings and straps. Oxford University Press, Oxford UK.

Khan, K.M., Bonar, F., Desmond, P.M., Cook, J.L., Young, D.A., Visentini, P.J., Fehrmann, M.W., Kiss, Z.S., O'Brien, P.A., Harcourt, P.R., Dowling, R.J., O'Sullivan, R.M., Crichton, K.J., Tress, B.M., Wark, J.D., 1996. Patellar tendinosis (jumper's knee): findings at histopathologic examination, US, and MR imaging. *Victorian Institute of Sport Tendon Study Group. Radiology* 200, 821-827.

Khan, K.M., Forster, B.B., Robinson, J., Cheong, Y., Louis, L., Maclean, L., Taunton, J.E., 2003. Are ultrasound and magnetic resonance imaging of value in assessment of Achilles tendon disorders? A two year prospective study. *Br J Sports Med* 37, 149-153.

Kjaer, M., 2004. Role of extracellular matrix in adaptation of tendon and skeletal muscle to mechanical loading. *Physiological reviews* 84, 649-698.

Klein Horsman, M.D., Koopman, H.F., van der Helm, F.C., Prose, L.P., Veeger, H.E., 2007. Morphological muscle and joint parameters for musculoskeletal modelling of the lower extremity. *Clin Biomech (Bristol, Avon)* 22, 239-247.

Komi, P.V., 1990. Relevance of in vivo force measurements to human biomechanics. *J Biomech* 23 Suppl 1, 23-34.

Komi, P.V., Fukashiro, S., Jarvinen, M., 1992. Biomechanical loading of Achilles tendon during normal locomotion. *Clinics in sports medicine* 11, 521-531.

Kongsgaard, M., Kovanen, V., Aagaard, P., Doessing, S., Hansen, P., Laursen, A.H., Kaldau, N.C., Kjaer, M., Magnusson, S.P., 2009. Corticosteroid injections, eccentric decline squat training and heavy slow resistance training in patellar tendinopathy. *Scand J Med Sci Sports* 19, 790-802.

Kongsgaard, M., Qvortrup, K., Larsen, J., Aagaard, P., Doessing, S., Hansen, P., Kjaer, M., Magnusson, S.P., 2010. Fibril morphology and tendon mechanical properties in patellar tendinopathy: effects of heavy slow resistance training. *Am J Sports Med* 38, 749-756.

Kongsgaard, M., Reitelseder, S., Pedersen, T.G., Holm, L., Aagaard, P., Kjaer, M., Magnusson, S.P., 2007. Region specific patellar tendon hypertrophy in humans following resistance training. *Acta Physiol (Oxf)* 191, 111-121.

Kose, O., Ege, T., Demiralp, B., Sanal, T., Bek, D., Basbozkurt, M., 2014. Prediction of the Presence of Plantaris Tendon Through Examination of Palmaris Longus Tendon: Is There a Link? *Int J Morphol* 32, 589-592.

Kubo, K., Kanehisa, H., Fukunaga, T., 2002. Effects of resistance and stretching training programmes on the viscoelastic properties of human tendon structures in vivo. *The Journal of physiology* 538, 219-226.



- Kubo, K., Kanehisa, H., Kawakami, Y., Fukunaga, T., 2000. Elasticity of tendon structures of the lower limbs in sprinters. *Acta physiologica Scandinavica* 168, 327-335.
- Kuhn, H.W., Tucker, A.W., 2014. Nonlinear programming, Traces and emergence of nonlinear programming. Springer, pp. 247-258.
- Kujala, U.M., Sarna, S., Kaprio, J., 2005. Cumulative incidence of achilles tendon rupture and tendinopathy in male former elite athletes. *Clinical journal of sport medicine : official journal of the Canadian Academy of Sport Medicine* 15, 133-135.
- Kuo, A.D., 2007. The six determinants of gait and the inverted pendulum analogy: A dynamic walking perspective. *Hum Mov Sci* 26, 617-656.
- Kuo, A.D., Donelan, J.M., Ruina, A., 2005. Energetic consequences of walking like an inverted pendulum: step-to-step transitions. *Exerc Sport Sci Rev* 33, 88-97.
- LaPrade, R.F., Morgan, P.M., Wentorf, F.A., Johansen, S., Engebretsen, L., 2007. The anatomy of the posterior aspect of the knee. An anatomic study. *J Bone Joint Surg Am* 89, 758-764.
- Lavagnino, M., Arnoczky, S.P., 2005. In vitro alterations in cytoskeletal tensional homeostasis control gene expression in tendon cells. *J Orthop Res* 23, 1211-1218.
- Lawrence, J.H., De Luca, C.J., 1983. Myoelectric signal versus force relationship in different human muscles. *Journal of applied physiology: respiratory, environmental and exercise physiology* 54, 1653-1659.
- Lersch, C., Grottsch, A., Segesser, B., Koebke, J., Bruggemann, G.P., Potthast, W., 2012. Influence of calcaneus angle and muscle forces on strain distribution in the human Achilles tendon. *Clin Biomech (Bristol, Avon)* 27, 955-961.
- Li, H.-Y., Hua, Y.-H., 2016. Achilles Tendinopathy: Current Concepts about the Basic Science and Clinical Treatments. *BioMed research international* 2016, 6492597-6492597.
- Lichtwark, G.A., Wilson, A.M., 2005. In vivo mechanical properties of the human Achilles tendon during one-legged hopping. *J Exp Biol* 208, 4715-4725.
- Lintz, F., Higgs, A., Millett, M., Barton, T., Raghuvanshi, M., Adams, M.A., Winson, I.G., 2011. The role of Plantaris Longus in Achilles tendinopathy: a biomechanical study. *Foot Ankle Surg* 17, 252-255.
- Mackay, I.R., McCulloch, A.S., 1990. Imaging the plantaris tendon with ultrasound. *British journal of plastic surgery* 43, 689-691.

- Madeleine, P., Bajaj, P., Sogaard, K., Arendt-Nielsen, L., 2001. Mechanomyography and electromyography force relationships during concentric, isometric and eccentric contractions. *J Electromyogr Kinesiol* 11, 113-121.
- Maffulli, N., Sharma, P., Luscombe, K.L., 2004. Achilles tendinopathy: aetiology and management. *Journal of the Royal Society of Medicine* 97, 472-476.
- Mafi, N., Lorentzon, R., Alfredson, H., 2001. Superior short-term results with eccentric calf muscle training compared to concentric training in a randomized prospective multicenter study on patients with chronic Achilles tendinosis. *Knee Surg Sports Traumatol Arthrosc* 9, 42-47.
- Maganaris, C.N., Baltzopoulos, V., Sargeant, A.J., 1998. Changes in Achilles tendon moment arm from rest to maximum isometric plantarflexion: in vivo observations in man. *The Journal of physiology* 510 ( Pt 3), 977-985.
- Maganaris, C.N., Baltzopoulos, V., Sargeant, A.J., 2006. Human calf muscle responses during repeated isometric plantarflexions. *Journal of biomechanics* 39, 1249-1255.
- Maganaris, C.N., Narici, M.V., Almekinders, L.C., Maffulli, N., 2004. Biomechanics and pathophysiology of overuse tendon injuries. *Sports medicine* 34, 1005-1017.
- Maganaris, C.N., Narici, M.V., Maffulli, N., 2008. Biomechanics of the Achilles tendon. *Disability and rehabilitation* 30, 1542-1547.
- Maganaris, C.N., Paul, J.P., 2002. Tensile properties of the in vivo human gastrocnemius tendon. *Journal of biomechanics* 35, 1639-1646.
- Magnusson, S.P., Aagaard, P., Rosager, S., Dyhre-Poulsen, P., Kjaer, M., 2001. Load-displacement properties of the human triceps surae aponeurosis in vivo. *The Journal of physiology* 531, 277-288.
- Malliaras, P., Barton, C.J., Reeves, N.D., Langberg, H., 2013. Achilles and patellar tendinopathy loading programmes : a systematic review comparing clinical outcomes and identifying potential mechanisms for effectiveness. *Sports medicine (Auckland, N.Z.)* 43, 267-286.
- Manal, K., Cowder, J.D., Buchanan, T.S., 2013. Subject-specific measures of Achilles tendon moment arm using ultrasound and video-based motion capture. *Physiol Rep* 1, e00139.
- Masci, L., Spang, C., van Schie, H.T., Alfredson, H., 2015. Achilles tendinopathy-do plantaris tendon removal and Achilles tendon scraping improve tendon structure? A prospective study using ultrasound tissue characterisation. *BMJ Open Sport Exerc Med* 1, e000005.

- Masci, L., Spang, C., van Schie, H.T., Alfredson, H., 2016. How to diagnose plantaris tendon involvement in midportion Achilles tendinopathy - clinical and imaging findings. *BMC Musculoskelet Disord* 17, 97.
- Mathiassen, S.E., Winkel, J., Hagg, G.M., 1995. Normalization of surface EMG amplitude from the upper trapezius muscle in ergonomic studies - A review. *J Electromyogr Kinesiol* 5, 197-226.
- Matthews, L.S., Ellis, D., 1968. Viscoelastic properties of cat tendon: effects of time after death and preservation by freezing. *Journal of biomechanics* 1, 65-71.
- Millard, M., Uchida, T., Seth, A., Delp, S.L., 2013. Flexing computational muscle: modeling and simulation of musculotendon dynamics. *Journal of biomechanical engineering* 135, 021005.
- Moissenet, F., Cheze, L., Dumas, R., 2014. A 3D lower limb musculoskeletal model for simultaneous estimation of musculo-tendon, joint contact, ligament and bone forces during gait. *J Biomech* 47, 50-58.
- Moritani, T., Muro, M., 1987. Motor unit activity and surface electromyogram power spectrum during increasing force of contraction. *European journal of applied physiology and occupational physiology* 56, 260-265.
- Moss, A., 1988. Is there an association between an absence of palmaris longus tendon and an absence of plantaris tendon? *Eur J Plast Surg* 11, 32-34.
- Muramatsu, T., Muraoka, T., Takeshita, D., Kawakami, Y., Hirano, Y., Fukunaga, T., 2001. Mechanical properties of tendon and aponeurosis of human gastrocnemius muscle in vivo. *Journal of Applied Physiology* 90, 1671-1678.
- Nayak, S.R., Krishnamurthy, A., Ramanathan, L., Ranade, A.V., Prabhu, L.V., Jiji, P.J., Rai, R., Chettiar, G.K., Potu, B.K., 2010. Anatomy of plantaris muscle: a study in adult Indians. *La Clinica terapeutica* 161, 249-252.
- Neviaser, A., Andarawis-Puri, N., Flatow, E., 2012. Basic mechanisms of tendon fatigue damage. *J Shoulder Elbow Surg* 21, 158-163.
- Nirschl, R.P., Pettrone, F.A., 1979. Tennis elbow. The surgical treatment of lateral epicondylitis. *J Bone Joint Surg Am* 61, 832-839.
- Nordin, M., Frankel, V.H., 2012. *Basic Biomechanics of the Musculoskeletal System*. Lippincott Williams & Wilkins.
- Olewnik, L., Wysiadecki, G., Polguy, M., Topol, M., 2017. Anatomic study suggests that the morphology of the plantaris tendon may be related to Achilles tendonitis. *Surg Radiol Anat* 39, 69-75.

- Onishi, H., Yagi, R., Akasaka, K., Momose, K., Ihashi, K., Handa, Y., 2000. Relationship between EMG signals and force in human vastus lateralis muscle using multiple bipolar wire electrodes. *J Electromyogr Kinesiol* 10, 59-67.
- Pearce, C.J., Carmichael, J., Calder, J.D., 2012. Achilles tendinopathy and plantaris tendon release and division in the treatment of non-insertional Achilles tendinopathy. *Foot Ankle Surg* 18, 124-127.
- Peck, D., Buxton, D.F., Nitz, A., 1984. A comparison of spindle concentrations in large and small muscles acting in parallel combinations. *Journal of morphology* 180, 243-252.
- Peers, K.H., Brys, P.P., Lysens, R.J., 2003. Correlation between power Doppler ultrasonography and clinical severity in Achilles tendinopathy. *International orthopaedics* 27, 180-183.
- Pollock, N., Dijkstra, P., Calder, J., Chakraverty, R., 2016. Plantaris injuries in elite UK track and field athletes over a 4-year period: a retrospective cohort study. *Knee Surg Sports Traumatol Arthrosc* 24, 2287-2292.
- Pourmoghaddam, A., Dettmer, M., O'Connor, D.P., Paloski, W.H., Layne, C.S., 2016. Measuring multiple neuromuscular activation using EMG - a generalizability analysis. *Biomedizinische Technik. Biomedical engineering* 61, 595-605.
- Pruim, G.J., Dejongh, H.J., Tenbosch, J.J., 1980. Forces Acting on the Mandible during Bilateral Static Bite at Different Bite Force Levels. *J Biomech* 13, 755-763.
- Raikova, R.T., Prilutsky, B.I., 2001. Sensitivity of predicted muscle forces to parameters of the optimization-based human leg model revealed by analytical and numerical analyses. *J Biomech* 34, 1243-1255.
- Rasmussen, J., Damsgaard, M., Voigt, M., 2001. Muscle recruitment by the min/max criterion - A comparative numerical study.
- Rees, J.D., Lichtwark, G.A., Wolman, R.L., Wilson, A.M., 2008. The mechanism for efficacy of eccentric loading in Achilles tendon injury; an in vivo study in humans. *Rheumatology (Oxford, England)* 47, 1493-1497.
- Reeves, N.D., Maganaris, C.N., Narici, M.V., 2003. Effect of strength training on human patella tendon mechanical properties of older individuals. *The Journal of physiology* 548, 971-981.
- Reiter, M., Ulreich, N., Dirisamer, A., Tscholakoff, D., Bucek, R.A., 2004. [Extended field-of-view sonography in Achilles tendon disease: a comparison with MR imaging]. *RoFo : Fortschritte auf dem Gebiete der Rontgenstrahlen und der Nuklearmedizin* 176, 704-708.

- Rio, E., Kidgell, D., Moseley, G.L., Gaida, J., Docking, S., Purdam, C., Cook, J., 2016. Tendon neuroplastic training: changing the way we think about tendon rehabilitation: a narrative review. *Br J Sports Med* 50, 209-215.
- Rouse, E.J., Hargrove, L.J., Perreault, E.J., Kuiken, T.A., 2014. Estimation of human ankle impedance during the stance phase of walking. *IEEE Trans Neural Syst Rehabil Eng* 22, 870-878.
- Sandrey, M.A., 2003. Acute and chronic tendon injuries: Factors affecting the healing response and treatment. *Journal of Sport Rehabilitation* 12, 70-91.
- Saxena, A., Bareither, D., 2000. Magnetic resonance and cadaveric findings of the incidence of plantaris tendon. *Foot Ankle Int* 21, 570-572.
- Sayana, M.K., Maffulli, N., 2007. Eccentric calf muscle training in non-athletic patients with Achilles tendinopathy. *J Sci Med Sport* 10, 52-58.
- Schlicht, S.M., Morrison, W.A., 1992. The plantaris tendon as a tendo-osseous graft. Part I. An anatomical study. *Journal of hand surgery (Edinburgh, Scotland)* 17, 467-470.
- Selvanetti, A., Cipolla, M., Puddu, G., 1997a. Overuse tendon injuries: Basic science and classification. *Operative Techniques in Sports Medicine* 5, 110-117.
- Selvanetti, A., Cipolla, M., Puddu, G., 1997b. Overuse tendon injuries: Basic science and classification. *Oper Techn Sport Med* 5, 110-117.
- Seynnes, O.R., Erskine, R.M., Maganaris, C.N., Longo, S., Simoneau, E.M., Grosset, J.-F., Narici, M.V., 2009. Training-induced changes in structural and mechanical properties of the patellar tendon are related to muscle hypertrophy but not to strength gains. *J Appl Physiol* 107, 523-530.
- Shapiro, L., Harish, M., Hargreaves, B., Staroswiecki, E., Gold, G., 2012. Advances in musculoskeletal MRI: technical considerations. *J Magn Reson Imaging* 36, 775-787.
- Sharma, P., Maffulli, N., 2005. Tendon injury and tendinopathy: healing and repair. *J Bone Joint Surg Am* 87, 187-202.
- Sharma, S., Khullar, M., Bhardwaj, S., 2015. Unilateral Accessory Plantaris Muscle: A Rare Anatomical Variation with Clinical Implications. *Glob J Med Res*.
- Sheehan, F.T., 2010. The instantaneous helical axis of the subtalar and talocrural joints: a non-invasive in vivo dynamic study. *J Foot Ankle Res* 3, 13.
- Slane, L.C., Thelen, D.G., 2014. Non-uniform displacements within the Achilles tendon observed during passive and eccentric loading. *J Biomech* 47, 2831-2835.

Slane, L.C., Thelen, D.G., 2015. Achilles tendon displacement patterns during passive stretch and eccentric loading are altered in middle-aged adults. *Med Eng Phys* 37, 712-716.

Smith, C., Young, I., Kearney, J., 1996. Mechanical properties of tendons: changes with sterilization and preservation. *Journal of biomechanical engineering* 118, 56-61.

Smith, J., Alfredson, H., Masci, L., Sellon, J.L., Woods, C.D., 2017. Differential Plantaris-Achilles Tendon Motion: A Sonographic and Cadaveric Investigation. *PM R* 9, 691-698.

Spang, C., Alfredson, H., Docking, S.I., Masci, L., Andersson, G., 2016. The plantaris tendon: a narrative review focusing on anatomical features and clinical importance. *The bone & joint journal* 98-B, 1312-1319.

Spang, C., Harandi, V.M., Alfredson, H., Forsgren, S., 2015. Marked innervation but also signs of nerve degeneration in between the Achilles and plantaris tendons and presence of innervation within the plantaris tendon in midportion Achilles tendinopathy. *Journal of musculoskeletal & neuronal interactions* 15, 197-206.

Spina, A.A., 2007. The plantaris muscle: anatomy, injury, imaging, and treatment. *J Can Chiropr Assoc* 51, 158-165.

Stephen, J.M., Marsland, D., Masci, L., Calder, J.D.F., Daou, H.E., 2018. Differential Motion and Compression Between the Plantaris and Achilles Tendons: A Contributing Factor to Midportion Achilles Tendinopathy? *Am J Sports Med* 46, 955-960.

Syha, R., Springer, F., Wurslin, C., Ipach, I., Ketelsen, D., Grozinger, G., Notohamiprodjo, M., Nikolaou, K., Claussen, C.D., Schick, F., Grosse, U., 2015. Tendinopathy of the achilles tendon: volume assessed by automated contour detection in submillimeter isotropic 3-dimensional magnetic resonance imaging data sets recorded at a field strength of 3 T. *Journal of computer assisted tomography* 39, 250-256.

Szaro, P., Witkowski, G., Smigielski, R., Krajewski, P., Ciszek, B., 2009. Fascicles of the adult human Achilles tendon - an anatomical study. *Ann Anat* 191, 586-593.

Thelen, D.G., Anderson, F.C., 2006. Using computed muscle control to generate forward dynamic simulations of human walking from experimental data. *Journal of biomechanics* 39, 1107-1115.

Thorpe, C.T., Streeter, I., Pinchbeck, G.L., Goodship, A.E., Clegg, P.D., Birch, H.L., 2010. Aspartic acid racemization and collagen degradation markers reveal an accumulation of damage in tendon collagen that is enhanced with aging. *J Biol Chem* 285, 15674-15681.

- Toumi, H., Lerguech, G., Cherief, M., Batakis, A., Hambli, R., Jennane, R., Best, T.M., Lespessailles, E., 2016. Implications of the calf musculature and Achilles tendon architectures for understanding the site of injury. *J Biomech* 49, 1180-1185.
- Tsirakos, D., Baltzopoulos, V., Bartlett, R., 1997. Inverse optimization: functional and physiological considerations related to the force-sharing problem. *Critical reviews in biomedical engineering* 25, 371-407.
- Uthoff, H.K., Sano, H., 1997. Pathology of failure of the rotator cuff tendon. *The Orthopedic clinics of North America* 28, 31-41.
- van Dijk, C.N., van Sterkenburg, M.N., Wiegerinck, J.I., Karlsson, J., Maffulli, N., 2011. Terminology for Achilles tendon related disorders. *Knee Surg Sports Traumatol Arthrosc* 19, 835-841.
- van Gils, C.C., Steed, R.H., Page, J.C., 1996. Torsion of the human Achilles tendon. *The Journal of foot and ankle surgery : official publication of the American College of Foot and Ankle Surgeons* 35, 41-48.
- van Sterkenburg, M.N., de Jonge, M.C., Sierevelt, I.N., van Dijk, C.N., 2010. Less promising results with sclerosing ethoxysclerol injections for midportion achilles tendinopathy: a retrospective study. *Am J Sports Med* 38, 2226-2232.
- van Sterkenburg, M.N., Kerkhoffs, G.M., Kleipool, R.P., Niek van Dijk, C., 2011a. The plantaris tendon and a potential role in mid-portion Achilles tendinopathy: an observational anatomical study. *J Anat* 218, 336-341.
- van Sterkenburg, M.N., Kerkhoffs, G.M., van Dijk, C.N., 2011b. Good outcome after stripping the plantaris tendon in patients with chronic mid-portion Achilles tendinopathy. *Knee Surg Sports Traumatol Arthrosc* 19, 1362-1366.
- van Sterkenburg, M.N., van Dijk, C.N., 2011. Mid-portion Achilles tendinopathy: why painful? An evidence-based philosophy. *Knee Surg Sports Traumatol Arthrosc* 19, 1367-1375.
- Vanderhooft, E., 1996. The frequency of and relationship between the palmaris longus and plantaris tendons. *American journal of orthopedics (Belle Mead, N.J.)* 25, 38-41.
- Verstraete, M.A., Van Der Straeten, C., De Lepeleere, B., Opsomer, G.J., Van Hoof, T., Victor, J., 2015. Impact of drying and thiel embalming on mechanical properties of achilles tendons. *Clin Anat* 28, 994-1001.
- Walton, J.M., 2003. *Pantelis Michelakis Achilles in Greek Tragedy* Cambridge: Cambridge University Press, 2002. 218 p. 40.00. ISBN: 0-521-81843-5, *New Theatre Quarterly*, pp. 395-395.

- Wang, J.H., 2006. Mechanobiology of tendon. *J Biomech* 39, 1563-1582.
- Ward, S.R., Eng, C.M., Smallwood, L.H., Lieber, R.L., 2009. Are current measurements of lower extremity muscle architecture accurate? *Clin Orthop Relat Res* 467, 1074-1082.
- Wehbe, M.A., 1992. Tendon graft donor sites. *The Journal of hand surgery* 17, 1130-1132.
- Weinert-Aplin, R.A., 2014. Development of a Foot and Ankle Musculoskeletal Model: Implications for Achilles Tendinopathy (Doctoral dissertation).
- Wening, J.V., Katzer, A., Phillips, F., Jungbluth, K.H., Lorke, D.E., 1996. [Detection of the tendon of the musculus plantaris longus--diagnostic imaging and anatomic correlate]. *Unfallchirurgie* 22, 30-35.
- White, W.L., 1960. The unique, accessible and useful plantaris tendon. *Plastic and reconstructive surgery and the transplantation bulletin* 25, 133-141.
- Wickiewicz, T.L., Roy, R.R., Powell, P.L., Edgerton, V.R., 1983. Muscle architecture of the human lower limb. *Clin Orthop Relat Res* 179, 275-283.
- Winter, D.A., 2009. *Biomechanics and motor control of human movement*, 4th ed. Wiley, Hoboken, N.J.
- Wren, T.A., Lindsey, D.P., Beaupre, G.S., Carter, D.R., 2003. Effects of creep and cyclic loading on the mechanical properties and failure of human Achilles tendons. *Ann Biomed Eng* 31, 710-717.
- Wren, T.A., Yerby, S.A., Beaupre, G.S., Carter, D.R., 2001. Mechanical properties of the human Achilles tendon. *Clin Biomech (Bristol, Avon)* 16, 245-251.
- Zanetti, M., Metzdorf, A., Kundert, H.P., Zollinger, H., Vienne, P., Seifert, B., Hodler, J., 2003. Achilles tendons: clinical relevance of neovascularization diagnosed with power Doppler US. *Radiology* 227, 556-560.
- Zeighami, A., Aissaoui, R., Dumas, R., 2018. Knee medial and lateral contact forces in a musculoskeletal model with subject-specific contact point trajectories. *J Biomech* 69, 138-145.
- Zelik, K.E., Honert, E.C., 2018. Ankle and foot power in gait analysis: Implications for science, technology and clinical assessment. *Journal of Biomechanics* 75, 1-12.



# Publications and presentations

## Conference presentations

1. Chia-Han Yeh, Anthony M.J. Bull, Angela E. Kedgley. 2018. The twisted fibre structure of the Achilles tendon in lower limb musculoskeletal modelling, World Congress of Biomechanics, Dublin, Ireland.
2. Chia-Han Yeh, James D. Calder, Anthony M.J. Bull, Angela E. Kedgley. 2017. Plantaris tendon geometry *in vivo*, European Society of Biomechanics, Seville, Spain.

## Posters

1. Chia-Han Yeh, James D. Calder, Jonathon Houghton, Anthony M.J. Bull, Angela E. Kedgley. 2018. Detecting the plantaris tendon *in vivo*: biomechanical implications of prevalence and anatomical variation for midportion Achilles tendinopathy, World Congress of Biomechanics, Dublin, Ireland.
2. Chia-Han Yeh, Anthony M.J. Bull, Angela E. Kedgley. 2018. The Lagrange Vector in musculoskeletal modelling, BioMedEng, London, UK.
3. Chia-Han Yeh, Anthony M.J. Bull, Angela E. Kedgley. 2016. The twisted fibre structure of the Achilles tendon in lower limb musculoskeletal modelling, MeiBioeng, Oxford, UK.

## **Appendix A**

### **The role of Lagrange multipliers in lower limb musculoskeletal modelling**

In chapter 5, the study produced results that showed that there is a significant effect on muscle force distribution in the Achilles tendon with different anatomical variants. The study utilised a musculoskeletal model and this chapter focuses on the optimization process that decides this distribution in such models. This chapter explores the underlying mathematics of the theorem of constrained optimisation and investigates its effect on muscle force distribution. This is a technical and numerical investigation of the solution predicted by the musculoskeletal model used in this thesis in order to provide further insights into muscle coordination.

## A.1 Introduction

Musculoskeletal models have been used to estimate the muscle and joint forces that occur during human movement. Such estimations are based on a combination of inverse dynamics and a constrained optimization process. The intersegmental forces and moments about each joint are calculated as the first step to represent the overall action of all the muscles crossing a joint. However, as the biomechanical function of these muscles often overlaps this forms an indeterminate system, which is termed muscle redundancy.

An optimization process can be applied to solve this problem. In musculoskeletal models, predefined anatomical parameters obtained from MRI and cadaveric dissection are often used to construct a model of the muscle pathways and a constrained optimization technique is applied to calculate the muscle forces during a motion. This process requires the explicit specification of an objective function. During the optimization process, the objective function is maximized or minimized whilst satisfying the kinetic constraints of movement and the degrees of freedom of the joints. Such an optimization process only considers the kinematic constraint of a single frame; and it is therefore also termed static optimization (Tsirakos et al., 1997).

The theory of constrained optimization was predominantly developed by the French mathematician, Joseph-Louis Lagrange. He introduced the concept of Lagrange multipliers to find optimal solutions under certain predefined constraints. In a musculoskeletal model, the Lagrange multipliers play a very powerful role because they directly affect the calculated muscle forces. However, there are few publications that discuss the meaning of Lagrange multipliers in these models, or explore their utility in

the physical interpretation of muscle force redundancy (Raikova and Prilutsky, 2001). Ait-Haddou et al. (2004) analysed the force distribution and the Lagrange multipliers and aims to facilitate the understanding of the Lagrange multipliers generated during the constrained optimization process (Ait-Haddou et al., 2004). They introduced a hyperplane that could differentiate the active and passive muscles. However, the idea of hyperplane is not easy to interpret geometrically.

The investigation of the multipliers themselves could provide insight into the muscle force distribution required to achieve a movement. The aim of this chapter was to clarify the physiological meaning of the Lagrange multiplier in the context of this thesis. Therefore, lower limb modelling of the gait cycle was analysed, with a focus on the contribution of muscles associated with Achilles tendon function.

## **A.2 Methods**

### **A.2.1 Anatomical parameters and kinematic data**

Nine previously-created subject-specific anatomical datasets containing the muscle paths of each participant, as described in Chapter 5, were used. The rotational Achilles tendon structure discussed in Chapter 5 was modelled as a single insertion. This enabled the results to be compared to those in the literature from other musculoskeletal models. The calculation of the location of the single insertion was discussed in Chapter 5. The same subject-specific gait data introduced in Chapter 5 was also used.

### **A.2.2 Musculoskeletal model**

The FreeBody model (Cleather and Bull, 2015), which was described in Chapter 5, was used to perform the optimization process and generate the Lagrange multipliers. In the FreeBody model, every joint has six degrees of freedom and the force and moment equilibrium of all axes are considered in the static optimization process. This results in a total of 22 degrees of freedom in the model and therefore a total of 22 kinetic constraints were defined in each frame. These constraints included the force equilibrium for the foot, shank, thigh, and patella in x, y, and z-directions and moment equilibrium for the foot, shank and thigh about the x, y, and z-axes. The moment equilibrium of the patella was simplified to the sagittal plane only (Cleather and Bull, 2015). To solve the constrained optimization, 22 Lagrange multipliers were assigned for the equality constraints and another 179 multipliers for inequality constraints, due to  $x_n$  being non-negative. Such inequality constraints fulfilled the Kuhn-Tucker condition (Kuhn and Tucker, 2014) and could be simplified as Equation 7.1 and Equation 7.2,

$$x_i \nabla_{x_i} L(x_i, \lambda) = 0, \quad i = 1, 2, \dots, 179 \quad \text{Equation 7.1}$$

$$\nabla_{\lambda_j} L(x, \lambda_j) = 0, \quad j = 1, 2, \dots, 22 \quad \text{Equation 7.2}$$

where

$$L(x, \lambda) = F(x) + \sum_j \lambda_j K_j(x) \quad \text{Equation 7.3}$$

$$F(x) = \sum_i (x_i / f_i)^3, \quad i = 1, \dots, 163 \quad \text{Equation 7.4}$$

$F(x)$ : the objective function;

$x_i$ : the magnitude of the  $n$ th muscle force;

$\lambda_j$ : the  $j^{\text{th}}$  Lagrange multiplier;

$f_i$ : the maximal muscle force of the  $i^{\text{th}}$  muscle;

$K_j(\mathbf{x})$  represents the  $j^{\text{th}}$  kinematic equality constraint, which is equivalent to the  $j^{\text{th}}$  row in Equation 6.5.

The Lagrange multipliers of each kinetic constraint are summarized in Table 6.1.

Lagrange multiplier	Kinetic constraints
$\lambda_1$	Foot anterior/posterior force equilibrium
$\lambda_2$	Foot superior/inferior force equilibrium
$\lambda_3$	Foot medial/lateral force equilibrium
$\lambda_4$	Shank anterior/posterior force equilibrium
$\lambda_5$	Shank superior/inferior force equilibrium
$\lambda_6$	Shank medial/lateral force equilibrium
$\lambda_7$	Thigh anterior/posterior force equilibrium
$\lambda_8$	Thigh superior/inferior force equilibrium
$\lambda_9$	Thigh medial/lateral force equilibrium
$\lambda_{10}$	Patella anterior/posterior force equilibrium
$\lambda_{11}$	Patella superior/inferior force equilibrium
$\lambda_{12}$	Patella medial/lateral force equilibrium
$\lambda_{13}$	Foot moment equilibrium in medial/lateral rotation
$\lambda_{14}$	Foot moment equilibrium in internal/external rotation
$\lambda_{15}$	Foot moment equilibrium in plantarflexion/dorsiflexion
$\lambda_{16}$	Shank moment equilibrium in adduction/abduction
$\lambda_{17}$	Shank moment equilibrium in internal/external rotation
$\lambda_{18}$	Shank moment equilibrium in flexion/extension
$\lambda_{19}$	Thigh moment equilibrium in adduction/abduction
$\lambda_{20}$	Thigh moment equilibrium in internal/external rotation
$\lambda_{21}$	Thigh moment equilibrium in flexion/extension
$\lambda_{22}$	Patellar tendon and quadriceps tendon force ratio

**Table 7.1 – The Lagrange multipliers in the FreeBody model and corresponding kinetic constraints.**

The constraints are defined in a reference coordinate system based on the participant's pelvic anatomical landmarks, where the x-axis points forward, the y-axis upward, and z-axis laterally to the right. This reference system does not represent the functional axes of each joint, but by aligning it with each participant's global coordinate frame, it mitigates the complexity of the discussion of the Lagrange multipliers across multiple segments. The equations of kinetic constraint were specified as Equation 6.5,

$$\begin{bmatrix} p_1^1 & \cdots & p_1^{179} \\ \vdots & \ddots & \vdots \\ p_{12}^1 & \cdots & p_{12}^{179} \\ q_1^1 & \cdots & q_1^{179} \\ \vdots & \ddots & \vdots \\ q_{10}^1 & \cdots & q_{10}^{179} \end{bmatrix} \begin{bmatrix} x_1 \\ \vdots \\ x_{179} \end{bmatrix} = \begin{bmatrix} k_1 \\ \vdots \\ k_{10} \\ l_1 \\ \vdots \\ l_{12} \end{bmatrix} \quad \text{Equation 7.5}$$

where

$p_n^m$ : the muscle line of action for the  $m^{th}$  muscle of  $n^{th}$  kinetic constraint equation;

$q_n^m$ : the effective moment arm of the  $m^{th}$  muscle of  $n^{th}$  kinetic constraint equation;

$x_n$ : the force magnitude of the  $n$ th muscle;

$k_n$ : the time derivatives of the linear momentum plus external force;

$l_n$ : the time derivatives of the angular momentum plus external torque.

As described in Chapter 5, 163 muscles are considered in the model. Another 15 joint contact force vectors and one patella tendon force are considered to formulate the equations of motion (Table 6.2). Therefore a total of 179 forces are calculated, with 163 muscle activations being specified in the objective function.



---

### Joint contact forces in FreeBody

---

Ankle joint contact forces in x-, y- and z-axes

Medial knee joint contact forces in x-, y-, and z-axes

Lateral knee joint contact forces in x-, y-, and z-axes

Patella femoral joint contact force in in x-, y-, and z-axes

Hip joint contact forces in x-, y-, and z-axes

---

**Table 7.2 – The 15 joint contact forces in the FreeBody model**

---

The calculation of muscle forces is achieved with constrained optimization. The objective function was the summation of the muscle activations cubed (Crowninshield and Brand, 1981). The constrained optimization algorithm in MATLAB (The Mathworks Inc., Natick, MA) was used to iteratively approach the optimal solution. In each frame, the Lagrange multipliers were returned if an optimal solution was found to satisfy the kinetic constraints. The optimal solution of the previous frame was used as the initial estimate for the algorithm to solve the next frame. Nine different initial values (0, 5, 10, 50, 100, 500, 1000) were set as an initial estimate of  $x$  to solve the first frame, to avoid obtaining a local minimum.

From Equation 6.1 and Equation 6.2, the optimal muscle force can be calculated by Equation 6.6

$$x_i = \sqrt{\frac{f_i^3}{3}} \sqrt{-(\lambda_1 p_1^i + \lambda_2 p_2^i + \dots + \lambda_{12} p_{12}^i + \lambda_{13} q_1^i + \dots + \lambda_{22} q_{10}^i)} \quad \text{Equation 7.6}$$

Equation 6.6 shows the optimal force can solely depend on the Lagrange multiplier and the components of the muscle lines of action and moment arm. This allows further simplification by grouping Lagrange Multipliers into 3D vectors as in Equation 6.7,

$$x_i = \sqrt{\frac{f_i^3}{3}} \sqrt{-\left(\sum_m V_m \cdot P_m^i + \sum_n U_n \cdot Q_n^i\right)} \quad \text{Equation 7.7}$$

where

$V_m$  : the 3D vector made by Lagrange multipliers for force equilibrium of the  $m^{\text{th}}$  segment;

$U_n$  : the 3D vector made by Lagrange multipliers for moment equilibrium of the  $n^{\text{th}}$  segment;

$P_m^i$  : the 3D vector of the  $i^{\text{th}}$  muscle line of action to the  $m^{\text{th}}$  segment;

$Q_n^i$  : the 3D vector of the  $i^{\text{th}}$  muscle effective moment arm to the  $n^{\text{th}}$  segment.

$V_m$  and  $U_n$  represent the grouping of Lagrange Multipliers and can be understood as 3D vectors. For ease of communication,  $V_m$  and  $U_n$  are termed ‘Lagrange Vectors’ in this study. The optimal force prediction is decided based on the summation of dot products of the Lagrange Vector and the vector representing the corresponding muscle line of action or moment arm. The muscle will be activated if  $x_i$  is a real number in the optimal solution.

The multipliers of each frame were analysed. The distribution of the multipliers and norm of Lagrange Vectors were characterized using median and interquartile range (IQR).

### **A.3 Results**

In a gait cycle, defined as being from heel strike to heel strike, the Lagrange multipliers changed smoothly and reached their extremum at the middle of the cycle (med: 49.5%, IQR: 47.5%-52%). The toe-off event happened at 62.2% of a gait cycle (IQR: 61.0%-62.8%). Two representative median multipliers ( $\lambda_7$  and  $\lambda_{13}$ ) in a gait cycle are shown in Figure 6.1.

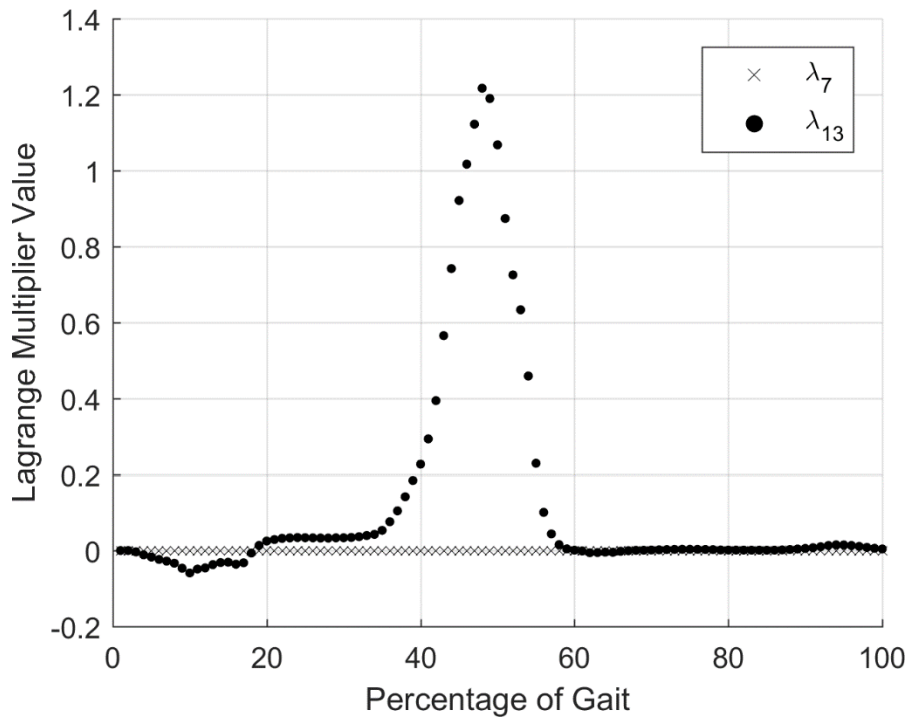


**Figure 7.1 – The median trajectory of two Lagrange multipliers during a walking trial (n = 9)**

$\lambda_7$  represents the Lagrange multiplier for thigh force equilibrium in the anterior/posterior axis, which remained closed to zero during the whole walking trial.  $\lambda_{13}$  represents the Lagrange multiplier for foot moment equilibrium in the anterior/posterior axis.

The extrema of all Lagrange multipliers and Lagrange Vectors, median and IQR are presented in Table 6.2. The multipliers of the thigh force equilibrium ( $\lambda_7$ ,  $\lambda_8$ , and  $\lambda_9$ ) remained almost zero, while the multiplier of the foot moment equilibrium ( $\lambda_{13}$ ) was the largest. The same pattern was seen in Lagrange Vectors. The largest norm was seen in the Lagrange Vector for foot moment equilibrium, while the smallest for hip force equilibrium. The extremums of the norms of the Lagrange Vectors are presented in Figure 6.2. The Lagrange Vectors summarize the magnitude of three components and provide a spatial understanding (Figure 6.3) of the Lagrange multipliers and their relationship with the muscle activations.

Lagrange multiplier	Median [IQR]	Lagrange Vector	Median norm [IQR]
$\lambda_1$	0.173 [0.063-0.303]		
$\lambda_2$	0.065 [0.032-0.154]	$V_1$	0.232 [0.130-0.614]
$\lambda_3$	0.134 [0.112-0.512]		
$\lambda_4$	0.134 [0.055-0.220]		
$\lambda_5$	0.044 [0.022-0.061]	$V_2$	0.157 [0.075-0.277]
$\lambda_6$	0.070 [0.048-0.173]		
$\lambda_7$	7e-7 [6e-7 to 9e-7]		
$\lambda_8$	9e-7 [8e-7 to 9e-7]	$V_3$	1e-6 [1.1e-6-1.2e-6]
$\lambda_9$	9e-7 [8e-7 to 1e-6]		
$\lambda_{10}$	0.133 [0.054-0.248]		
$\lambda_{11}$	0.033 [0.017-0.043]	$V_4$	0.155 [0.075-0.296]
$\lambda_{12}$	0.072 [0.050-0.169]		
$\lambda_{13}$	1.763 [0.930-4.854]		
$\lambda_{14}$	1.090 [0.576-3.084]	$U_1$	2.078 [1.249-5.652]
$\lambda_{15}$	0.668 [0.076-1.304]		
$\lambda_{16}$	0.160 [0.128-0.388]		
$\lambda_{17}$	0.100 [0.063-0.432]	$U_2$	0.220 [0.148-0.918]
$\lambda_{18}$	0.072 [0.041-0.366]		
$\lambda_{19}$	0.168 [0.104-0.379]		
$\lambda_{20}$	0.092 [0.062-0.446]	$U_3$	0.369 [0.175-1.406]
$\lambda_{21}$	0.316 [0.127-0.651]		
$\lambda_{22}$	0.002 [0.002-0.009]	$U_4$	0.002 [0.002-0.009]

**Table 7.3 – The median and IQR of extrema of Lagrange multipliers and Lagrange vectors.**

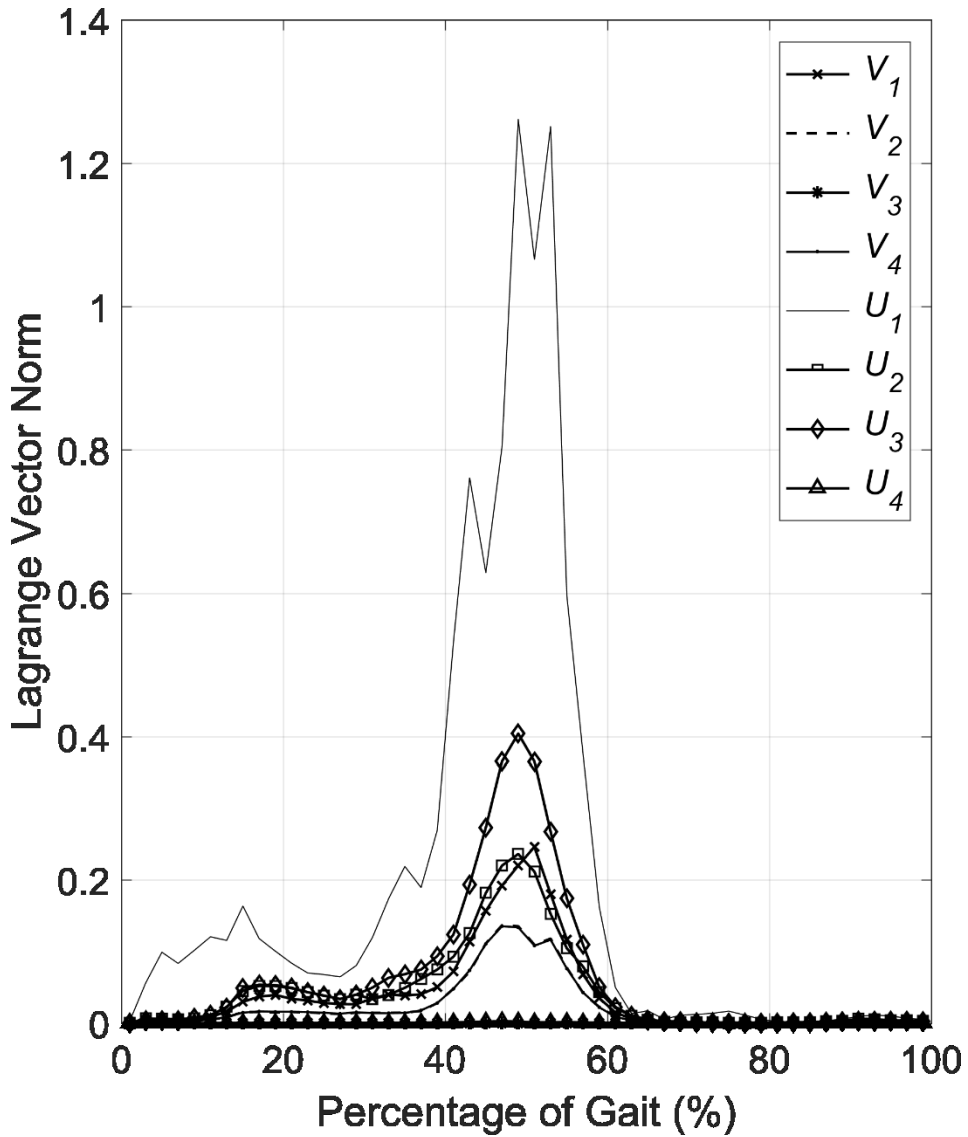


**Figure 7.2 – The median trajectory of the norms of all the Lagrange Vectors for all nine participants.**

The physical meaning of the Lagrange Vectors  $V_i$  and  $U_i$  are described in Table 6.1. The largest norm was seen in  $U_1$ , which represents the Lagrange Vector of foot moment equilibrium.

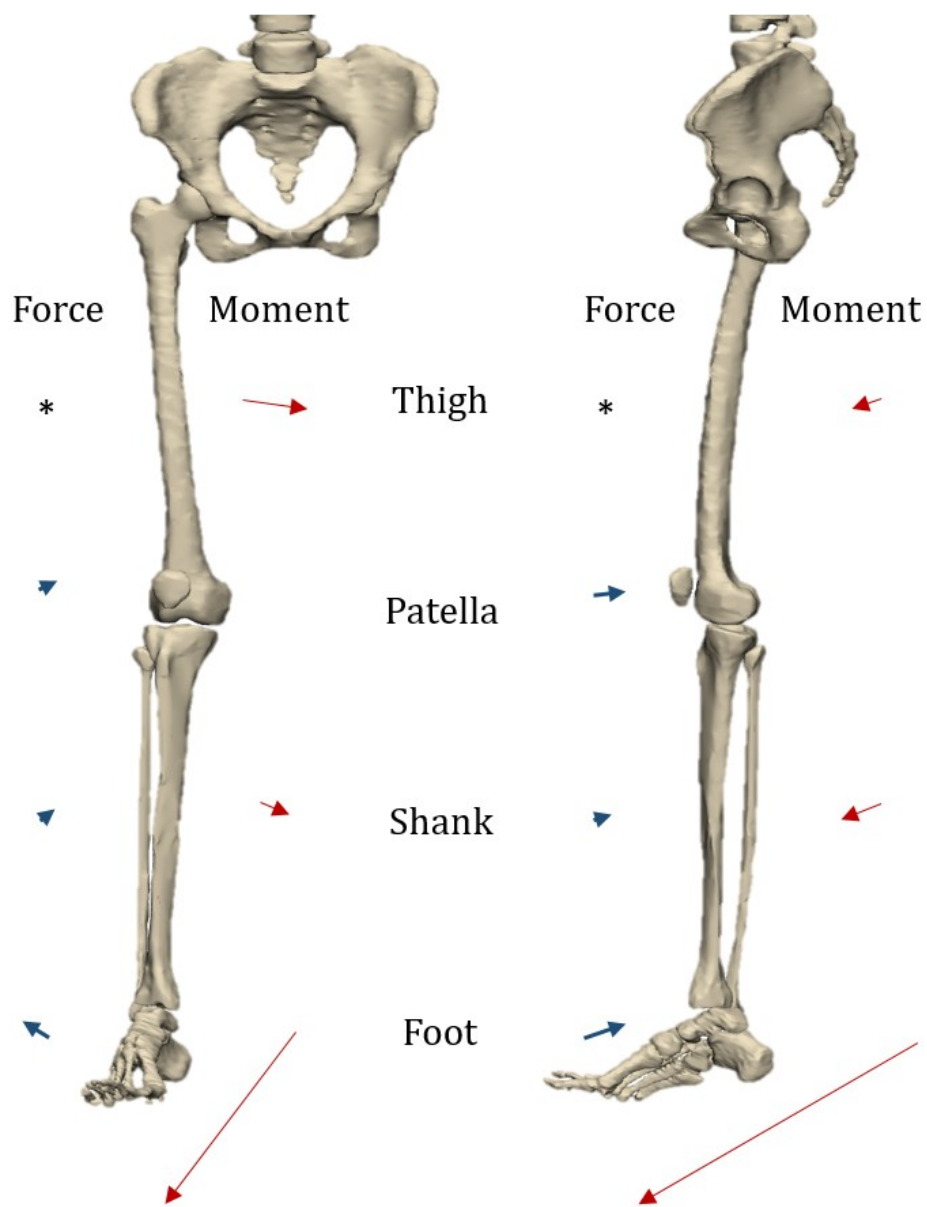


**Figure 7.3 – The anterior and medial projection of the Lagrange Vector.**

The hip force Vector is marked as \* because it is too small.

## **A.4 Discussion**

This study investigated the effect of the Lagrange multipliers in a 3D space and proposed a novel ‘Lagrange Vector’. Few studies in the literature have mentioned the role of Lagrange multipliers in musculoskeletal modelling (Moissenet et al., 2014; Raikova and Prilutsky, 2001; Zeighami et al., 2018) and their potential importance has been neglected. This representation enables improved understanding of the spatial interaction of muscle force optimization.

### **A.4.1 The magnitude of Lagrange multipliers**

Lagrange multipliers influence the muscle force optimization. As shown in Equation 6.6, the multipliers can be seen as a weighting factor for each anatomical parameter (i.e. muscle lines of action and muscle effective moment arm) used for muscle force prediction. The multipliers for thigh force equilibrium remained close to zero throughout the gait cycle. Therefore, the muscle lines of action applied to the thigh segment had a minimal effect on the prediction of the muscle forces. This observation supports the simplified inverted pendulum model of gait, in which no active work is needed to support the centre of mass during single support phase (Kuo, 2007; Kuo et al., 2005).

The largest multipliers were observed for ankle moment equilibrium. This suggests that the prediction of muscle forces will be greatly affected if the muscle moment arm of the foot is changed. This is intuitively reasonable, as the ankle provides a large torque to propel the body forward. In fact, previously the Achilles tendon insertion was identified as the most sensitive parameter to the overall muscle force prediction in lower



limb musculoskeletal modelling (Carbone et al., 2012). A large foot multiplier, but relatively small shank and thigh multipliers, identified in this study further explain why perturbation of the origins of muscles connected to the Achilles tendon will not affect the overall force output as much as a perturbation of the Achilles tendon insertion. As the insertion changes, large foot multipliers will amplify the difference in muscle lines of action and moment arms in the foot, while small shank multipliers will not amplify the changes to such an extent and therefore only have a minor effect on the resultant muscle forces.

Large inter-participant IQRs for the extrema were noticed. This variation could come from both anatomical variance and the kinematic differences between different subjects when walking. However, the small magnitude of hip force multipliers and large foot moment multipliers were consistent across all participants. This suggests that the model is taking a similar force prediction strategy for muscles that connect to the hip and ankle despite all the existing variation.

The optimization used an objective function that sought to minimise the summation of muscle activation to the power of three, which is the most commonly used objective function in lower limb musculoskeletal modelling (Erdemir et al., 2007). In the literature, the power of the cost function has varied between two and five, but this has been shown to result in only small differences in the resultant forces (Crowninshield and Brand, 1981). Future work could include investigating the interaction between Lagrange multipliers and objective functions.

The static optimization method has been used in lower limb musculoskeletal modelling for more than three decades. However, the value of Lagrange multipliers has not been discussed previously. One possible reason is that the objective function used often lack physiological meaning. Such objective functions act as a surrogate to be

minimized, but the final value of the objective function is not of interest, as it does not directly represent physiological parameters, such as energy or stability. This contrasts with the application of Lagrange multipliers in other fields, such as for minimizing a budget or maximizing profit, where the magnitude of the multiplier can be used as a guide to improve the optimal result (Intriligator, 2002). This study showed that Lagrange multipliers could provide insight into human motion, explain model behaviour, and potentially be used to craft an alternative objective function.

### **A.4.2 Lagrange Vector**

The concept of a Lagrange Vector was proposed, which can simplify the force distribution formula (Equation 6.7) and provide a graphical understanding of the multipliers.

The Lagrange Vector can be interpreted in different ways. To begin with, the transformation matrix between different coordinate frames can be applied to the Lagrange Vector. The precise weight of the vector in each direction of a segmental coordinate frame can be identified. This helps to explain the model sensitivity with respect to different functional axes. The norm of the Lagrange Vector can also be used as an indicator of the sensitivity to overall force prediction of each segment. If a particular Lagrange Vector has a large norm, the muscles inserting to or originating from the corresponding segment will have a large effect on the predicted force for those muscles. Furthermore, Lagrange Vectors provide a geometric explanation of the optimization results. As shown in Figure 6.4, the activation of a muscle is dependent on four components: the dot products of the muscle line of action and the moment arm with respect to the proximal and distal segments. If these four components sum to be positive, the muscle will be activated. If the summation is negative, the muscle will not

be activated. Thus, the summation further quantifies ‘how far’ a muscle is from being activated. This information is valuable when analysing the digitized muscle lines of action, which have been reported to have an error of up 5 mm during the digitization process (Klein Horsman et al., 2007). The Lagrange Vector provides a guide to correct this error.

---

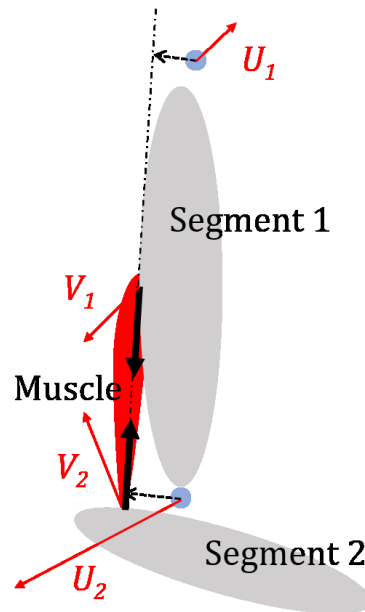


**Figure 7.4 – The illustration of a spatial understanding of the Lagrange Vector.**

The red arrows represent the Lagrange Vectors. The thick solid arrows represent the muscle line of action. The dashed arrows represent the muscle moment arms. The blue dot represents the instantaneous centre of rotation.

---

The Lagrange Vector also provides insight into muscle coordination and co-activation. As the Lagrange Vectors are shared by all the muscles, the norm of the vector can be understood as the co-activation level of the muscles that insert to and originate from the same segment. For example, the tibialis anterior, peroneus longus and soleus muscles originate from the shank and insert to the foot in the model. Anatomically they are innervated by the deep peroneal nerve, superficial peroneus

nerve, and tibial nerve, respectively, and these three nerves share a common origin, the sciatic nerve. The force calculation of these three muscles is decided by their own muscle lines of action, moment arms, and the four shared Lagrange Vectors, which are decisive as to whether a muscle is in favour of being activated (Table 6.5).

---

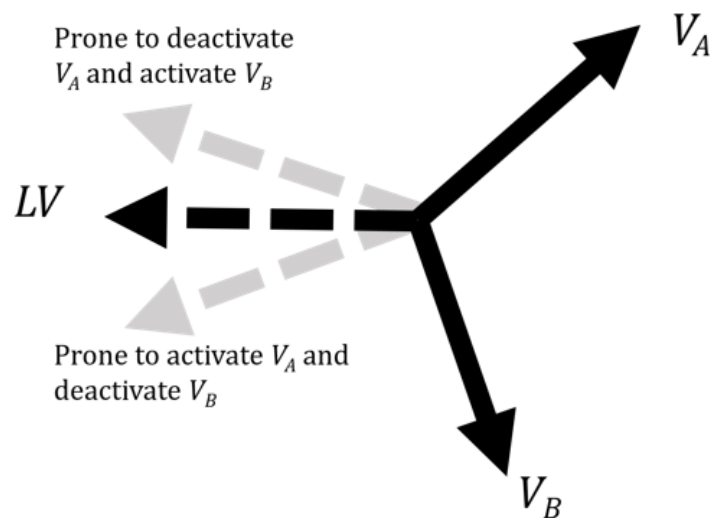


**Figure 7.5 – The orientation of the Lagrange Vector (LV) is decisive as to muscle activation.**

---

There are several limitations to this study. First, FreeBody is a segment-based model built on digitized anatomical parameters. This digitization process could introduce error and has been shown to overestimate the muscle and joint contact forces (Fregly et al., 2012; Gerus et al., 2013; Moissenet et al., 2014). Thus, the Lagrange Vector and multipliers also will have been overestimated. Therefore, this study focused on the relationship between Lagrange Vectors as a representation of the model behaviour, such as why some muscles tend to be activated but some are not, instead of comparing the actual values of the vector components. Second, the joints are simulated as floating

joints which are freely movable in six degrees of freedom. Constraining a joint will reduce the dimension of the Lagrange Vector. However, the norm of a reduced two-dimensional or one-dimensional vector is still representative of the activation level and the weighting factor for muscle force prediction. Finally, only level walking gait trials were analysed and only one musculoskeletal model was used to perform this experiment. Gait is a well-understood activity of human motion and has been modelled by other research groups. A different Lagrange Vector pattern is expected for other activities. A similar analysis could be carried out with other models, as long as the constrained optimization technique is used.

There are still many unknowns in the interaction between the Lagrange Vectors, kinematics, anatomical parameters, and objective functions. Further investigation is required to clarify these relationships. From a modelling perspective, as all the muscles on the same segments share the same sets of Lagrange Vector, it can provide insight into the coordination of muscles or even inform an understanding of high-level control strategy.

## **A.5 Conclusion**

The analysis of the Lagrange multipliers that results from the optimisation process in musculoskeletal modelling is useful to improve understanding of the model behaviour in distributing muscle forces. The Lagrange Vector is a representation that groups the multipliers and provides a geometric interpretation. In human gait modelling, a large norm in the Lagrange Vector for foot moment equilibrium and a small norm for

thigh force equilibrium were observed. The analysis of the Lagrange Vector can quantify the activation and deactivation tendency of muscles. The Lagrange Vectors for a given segment are shared by all muscles that originate from or insert on that segment and can be understood as a high-level estimation of muscle coordination and co-activation factor.

Chapters 5 and 6 covered the fundamental characteristics of lower limb musculoskeletal modelling, such as the insertion of Achilles tendon and the importance of the foot moment in the prediction of muscle forces. In the next chapter, we will use the model to analyse rehabilitation exercises.

# Appendix B Permissions for reproduction of figures

## Permissions for reproduction of figures

---

### ELSEVIER LICENSE TERMS AND CONDITIONS

Oct 25, 2018

---

This Agreement between Imperial College London -- Chia-Han Yeh ("You") and Elsevier ("Elsevier") consists of your license details and the terms and conditions provided by Elsevier and Copyright Clearance Center.

License Number	4413280877073
License date	Aug 20, 2018
Licensed Content Publisher	Elsevier
Licensed Content Publication	Annals of Anatomy - Anatomischer Anzeiger
Licensed Content Title	Fascicles of the adult human Achilles tendon – An anatomical study
Licensed Content Author	Paweł Szaro, Grzegorz Witkowski, Robert Śmigieński, Paweł Krajewski, Bogdan Ciszek
Licensed Content Date	Nov 20, 2009
Licensed Content Volume	191
Licensed Content Issue	6
Licensed Content Pages	8
Start Page	586
End Page	593
Type of Use	reuse in a thesis/dissertation
Intended publisher of new work	other
Portion	figures/tables/illustrations
Number of figures/tables/illustrations	1
Format	both print and electronic
Are you the author of this Elsevier article?	No
Will you be translating?	No
Original figure numbers	fig 6
Title of your thesis/dissertation	Biomechanics of Midportion Achilles tendinopathy
Expected completion date	Nov 2018
Estimated size (number of pages)	400
Requestor Location	Imperial College London Imperial College London  London, London SW7 2AZ United Kingdom Attn: Imperial College London
Publisher Tax ID	GB 494 6272 12

Permission to reproduce figures from Szaro et al.(2009) in Figure 2.9 and Figure 5.2

---

---

## JOHN WILEY AND SONS LICENSE TERMS AND CONDITIONS

Oct 25, 20

---

This Agreement between Imperial College London -- Chia-Han Yeh ("You") and John Wiley and Sons ("John Wiley and Sons") consist of your license details and the terms and conditions provided by John Wiley and Sons and Copyright Clearance Center.

License Number	4413280734318
License date	Aug 20, 2018
Licensed Content Publisher	John Wiley and Sons
Licensed Content Publication	Scandinavian Journal of Medicine & Science In Sports
Licensed Content Title	The twisted structure of the human Achilles tendon
Licensed Content Author	M. Edama, M. Kubo, H. Onishi, et al
Licensed Content Date	Dec 30, 2014
Licensed Content Volume	25
Licensed Content Issue	5
Licensed Content Pages	7
Type of Use	Dissertation/Thesis
Requestor type	University/Academic
Format	Print and electronic
Portion	Figure/table
Number of figures/tables	2
Original Wiley figure/table number(s)	Fig 5,6
Will you be translating?	No
Title of your thesis / dissertation	Biomechanics of Midportion Achilles tendinopathy
Expected completion date	Nov 2018
Expected size (number of pages)	400
Requestor Location	Imperial College London Imperial College London
	London, London SW7 2AZ United Kingdom Attn: Imperial College London
Publisher Tax ID	EU826007151

Permission to reproduce figures from Edama et al. (2014) in Figure 2.9 and Figure 5.3.

---



---

## WOLTERS KLUWER HEALTH, INC. LICENSE TERMS AND CONDITIONS

Oct 25, 20

---

---

This Agreement between Imperial College London -- Chia-Han Yeh ("You") and Wolters Kluwer Health, Inc. ("Wolters Kluwer Health, Inc.") consists of your license details and the terms and conditions provided by Wolters Kluwer Health, Inc. and Copyright Clearance Center.

License Number	4410430219621
License date	Aug 15, 2018
Licensed Content Publisher	Wolters Kluwer Health, Inc.
Licensed Content Publication	Clinical Orthopaedics and Related Research
Licensed Content Title	The Achilles Tendon Insertion is Crescent-shaped: An In Vitro Anatomic Investigation
Licensed Content Author	Heinz Lohrer, Sabine Arentz, Tanja Nauck, et al
Licensed Content Date	Sep 1, 2008
Licensed Content Volume	466
Licensed Content Issue	9
Type of Use	Dissertation/Thesis
Requestor type	Individual Account
STM publisher name	
Portion	Figures/table/illustration
Number of figures/tables/illustrations	1
Figures/tables/illustrations used	3
Author of this Wolters Kluwer article	No
Title of your thesis / dissertation	Biomechanics of Midportion Achilles tendinopathy
Expected completion date	Nov 2018
Estimated size(pages)	400
Requestor Location	Imperial College London Imperial College London  London, London SW7 2AZ United Kingdom Attn: Imperial College London
Publisher Tax ID	EU826013006
Billing Type	Invoice
Billing Address	Imperial College London Imperial College London  London, United Kingdom SW7 2AZ Attn: Imperial College London

Permission to reproduce figures from Lohrer et al.(2008) in Figure 2.7

---

---

## JOHN WILEY AND SONS LICENSE TERMS AND CONDITIONS

Oct 25, 20

---

This Agreement between Imperial College London -- Chia-Han Yeh ("You") and John Wiley and Sons ("John Wiley and Sons") consist of your license details and the terms and conditions provided by John Wiley and Sons and Copyright Clearance Center.

License Number	4410421132115
License date	Aug 15, 2018
Licensed Content Publisher	John Wiley and Sons
Licensed Content Publication	Journal of Anatomy
Licensed Content Title	The plantaris tendon and a potential role in mid-portion Achilles tendinopathy: an observational anatomical study
Licensed Content Author	Maayke N. van Sterkenburg, Gino M. M. J. Kerkhoffs, Roeland P. Kleipool, et al
Licensed Content Date	Feb 17, 2011
Licensed Content Volume	218
Licensed Content Issue	3
Licensed Content Pages	6
Type of Use	Dissertation/Thesis
Requestor type	University/Academic
Format	Print and electronic
Portion	Figure/table
Number of figures/tables	2
Original Wiley figure/table number(s)	Figure 2, Figure 4
Will you be translating?	No
Title of your thesis / dissertation	Biomechanics of Midportion Achilles tendinopathy
Expected completion date	Nov 2018
Expected size (number of pages)	400
Requestor Location	Imperial College London Imperial College London  London, London SW7 2AZ United Kingdom Attn: Imperial College London
Publisher Tax ID	EU826007151

Permission to reproduce figures from van Sterkenburg et al. (2011) in Figure 2.6.

---

---

## WOLTERS KLUWER HEALTH LICENSE TERMS AND CONDITIONS

Oct 25, 201

---

This Agreement between Imperial College London -- Chia-Han Yeh ("You") and Wolters Kluwer Health ("Wolters Kluwer Health") consists of your license details and the terms and conditions provided by Wolters Kluwer Health and Copyright Clearance Center.

License Number	4455850607229
License date	Oct 25, 2018
Licensed Content Publisher	Wolters Kluwer Health
Licensed Content Publication	WK Health Book
Licensed Content Title	Basic Biomechanics of the Musculoskeletal System
Licensed Content Author	Margareta Nordin DirSci, Victor H. Frankel MD, PhD
Licensed Content Date	Jan 1, 2012
Type of Use	Dissertation/Thesis
Requestor type	academic/educational
Format	print and electronic
Portion	figures/tables/illustrations
Number of figures/tables/illustrations	1
The ID numbers of the figures/tables/illustrations are...	figure 9-4
Will you be translating?	no
Reusing current or a previous edition	current edition
Circulation/distribution	20
Title of your thesis / dissertation	Biomechanics of Midportion Achilles tendinopathy
Expected completion date	Nov 2018
Estimated size (number of pages)	400
Requestor Location	Imperial College London Imperial College London  London, London SW7 2AZ United Kingdom Attn: Imperial College London
Billing Type	Invoice
Billing Address	Imperial College London Imperial College London  London, United Kingdom SW7 2AZ Attn: Imperial College London - - - - -

Permission to reproduce figures from Nordin and Frankel (2012) in Figure 2.3.

---



**Title:** Heavy-Load Eccentric Calf Muscle Training For the Treatment of Chronic Achilles Tendinosis  
**Author:** Håkan Alfredson, Tom Pietilä, Per Jonsson, et al  
**Publication:** American Journal of Sports Medicine  
**Publisher:** SAGE Publications  
**Date:** 05/01/1998  
Copyright © 1998, © SAGE Publications

Logged in as:  
Chia-Han Yeh  
Imperial College London  
Account #:  
3001321724

[LOGOUT](#)

#### Gratis Reuse

Permission is granted at no cost for use of content in a Master's Thesis and/or Doctoral Dissertation. If you intend to distribute or sell your Master's Thesis/Doctoral Dissertation to the general public through print or website publication, please return to the previous page and select 'Republish in a Book/Journal' or 'Post on intranet/password-protected website' to complete your request.

Permission to reproduce figures from Alfredson et al.(1998) in Figure 2.10

---



**Title:** Heavy Slow Resistance Versus Eccentric Training as Treatment for Achilles Tendinopathy  
**Author:** Rikke Beyer, Mads Kongsgaard, Birgitte Hougs Kjær, et al  
**Publication:** American Journal of Sports Medicine  
**Publisher:** SAGE Publications  
**Date:** 07/01/2015  
Copyright © 2015, © SAGE Publications

Logged in as:  
Chia-Han Yeh  
Imperial College London  
Account #:  
3001321724

[LOGOUT](#)

#### Gratis Reuse

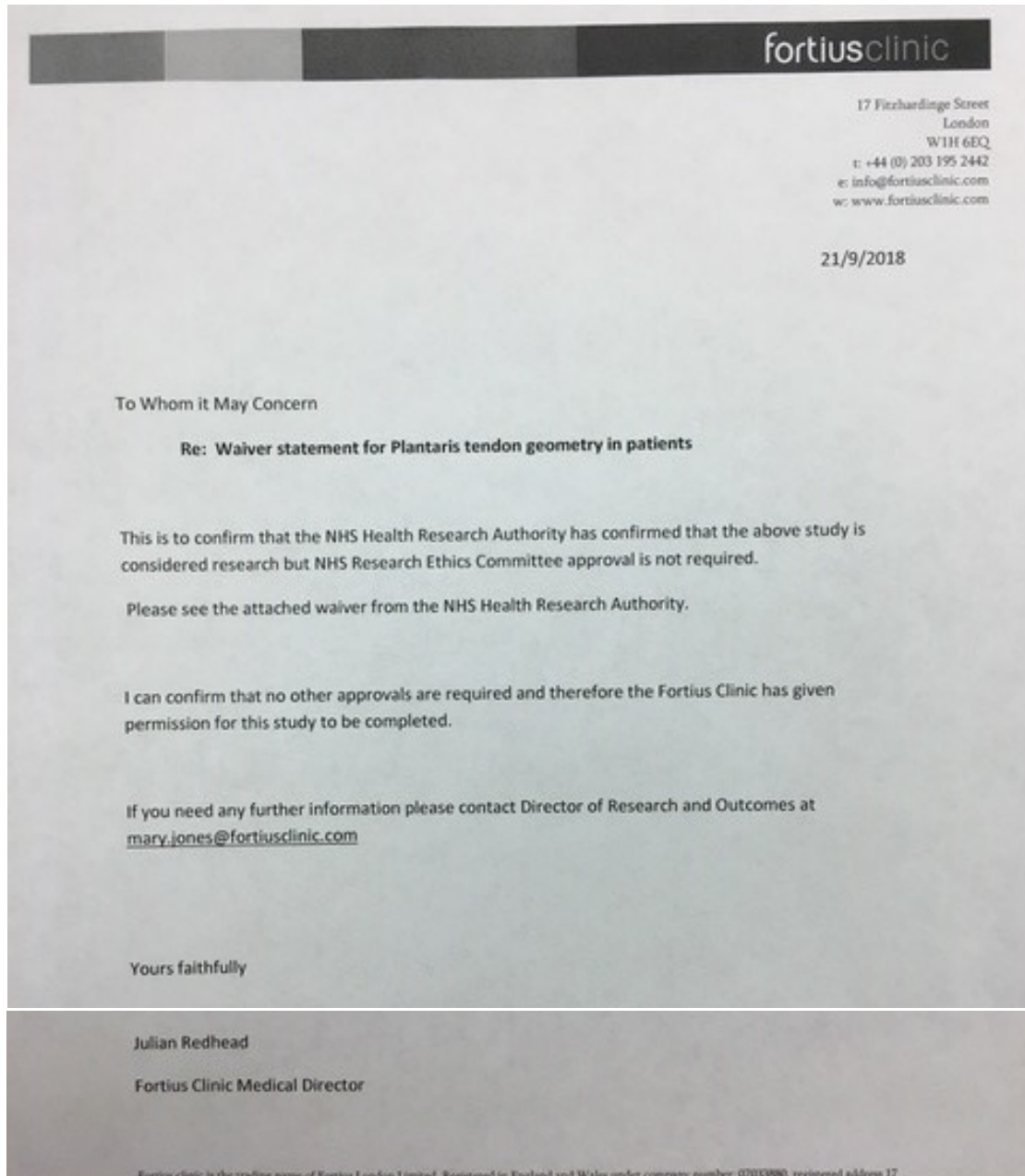
Permission is granted at no cost for use of content in a Master's Thesis and/or Doctoral Dissertation. If you intend to distribute or sell your Master's Thesis/Doctoral Dissertation to the general public through print or website publication, please return to the previous page and select 'Republish in a Book/Journal' or 'Post on intranet/password-protected website' to complete your request.

Permission to reproduce figures from Beyer et al. (2015) in Figure 2.11.

---

# Appendix C Waiver statement

Waiver statement for accessing the medical imaging database



## Ethics Approval (18IC4371)



**Imperial College Research Ethics Committee**  
Imperial College London  
Room 221  
Medical School Building  
St Marys Campus  
London  
W2 1PG  
Tel: +44 (0)207 594 9484  
[researchethicscommittee@imperial.ac.uk](mailto:researchethicscommittee@imperial.ac.uk)

Angela Kedgley  
Bioengineering Department  
Royal School of Mines  
Imperial College London  
London, SW7 2AZ

2<sup>nd</sup> July 2018

Dear Dr Kedgley

**Study Title: Modelling Achilles and plantaris tendons during rehabilitation activities**

**ICREC reference: 18IC4371**

The above Notice of Amendment was reviewed by the Joint Research Compliance Office on 29/06/18

The Joint Research Compliance Office (JRCO) have reviewed the revised documents you submitted and would like to grant full approval to this study on the basis described in the Notice of Amendment.

### **Documents**

The documents reviewed were:

- Notice of Amendment Achilles MSk model
- Patient Information Sheet Achilles MSk model (v3 25/06/18)
- Patient email Achilles MSk model (v3 25/06/18)
- Consent Form Achilles MSk model (v2 25/06/18)
- Protocol Achilles MSk model (v2 25/06/18)

Yours sincerely,

Gary Roper,  
Head of Regulatory Compliance,  
Imperial College London

## Ethics Approval (16IC3385)



**Imperial College Research Ethics Committee**  
Imperial College London  
Room 221  
Medical School Building  
St Marys Campus  
London  
W2 1PG  
Tel: +44 (0)207 594 9484  
[researchethicscommittee@imperial.ac.uk](mailto:researchethicscommittee@imperial.ac.uk)

Dr Angela Kedgley  
Imperial College London  
Department of Bioengineering  
London  
SW7 2AZ

11 June 2016

Dear Dr Kedgley,

**Study Title: Geometry of loaded achilles and plantaris tendons in MRI.**

**ICREC reference: 16IC3385**

The above study was approved by your Head of Department on 22/05/16 and by the Joint Research Compliance Office on 08/07/16.

Under the Imperial College Research Ethics Committee process, a study that has been reviewed by the Joint Research Compliance Office and Head of Division/Department (or Principal), where no significant ethical issues have been identified in the protocol or ethics application, can be approved without requiring it to go to full committee.

#### **Documents**

The documents reviewed were:

- ICREC Application form
- Protocol (v3 24/06 /16)
- Participant information sheet (v2 16/06/16)
- Consent form (v2 16/06/16)
- Recruitment email (v1 01/06/16)
- Recruitment poster (v2 12/07/16)
- Peer review letter (17/06/16)
- Sponsorship and indemnity form

Yours sincerely,

Gary Roper,  
Head of Regulatory Compliance,  
Imperial College London

Imperial College of Science, Technology and Medicine